Supplement of Atmos. Meas. Tech., 17, 765–782, 2024
https://doi.org/10.5194/amt-17-765-2024-supplement


Atmospheric Measurement Techniques
Open Access
EGU

*Supplement of*

# Single-blind test of nine methane-sensing satellite systems from three continents

**Evan D. Sherwin et al.**

*Correspondence to:* Evan D. Sherwin (evansherwin@lbl.gov)

# S1. Supplementary methods

## S1.1. Advancing Development of Emissions Detection Protocol

The single-blind controlled methane release testing in this study followed the Advancing Development of Emissions Detection (ADED) protocol, developed at the Methane Emissions Technology Evaluation Center (METEC) in Colorado (Zimmerle, 2022).

We followed protocols from Section 10, "Aerial Survey Emission Detection And Quantification," which was designed to apply to remote sensing technologies in general, including satellites (Zimmerle, 2022).

Documentation of the system under test is included both within this paper as well as in the "Performer Info" tab of the data spreadsheets submitted by each team, which are available in the data and code repository associated with this paper. Submitted emissions estimates used the standard template spreadsheet for the Aerial Survey Emission Detection And Quantification version of the ADED protocol (Zimmerle, 2022).

Following Section 10.1.1 of the ADED protocol, all teams were required to notify the Stanford team in advance of the flight pattens they intended to fly, including orientation. Teams were required to explain any deviations from this flight plan, e.g. due to inclement weather conditions (Zimmerle, 2022).

Following Section 10.4.1 of the ADED protocol, the test location was at least 1 km away from all potential confounding methane sources, e.g. the local landfill, and from all nearby water features (Zimmerle, 2022).

## S1.2. Flow rate estimation

Unless otherwise specified, all methane flow rate estimates are the average flow rate over the five minutes preceding a timestamp. Meters produce a whole-gas mass flow rate, which we convert to a methane flow rate using the methane fraction provided in natural gas composition measurements conducted at the two metering stations upstream of the vendor from which we purchased compressed natural gas. For each truck refill, we estimate the methane mole fraction as the average of the daily measurements from the five previous days leading up to and including the refill, averaging over both metering stations, as discussed in (El Abbadi et al., 2023).

## S1.3. Exclusion criteria

Stanford excluded emissions for the following reasons:

1. If there was a system malfunction resulting in an emission without reliable metering.
2. If the team was notified in advance that Stanford would not be releasing on a given day.
3. If a satellite was tasked without notice to a date outside of the testing period or on a United States national holiday.
4. Stanford release planners were unaware of 14 Sentinel-2 overpasses during the testing period and excluded them from analysis. These include overpasses on October 11$^{th}$, 14$^{th}$, 16$^{th}$, 19$^{th}$, 21$^{st}$, 24$^{th}$, 29$^{th}$, and 31$^{st}$, and November 3$^{rd}$, 10$^{th}$, 13$^{th}$, 20$^{th}$, 23$^{rd}$, and 30$^{th}$.

5. Before analyzing results, we had planned to exclude all emissions with metered flow standard deviation, accounting for all sources of variability and uncertainty, greater than 10%. In practice, the only emission that met this threshold was the sole valid GF5 overpass, which was rescheduled without notice to one minute after the emission was shut down. As a result, we include this emission in the main paper, with the appropriate caveats.

Teams were allowed to exclude measurements for any reason. In practice, the most common reason given was cloud cover.

### S1.4. Excluded nonzero ZY1 release

We exclude the October 20$^{th}$ ZY1 release from analysis in the main manuscript due to a system malfunction in the release and metering apparatus. As a result of the malfunction, there was no log of the precise meter readings. Because of the system malfunction, the Stanford field team cut gas approximately one minute before the ZY1 overpass. However, all three teams analyzing ZY1 data detected methane in the acquired spectral data.

In supplementary analysis, we use the targeted rate of 0.998 t(gas)/h as our central estimate, and add a symmetric 95% confidence interval based on the maximum measured release value of 1.607 t(gas)/h, resulting in a lower-end error bar estimated at 0.389 t(gas)/h. This translates to an estimated methane emission rate of 0.944 [0.367, 1.520] t($CH_4$)/h.

### S1.5. Total emissions during testing

We estimate total methane emissions released while testing satellites, not including methane released during the two-month testing period to evaluate other technologies. As a rule, we held each release at a constant volume for 15 minutes before a satellite passed overhead, and for five minutes afterward. For simplicity, we assume by default that all releases were held for 20 minutes at the 5-minute average volume before the satellite passed overhead. Across the full dataset, there are 47 unique satellite overpass timestamps during nonzero methane releases. This naïve approach, which does not account for near-simultaneous overpasses, would estimate total emissions at 10.7 t($CH_4$).

In some cases, multiple satellites passed overhead within 20 minutes or less. In those cases, we subtract out methane associated with any overlapping period. This occurred on October 10$^{th}$, 17$^{th}$, 26$^{th}$, and 29$^{th}$, as well as November 8$^{th}$, 10$^{th}$, 15$^{th}$, 17$^{th}$, 18$^{th}$, 28$^{th}$, and 29$^{th}$. See the replication code, in the script entitled “SatelliteTestingMain.ipynb.”

After accounting for these overlapping release periods for satellite overpasses occurring close in time, total estimated emissions from this test fall to 7.7 t($CH_4$).

## S2. Participating satellites

*This section is adapted in part, with permission, from (Sherwin et al., 2023).*

Nine satellite constellations were available to collect measurements during the study period of October 10$^{th}$-November 30$^{th}$, 2022. This included targeted satellites systems EnMAP, Gaofen 5

(GF5), GHGSat C, PRISMA, WorldView-3, and Ziyuan 1 (ZY1) which must be tasked to focus on a particular area, as well as global-coverage satellites Huanjing 2 (HJ2), Landsat 8/9, and Sentinel-2, which passively collect data from nearly all inhabited areas of the world (ESA, 2022a, b; OHBI, 2022; USGS, 2022a; ESA, 2021c, 2022c).

**Error! Reference source not found.** summarizes the spectral resolution, spatial coverage, constellation size, swath width, revisit time, and data availability.

Note that only the GHGSat instruments were originally designed for the primary purpose of detecting and quantifying methane emissions. With the remaining satellites, researchers have developed methane retrieval techniques based on existing data, e.g. citations (Varon et al., 2021; Lauvaux et al., 2022; Irakulis-Loitxate et al., 2021, 2022).

### S2.1. EnMAP

The Environmental Mapping and Analysis Program (EnMAP) satellite is a collaborative effort led by the German Space Agency and the German Research Center for Geosciences. The satellite launched on April 1, 2022. This targeted hyperspectral instrument uses spectral bands ranging from 420-2,450 nm at 10 nm spectral resolution, with a 30 km swath, operating with a 4-day maximum revisit frequency and 27-day nadir revisit frequency (EnMAP, 2023; Jacob et al., 2022). Data from EnMAP are publicly available, and the satellite can be tasked upon request (EnMAP, 2022).

### S2.2. Gaofen 5 (GF5)

The Gaofen 5-02 (GF5) Advanced Hyperspectral Imager satellite is the latest in a series of GF5 satellites launched by the Chinese government on September 7, 2021 (Luo et al., 2023). This targeted hyperspectral instrument uses spectral bands ranging from 759-2,058 nm, with 30x30 m spatial and a 60 km swath (Luo et al., 2023; Zhang et al., 2022). The spectral resolution of the instrument is unclear from the existing literature. Based on the satellite overpass dates submitted by NJU for the testing period, October 15$^{th}$, November 15$^{th}$, November 23$^{rd}$, and November 30$^{th}$, it appears that GF5-02 is capable of revisiting a location within at least 7 days. Data from GF5 can be made available upon request from the relevant government agencies.

### S2.3. GHGSat C

At the time of testing, the GHGSat C satellite series consisted of a constellation of eight instruments launched by the Canada-based private company GHGSat. GHGSat C1 launched on September 2$^{nd}$, 2020, followed by GHGSat C2 on January 24$^{th}$, 2021 and GHGSat C3-C5 launched May 25, 2022 (GHGSat, 2022). GHGSat C6-C8 were launched on April 15$^{th}$, 2023 (GHGSat, 2023). The precursor GHGSat-D satellite was launched on June 22$^{nd}$, 2016. Several additional satellites are scheduled to launch in the coming years, with a goal of achieving a 10-satellite constellation by 2023 (ESA, 2022a).

GHGSat C satellites each complete 15 orbits per day, with an average repeat cycle of approximately 14-days. Each satellite is equipped with a multispectral Wide-Angle Fabry-Perot (WAF-P) Imaging Spectrometer, focusing on a proprietary combination of unpolarized short-wave infrared frequencies from 1630-1675 nm with 0.3 nm spectral resolution and 25m spatial resolution, as well as a secondary VIS-1 Visible Sensor in the optical frequency range at <20m

spatial resolution (ESA, 2022a; Jacob et al., 2022). The sensors have a 12 km-wide field-of-view, which can be targeted toward a desired location. GHGSat claims a detection threshold of 0.1 t($CH_4$)/h at 3 m/s winds, with methane column density precision at 1% of background (ESA, 2022a).

GHGSat operates commercially, but offers access to data archives as well as tasking to scientific researchers for select proposals (ESA, 2021b).

### S2.4. Huanjing 2 (HJ2)

Huanjing 2 (HJ2) is a constellation of two satellites, HJ2A and HJ2B, launched by the Chinese government in 2020 (Zhong et al., 2021). This system has an 800 km swath (Zhong et al., 2021). The spectral bands from data files shared with all teams include 100 visible to near infrared (VNIR) bands from 450-920 nm, with 115 short-wave infrared (SWIR) bands from 900-2500 nm. Based on the satellite overpass dates submitted by NJU for the testing period, November 2nd and November 6th, it appears that HJ2B is capable of revisiting a location within at least 4 days. Data from HJ2 can be made available upon request from the relevant government agencies.

### S2.5. Landsat 8/9

Launched on February 11th, 2013 and September 27th, 2021, respectively, the Landsat 8 and 9 satellites are is the product of a collaboration between the National Aeronautics and Space Administration (NASA) and the United States Geological Survey (USGS), both agencies of the United States government (USGS, 2022a; NASA, 2023). Both instruments have global coverage, collecting data for all inhabited areas of the world every 16 days (with the two instruments 8 days out of phase) with a 185 km swath. Both satellites host a 9-band operational land imager, including two SWIR bands at 1570-1650 nm and 2110-2290 nm at 200 nm spectral resolution, as well as four visible bands, all at 30 m spatial resolution. An onboard thermal infrared sensor also collects two bands at 10,600-11,190 nm and 11,500-12,510 nm, both at 100 m resolution (USGS, 2022a; NASA, 2023; Jacob et al., 2022). All data from Landsat 8 and 9 are publicly available on the USGS website (USGS, 2022b).

### S2.6. PRISMA

Launched March 19th, 2019, the PRISMA (PRecursore IperSpettrale della Missione Applicativa) satellite is a product of the Italian Space Agency (ASI), contracting through Orbitale Hochtechnologie Bremen (OHB) Italia S.p.A. This targeted hyperspectral instrument uses spectral bands ranging from 400-2,500 nm with 10 nm spectral resolution, 30x30 m spatial resolution, and a 30 km swath, operating with a 7-day maximum revisit frequency and 29-day nadir repetition cycle. Data from PRISMA are publicly available, and the satellite can be tasked upon request (OHBI, 2022; ESA, 2012; Jacob et al., 2022).

### S2.7. Sentinel-2

The two-satellite Sentinel-2 constellation consists of Sentinel 2A, launched June 23rd, 2015, and Sentinel 2B, launched March 7, 2017 as part of the European Union's Copernicus program (ESA, 2017). The satellites operate in the same 10-day polar orbit offset by 180°, resulting in 5-day revisit times at the equator, falling to 2-3 days at mid-latitudes. Each satellite collects data for all inhabited areas of the world each orbit with a 290 km swath with thirteen spectral bands in the SWIR and VNIR ranges. This includes four bands at 10 m resolution, six bands at 20m

resolution (including Band 12 at 2190 nm in the SWIR range at 200 nm spectral resolution), and three bands at 60m resolution (ESA, 2015; Jacob et al., 2022). All data from Sentinel-2 are publicly available at (ESA, 2021a).

Due to a miscommunication, Stanford did not conduct releases for 17 of the 23 Sentinel-2 overpasses during the study period. These data points are excluded from all analysis. Teams had access to the imagery collected during those overpasses, but would not necessarily know whether we were conducting releases at those times.

### S2.8. WorldView-3

Launched August 13th, 2014, the WorldView-3 satellite is owned and operated by United States-based company Maxar. This multispectral instrument measures in one panchromatic band, eight multispectral bands in the visible near infrared range, eight SWIR bands (1195-2365 nm at 50 nm spectral resolution), and twelve bands covering clouds, aerosols, vapors, ice, and snow. This targeted instrument has an 13.1 km swath, 3.7x3.7 m spatial resolution, and a 1-day revisit frequency and a repetition cycle of 4.5 days at 20° off-nadir for maximum resolution (ESA, 2022b; Jacob et al., 2022).

WorldView-3 operates commercially. Researchers may submit proposals to access data archives and request satellite tasking (ESA, 2022d).

### S2.9. Ziyuan 1

Ziyuan 1-02E (ZY1) Advanced Hyperspectral Imager satellite is the latest in a series of ZY1 satellites launched by the Chinese government on December 26th, 2021 (Song et al., 2022). This targeted hyperspectral instrument uses 76 visible and near infrared bands at 10 nm spectral resolution, with 90 short-wave infrared bands at 20 nm spectral resolution, both with a 60 km swath and 30 m pixels (Song et al., 2022). Based on the satellite overpass dates submitted by NJU for the testing period, October 20th, 21st, 23rd, 26th, and 27th, it appears that ZY1 is capable of revisiting a location as frequently as every day. Data from ZY1 can be made available upon request from the relevant government agencies.

### S2.10. Data submission timeline

Table S1. Data submission timeline by stage for each team. Includes the dates at which 1) teams submitted fully blind Stage 1 results, 2) teams received unblinded in situ wind data from the on-site 10 m ultrasonic anemometer, and 3) teams submitted Stage 2 results using in situ wind measurements. All teams were provided with satellite data as the Stanford team received it. In some instances, providing data to the Stanford team, with the final spectral data arriving February 15th, 2023. This data availability delay introduced additional latency into Stage 1 submission that was beyond teams' control.

| Operator | Submitted Stage 1 | Received Wind Data | Submitted Stage 2 |
|---|---|---|---|
| GHGSat | 5-Feb-23 | 23-Feb-23 | 2-Mar-23 |
| Kayrros | 2-Mar-23 | 3-Mar-23 | 7-Mar-23 |
| LARS | 2-Mar-23 | 2-Mar-23 | 3-Mar-23 |
| Maxar | 1-Mar-23 | 3-Mar-23 | 6-Mar-23 |
| NJU | 2-Mar-23 | 2-Mar-23 | 7-Mar-23 |
| Orbio Earth | 16-Feb-23 | 23-Feb-23 | 6-Mar-23 |

# S3. Participating teams

*This section is adapted in part, with permission, from (Sherwin et al., 2023).*

Six teams participated in this single-blind study, each using data from a subset of the nine participating satellites.

We invited all teams of which we were aware that estimate methane emissions from any of the nine participating satellites. Teams that declined to participate are listed at the end.

Each team was given the option to produce methane retrievals for up to five participating satellites. GHGSat was the only company with access to data from GHGSat C satellites and was thus the only team able to produce an estimate from that satellite, as shown in Table S1.

Table S1. Satellites (columns) analyzed by each team (rows). The final column is the reported source for 10 m wind data for fully blind estimates.

| Team | GHGSat | Kayrros | LARS | Maxar | NJU | Orbio Earth |
|---|---|---|---|---|---|---|
| EnMAP | | X | X | X | X | |
| GF5 | | X | X | | X | |
| GHGSat C | X | | | | | |
| HJ2 | | | X | | X | |
| Landsat | | X | | X | X | |
| PRISMA | | X | X | X | X | |
| Sentinel-2 | X | X | | X | X | X |
| WorldView-3 | | X | X | X | X | |
| ZY1 | | X | X | | X | |
| Wind source | GEOS-FP | ECMWF ERA5, HRRR | ECMWF ERA5, GEOS-FP | Wunderground.com, Windy.com | GEOS-FP | GEOS-FP |

In fully blind stage 1 estimates, most teams used wind reanalysis data from NASA Goddard Earth Observing System-Fast Processing (NASA GEOS-FP) at 10 m, Fifth generation European Centre for Medium-Range Weather Forecasts Atmospheric Reanalysis of the global climate (ECMWF ERA5), or both (NASA, 2021; ECMWF, 2022). Kayrros supplemented ECMWF ERA5 data with the National Oceanographic and Atmospheric Administration (NOAA) High Resolution Rapid Refresh (HRRR) reanalysis product, which focuses on the United States (NOAA, 2022). Maxar used data from Wunderground.com for the Phoenix Sky Harbor airport for most estimates, with WorldView-3 estimates averaging wind speed data from Windy.com for the three weather stations nearest the test site, Casa Grande Municipal Airport, FW1331 Casa Grande, and FW9639 Casa Grande.

See Performer Information spreadsheets in the data and code repository for additional detail on the wind speed used by each team.

### S3.1. GHGSat

GHGSat is a private company, based in Canada, specializing in remote sensing of greenhouse gas emissions. GHGSat owns a constellation of satellites, currently including GHGSat D as well as the more recent GHGSat C1-C8 instruments, with further satellites scheduled for launch in coming years (CEOS, 2018). GHGSat also submitted estimates for Sentinel-2.

Firmware installed on the instruments was as follows:
GHGSat C2 Firmware version: 10.9.3-gb41c76f
GHGSat C2 Observation script: N251A98E.GSB
GHGSat C3+ Firmware version: 10.29.0
GHGSat C3+ Observation script for: NE36DDC3.GSB

Methane retrievals were then conducted using toolchain version 9.8.0, via the ghg-ops-srr

v0.11.1 source rate retrieval algorithm. See the "Performer Info" tab of the GHGSat reported data spreadsheet, included in the data and code repository, for further detail.

### S3.2. Kayrros

Kayrros is a private company specializing in reanalysis of public and private satellite data, with a major area of focus in remote sensing of methane. Kayrros produced estimates for all satellites except GHGSat C and HJ2.

See the "Performer Info" tab of the Kayrros reported data spreadsheets (available in the data and code repository) for further detail on the approach used in this test.

### S3.3. Land and Atmosphere Remote Sensing group (Universitat Politècnica de València)

Researchers Prof. Luís Guanter, Javier Roger Juan, Dr. Javier Gorroño Viñegla of Universitat Politècnica de València in the Land and Atmosphere Remote Sensing (LARS) group in Spain produced estimates for all satellites except GHGSat C, LandSat, and Sentinel-2.

LARS researchers did not report the details of their retrieval algorithms in this study but did so in other studies. In Irakulis-Loitxate et al., the LARS group used a matched filter-based method for PRISMA, ZY1 retrievals in (Irakulis-Loitxate et al., 2021), and for Sentinel-2 and Landsat 8 retrievals in (Irakulis-Loitxate et al., 2022). In Sánchez-García et al. (Sánchez-García et al., 2022), the LARS group applies a retrieval method derived from (Frankenberg et al., 2016; Varon et al., 2018) to estimate methane emission rates using WorldView-3.

Dr. Gorroño Viñegla submitted fully blinded WorldView-3 quantification estimates after winds had been unblinded to J. Roger Juan. Although Stanford researchers are confident Dr. Gorroño Viñegla did not receive in situ wind measurements before submitting these results, we do not include them in the main analysis for consistency across all teams and to maintain a strict standard for integrity of the blind. We include these results, as well as results using in situ wind submitted after the conclusion of the blind, in the SI, Section S4 with appropriate caveats. The fact that results submitted using in situ wind differ substantially from initial blinded results further points to the integrity of fully blinded results.

### S3.4. Maxar

Maxar is a private company based in the United States, both operating and analyzing data from satellites (Hayden and Christy, 2023). In particular, Maxar owns and operates the WorldView-3 satellite, using it and other satellites to, among other things, detect and quantify methane emissions. Maxar submitted estimates for EnMAP, Landsat, PRISMA, Sentinel-2, and WorldView-3. Maxar submitted PRISMA quantification estimates for stage 2 only.

See (Hayden and Christy, 2023) for additional discussion of their approach to methane sensing.

### S3.5. Nanjing University

Researchers Fei Li, Prof. Huilin Chen, and Prof. Yongguang Zhang of Nanjing University in China produced estimates for all satellites except GHGSat C.

NJU used an integrated mass enhancement (IME) model to estimate emission rates, multiplying pixel-wise IME by wind speed and dividing that product by the length of the masked plume. See the "Performer Info" tab of the NJU reported data spreadsheets (available in the data and code repository) for further detail on the approach used in this test.

### S3.6. Orbio Earth

Orbio Earth is a Germany-based company focusing on detecting and quantifying methane emissions using satellite data (Orbio, 2023). Orbio Earth submitted estimates for Sentinel-2 only.

According to the "Performer info" sheet of their submitted results, they employ "5 stage multi-spectral reflectance process using adaptations and combinations of peer-reviewed modelling approaches, including but not limited to Varon et al. 2021, Varon et al 2018, Ehret et al 2022, Gorroño et al 2023. Based on creating a prediction of the background reflectance of the site and comparing it to the real reflectance." All submissions used "Model version 16_2" of the Orbio Earth software system.

### S3.7. Harvard University [declined to participate]

Dr. Daniel Varon of Harvard University developed the first method for estimating methane emissions from Sentinel-2 data (Varon et al., 2021). Dr. Varon participated in a previous single-blind test, producing estimates for Sentinel-2 (Sherwin et al., 2023), and declined to participate in this round of testing due to limited availability.

### S3.8. Satelytics [declined to participate]

Satelytics is a multifaceted business intelligence company based in the United States, focused on synthesizing satellite data into actionable insights (Satelytics, 2023). Satelytics offers a methane detection and quantification service based on satellite data and was invited to participate in this test, but declined to do so.

### S3.9. Stichting Ruimte Onderzoek Nederland (SRON) [declined to participate]

SRON is the Dutch government space agency, which has a significant focus on remote sensing of methane emissions. In a previous single-blind test, Dr. Sudhanshu Pandey produced estimates for Sentinel-2 and Landsat 8 on behalf of SRON (Sherwin et al., 2023). SRON declined to participate in this round of testing due to personnel limitations.

# S4. Supplementary results

## S4.1. Supplementary regression results

*Parts of this section are adapted with permission from (Sherwin et al., 2023).*

To estimate the overall quantification accuracy, goodness of fit, and error distribution of all quantified methane emission estimates, we apply a linear regression. For reasons described in (Sherwin et al., 2023), we fix the $y$-intercept at zero in the regression, shown in Eq. (1).

$$y = \beta x \quad (1)$$

Where $x$ is the mean metered emission rate, and y is the central emissions estimate provided by participating teams. These $x$ and $y$ values correspond to the markers in Figure 4.

The regression only includes quantified emissions, and does not include emissions that were not detected. We do this to assess the error distribution of detected emissions.

Table S2. Regression results for stages 1 and 2 based on the fixed-intercept ordinary least squares regression in Eq. (1). Maxar submitted quantification estimates for PRISMA in stage 2 only, adding two true positive data points to the stage 2 regression results.

| | Stage 1 | Stage 2 |
|---|---|---|
| *B* | 1.139 [0.832, 1.446] | 1.248 [1.037, 1.459] |
| Standard error | 0.152 | 0.105 |
| t-statistic | 7.502 | 11.937 |
| No. Observations | 41 | 43 |
| Degrees of freedom (Residuals) | 40 | 42 |
| Degrees of freedom (Model) | 1 | 1 |
| Uncentered $R^2$ | 0.585 | 0.772 |
| Centered $R^2$ | 0.574 | 0.767 |
| F-statistic | 56.3 | 142.5 |

$R^2$ values are presented in uncentered format, which is standard for regression specifications without a y-intercept term. As a result, these $R^2$ values are not directly comparable with the centered $R^2$ values produced in regressions with a y-intercept. Centered $R^2$ values, directly comparable with $R^2$ values from regressions with a nonzero y-intercept term, are also shown in Table.

Note that these regressions treat each estimate from each team and satellite as independent and identically distributed observations. This aggregation is necessary to produce a meaningful regression due to the small sample size for each satellite and team, but the results of this analysis should be treated as a rough illustration of the general capabilities of the participating satellites and teams as a whole. Detailed characterization of the quantification accuracy from individual satellites and teams will require more data points.

## S4.2. Regression results excluding Maxar

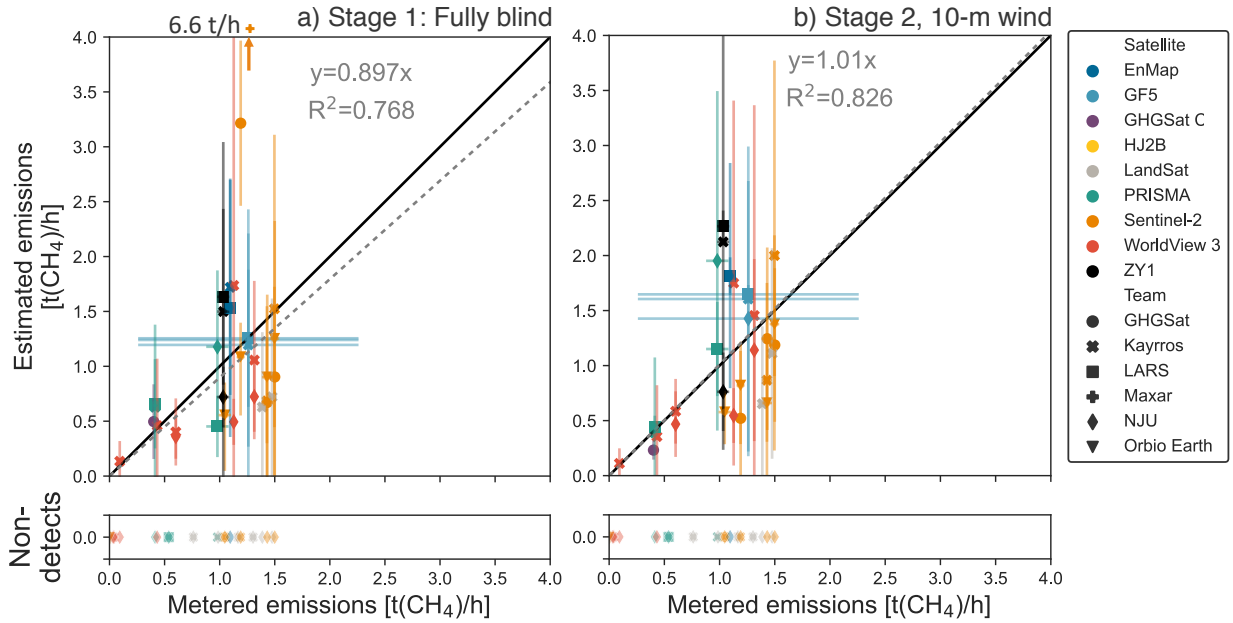


Figure S1. Methane quantification performance by satellite and team, excluding estimates from Maxar, who realized after submission that their estimates were artificially high due to use of a deprecated spectral library. Metered emissions compared with single-blind estimates for each overpass with successfully reported data, with 95% X and Y confidence intervals. a) Fully blind stage 1 results using modeled wind speed estimates. Note one Sentinel-2 estimate exceeds the y-axis limit at 6.6 t($CH_4$)/h. b) Stage 2 results using on-site 10 m wind speed and direction measurements. LARS WorldView-3 quantification estimates are excluded from the main analysis, as stage 1 estimates were submitted after wind data had been unblinded to a member of the LARS team not involved in analyzing WorldView-3 data, while corresponding stage 2 estimates were submitted after release volumes were unblinded. The grey dashed lines represent an ordinary least squares fit with the intercept fixed at zero, with slope and uncentered $R^2$ displayed. The black solid lines denote exact 1:1 agreement. See the SI, Section S4 for satellite- and team-specific results.

## S4.3. Error statistics by satellite and team

Recall in interpreting these results that Maxar concluded after results were unblinded that their results were high by a factor of roughly 2.3 due to use of a deprecated spectral library (Hayden and Christy, 2023).

Table S3. Stage 1 (fully blind) summary statistics of quantified (non-zero) emissions by satellite, across all teams. Excludes LARS WorldView-3 quantification estimates, consistent with the main analysis, because their Stage 1 results were submitted after winds had been unblinded to a member of the LARS team analyzing other satellites. We report min, mean, max, and standard deviation.

| Stage 1 | | | | | |
|---|---|---|---|---|---|
| | Count | Min | Mean | Max | $\sigma$ |
| EnMAP | 3 | 40% | 55% | 68% | 14% |
| Gaofen 5 | 3 | -5% | -2% | 0% | 2% |
| GHGSat C | 1 | 24% | 24% | 24% | NA |
| Huanjin 2B | 0 | NA | NA | NA | NA |
| LandSat 8/9 | 2 | -55% | -53% | -51% | 3% |
| PRISMA | 4 | -54% | 19% | 59% | 52% |
| Sentinel-2 | 11 | -53% | 38% | 456% | 153% |
| WorldView-3 | 14 | -56% | 33% | 192% | 74% |
| Ziyuan 1 | 6 | -30% | 39% | 131% | 58% |

Table S4. Stage 2 (with 10 m in situ wind measurements) summary statistics of quantified (non-zero) emissions by satellite, across all teams. Excludes LARS WorldView-3 quantification estimates, consistent with the main analysis. Maxar submitted PRISMA quantification estimates in stage 2 only.

| Stage 2 | | | | | |
|---|---|---|---|---|---|
| | Count | Min | Mean | Max | $\sigma$ |
| EnMAP | 3 | 65% | 75% | 93% | 16% |
| Gaofen 5 | 3 | 13% | 24% | 31% | 9% |
| GHGSat C | 1 | -42% | -42% | -42% | NA |
| Huanjin 2B | 0 | NA | NA | NA | NA |
| LandSat 8/9 | 2 | -53% | -39% | -25% | 20% |
| PRISMA | 6 | -24% | 46% | 181% | 79% |
| Sentinel-2 | 11 | -56% | 4% | 193% | 76% |
| WorldView-3 | 14 | -52% | 40% | 140% | 67% |
| Ziyuan 1 | 6 | -51% | 35% | 119% | 70% |

Table S5. Stage 1 (fully blind) summary statistics of quantified (non-zero) emissions by team, across all satellites.

| Stage 1 | | | | | |
|---|---|---|---|---|---|
| | Count | Min | Mean | Max | $\sigma$ |
| GHGSat | 4 | -53% | 25% | 170% | 102% |
| Kayrros | 14 | -55% | 13% | 131% | 54% |
| LARS | 6 | -54% | 24% | 59% | 44% |
| Maxar | 11 | -14% | 125% | 456% | 136% |
| NJU | 7 | -56% | -24% | 20% | 27% |
| Orbio Earth | 4 | -47% | -27% | -9% | 18% |

Table S6. Stage 2 (with 10 m in situ wind measurements) summary statistics of quantified (non-zero) emissions by team, across all satellites.

| Stage 2 | | | | | |
|---|---|---|---|---|---|
| | Count | Min | Mean | Max | $\sigma$ |
| GHGSat | 4 | -56% | -33% | -13% | 20% |
| Kayrros | 14 | -53% | 16% | 106% | 44% |
| LARS | 6 | 8% | 42% | 119% | 43% |
| Maxar | 11 | -24% | 101% | 193% | 69% |
| NJU | 7 | -52% | -7% | 99% | 52% |
| Orbio Earth | 4 | -54% | -34% | -8% | 20% |

## S4.4. Aggregate error statistics

Table S7. Summary statistics of the percent error of estimated emission rates, as well as stage 1 wind speed error. Compares central estimates with 5-minute mean measured emissions. Note that although the standard deviation of the percent error distribution falls slightly after wind unblinding in stage 2, the inter-quartile range between the 25$^{th}$ and 75$^{th}$ percentiles (P25 and P75, respectively) of the error distribution is larger in stage 2. Includes results excluding Maxar submissions both because Maxar concluded after results were unblinded that their results were high by a factor of two due to use of a deprecated spectral library (Hayden and Christy, 2023) and because Maxar submitted only stage 2 estimates for PRISMA.

| **Metric** | **Stage 1 (fully blind)** | **Stage 2 (measured wind)** | **Stage 1 (exclude Maxar)** | **Stage 2 (exclude Maxar)** | **Wind speed** |
|---|---|---|---|---|---|
| **Mean** | 29% | 27% | 4% | 4% | 18% |
| **Standard deviation** | 90% | 67% | 54% | 47% | 156% |
| **Min** | -56% | -56% | -56% | -56% | -87% |
| **P25** | -34% | -24% | -40% | -29% | -49% |
| **P50 (median)** | 4% | 12% | -5% | -6% | -36% |
| **P75** | 55% | 66% | 44% | 29% | -10% |
| **Max** | 456% | 193% | 170% | 119% | 645% |
| **Inter-quartile range (P75-P25)** | 89% | 90% | 84% | 58% | 39% |

## S4.5. Detection summary

Table S8. Detection results by satellite and team. A tabular representation of Figure 2. Note that measurements for which Stanford filtered for all teams were excluded from Figure 2 but are included here in the # Stan. Filtered column.

| Satellite/ Team | # True positive | # False negative | # True negative | # False positive | # Op. filtered | # Stan. Filtered | # Not tasked | Total |
|---|---|---|---|---|---|---|---|---|
| EnMap/ Kayrros | 1 | 0 | 4 | 0 | 0 | 0 | 0 | 5 |
| EnMap/ LARS | 1 | 0 | 1 | 0 | 0 | 3 | 0 | 5 |
| EnMap/ MAXAR | 1 | 0 | 1 | 0 | 0 | 3 | 0 | 5 |
| EnMap/ NJU | 0 | 1 | 1 | 0 | 0 | 3 | 0 | 5 |
| GF5/ Kayrros | 1 | 0 | 0 | 0 | 0 | 1* | 0 | 2 |
| GF5/ LARS | 1 | 0 | 0 | 0 | 0 | 1* | 0 | 2 |
| GF5/ NJU | 1 | 0 | 0 | 0 | 0 | 1* | 0 | 2 |
| GHGSat C/ GHGSat | 1 | 0 | 1 | 0 | 3 | 2* | 5 | 12 |
| HJ2B/ LARS | 0 | 0 | 1 | 0 | 0 | 0 | 0 | 1 |
| HJ2B/ NJU | 0 | 0 | 1 | 0 | 0 | 0 | 0 | 1 |
| LandSat/ Kayrros | 2 | 4 | 2 | 0 | 0 | 4* | 0 | 12 |
| LandSat/ MAXAR | 0 | 6 | 2 | 0 | 0 | 4* | 0 | 12 |
| LandSat/ NJU | 0 | 6 | 2 | 0 | 0 | 4* | 0 | 12 |
| PRISMA/ Kayrros | 1 | 2 | 2 | 0 | 0 | 3* | 2 | 10 |
| PRISMA/ LARS | 2 | 1 | 2 | 0 | 0 | 3* | 2 | 10 |
| PRISMA/ MAXAR | 2 | 1 | 2 | 0 | 0 | 3* | 2 | 10 |
| PRISMA/ NJU | 1 | 2 | 2 | 0 | 0 | 3* | 2 | 10 |
| Sentinel-2/ GHGSat | 3 | 1 | 2 | 0 | 0 | 17* | 0 | 8 |
| Sentinel-2/ Kayrros | 2 | 2 | 2 | 0 | 0 | 17* | 0 | 8 |

| | | | | | | | | |
|---|---|---|---|---|---|---|---|---|
| Sentinel-2/ MAXAR | 2 | 2 | 2 | 0 | 0 | 17* | 0 | 8 |
| Sentinel-2/ NJU | 0 | 4 | 2 | 0 | 0 | 17* | 0 | 8 |
| Sentinel-2/ Orbio Earth | 4 | 0 | 2 | 0 | 0 | 17* | 0 | 8 |
| WorldView-3/Kayrros | 5 | 2 | 0 | 0 | 0 | 3* | 0 | 10 |
| WorldView-3/LARS | 3 | 2 | 0 | 0 | 2 | 3* | 0 | 10 |
| WorldView-3/MAXAR | 6 | 1 | 0 | 0 | 0 | 3* | 0 | 10 |
| WorldView-3/NJU | 3 | 4 | 0 | 0 | 0 | 3* | 0 | 10 |
| ZY1/ Kayrros | 1 | 0 | 0 | 0 | 0 | 3* | 0 | 4 |
| ZY1/ LARS | 1 | 0 | 0 | 0 | 0 | 3* | 0 | 4 |
| ZY1/ NJU | 1 | 0 | 0 | 0 | 0 | 3* | 0 | 4 |
| Total | 46 | 41 | 34 | 0 | 5 | 144 | 13 | 283 |

* These measurements were filtered for all teams and not included in Figure 2.

Table S9. Ground truth for detection by satellite. Includes the count of non-zero emissions as well as zero-emission controls given to each satellite for all measurements (all instances in which the satellite passed overhead), not including data points excluded by Stanford for all teams, including overpasses in which the satellite was not tasked.

| Satellite | # Non-zero | # Zero |
|---|---|---|
| EnMAP | 4 | 1 |
| Gaofen 5 | 1 | 0 |
| GHGSat C | 9 | 1 |
| Huanjin 2B | 0 | 1 |
| LandSat 8/9 | 7 | 3 |
| PRISMA | 4 | 3 |
| Sentinel-2 | 4 | 2 |
| WorldView-3 | 7 | 0 |
| Ziyuan 1 | 1 | 0 |
| Total | 37 | 11 |

## S4.6. Supplementary figures

Underlying data and code to reproduce these figures are available in the data and code repository for this paper, particularly in "Satellite_results_consolidated_clean_20230627.csv".

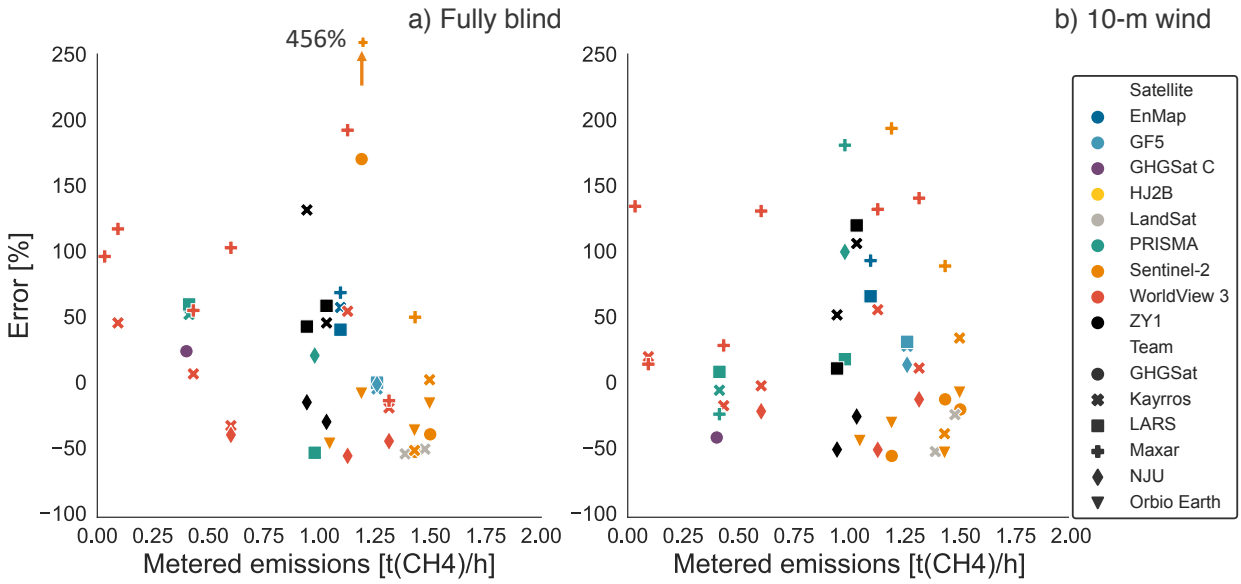


Figure S2. Percent error for Stage 1 (fully blind) and Stage 2 (with measured 10 m wind speed and direction).

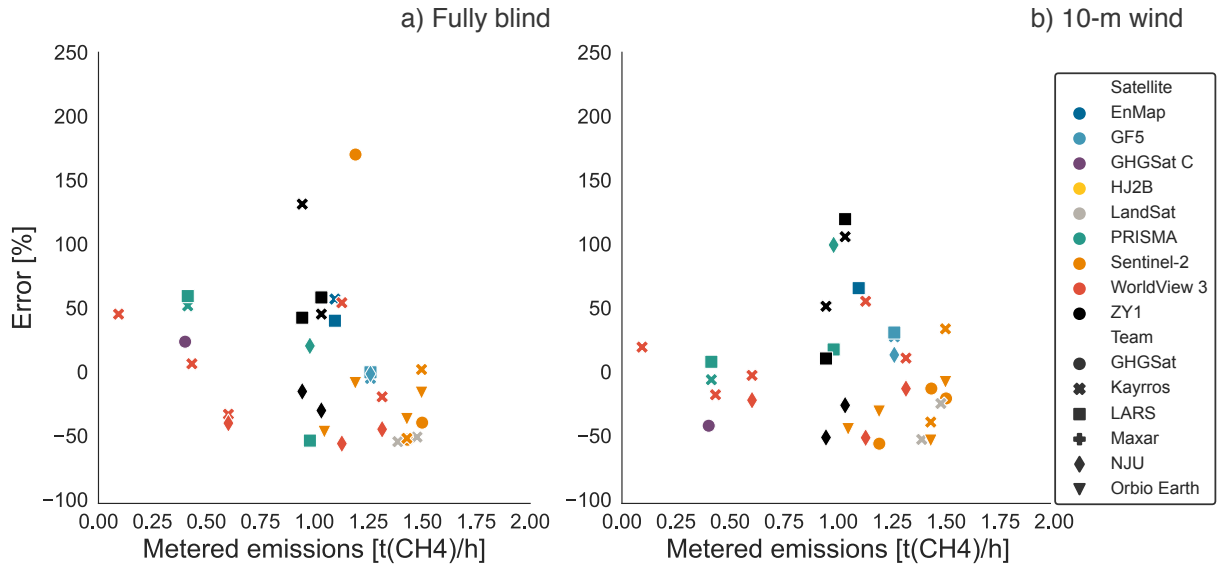


Figure S3. Percent error excluding Maxar estimates, which Maxar now believes were artificially high by a factor of 2.3 (Hayden and Christy, 2023). Stage 1 (fully blind) and Stage 2 (with measured 10 m wind speed and direction).

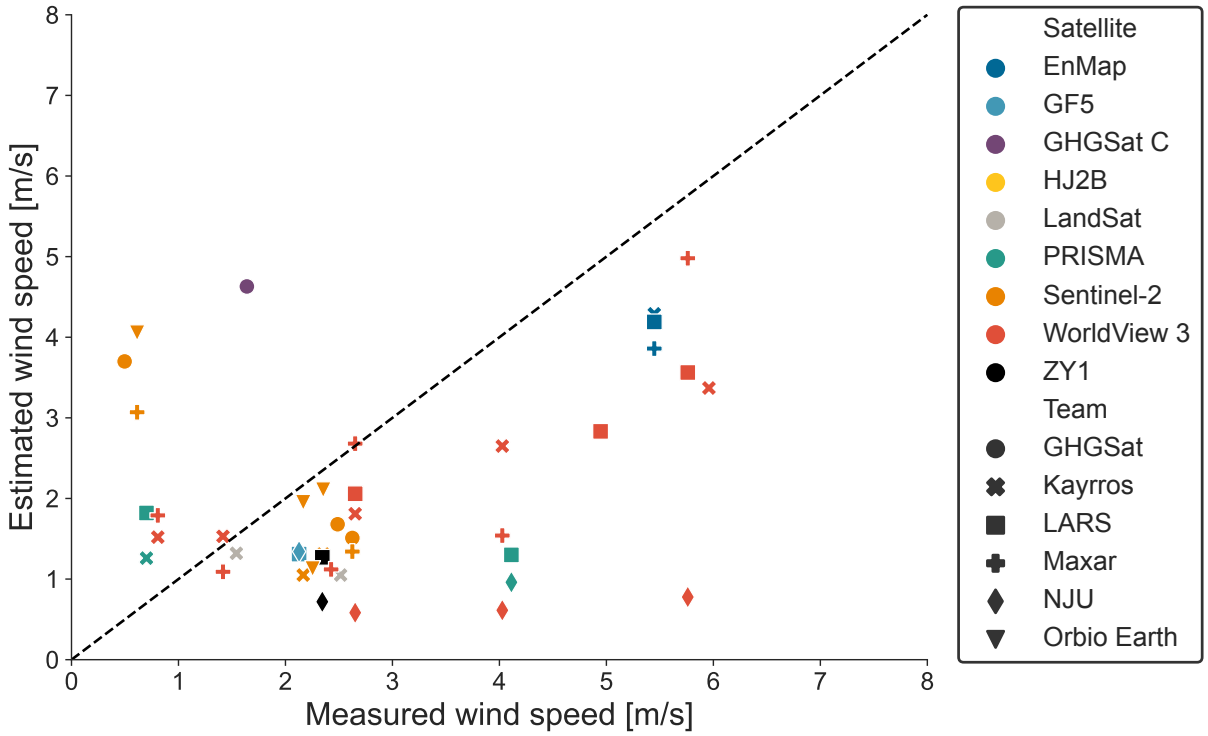


Figure S4. Parity chart of wind speed estimates used by teams in Stage 1 compared with 5-minute averages from the 10 m ultrasonic anemometer. Only includes wind speeds for nonzero quantified emissions that passed Stanford and operator quality control. The black dashed line denotes exact 1:1 agreement.

### S4.6.1. Team-specific results

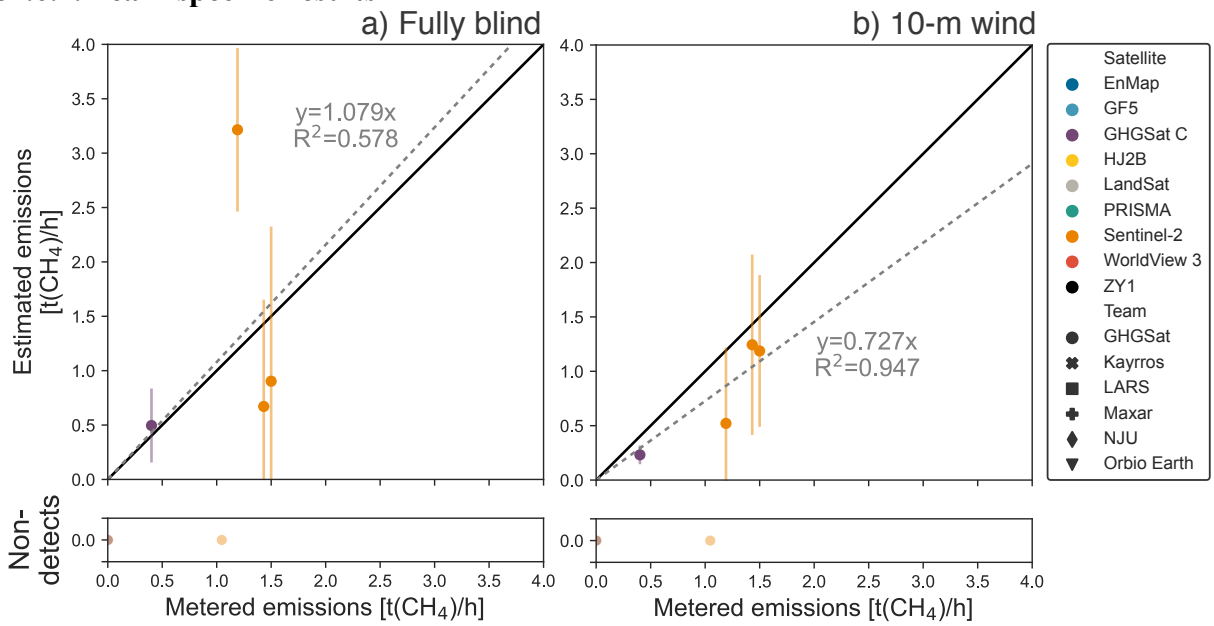


Figure S5. Quantification performance for GHGSat across all satellites, with 95% X and Y confidence intervals. a) presents fully blinded results, while in b) were produced using 10 m in situ wind measurements. The black solid line denotes exact 1:1 agreement. Fitted slope and uncentered $R^2$ shown for an ordinary least squares fit with the intercept fixed at zero (gray dashed line).

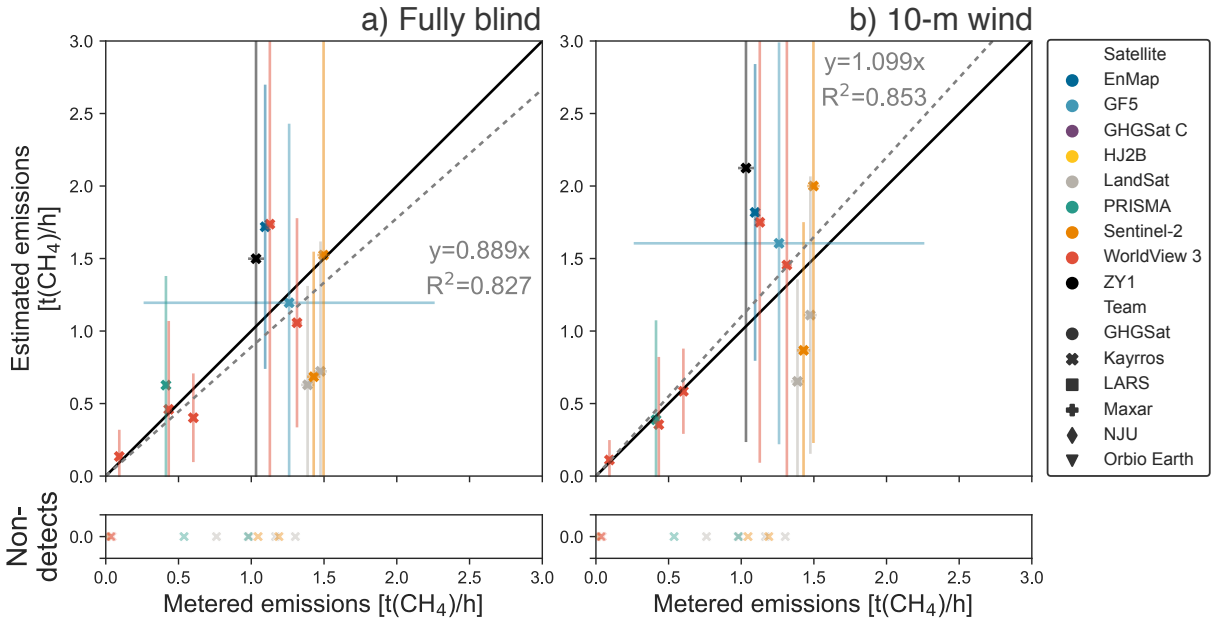


Figure S6. Quantification performance for Kayrros across all satellites, with 95% X and Y confidence intervals. a) presents fully blinded results, while in b) were produced using 10 m in situ wind measurements. The black solid line denotes exact 1:1 agreement. Fitted slope and uncentered $R^2$ shown for an ordinary least squares fit with the intercept fixed at zero (gray dashed line).

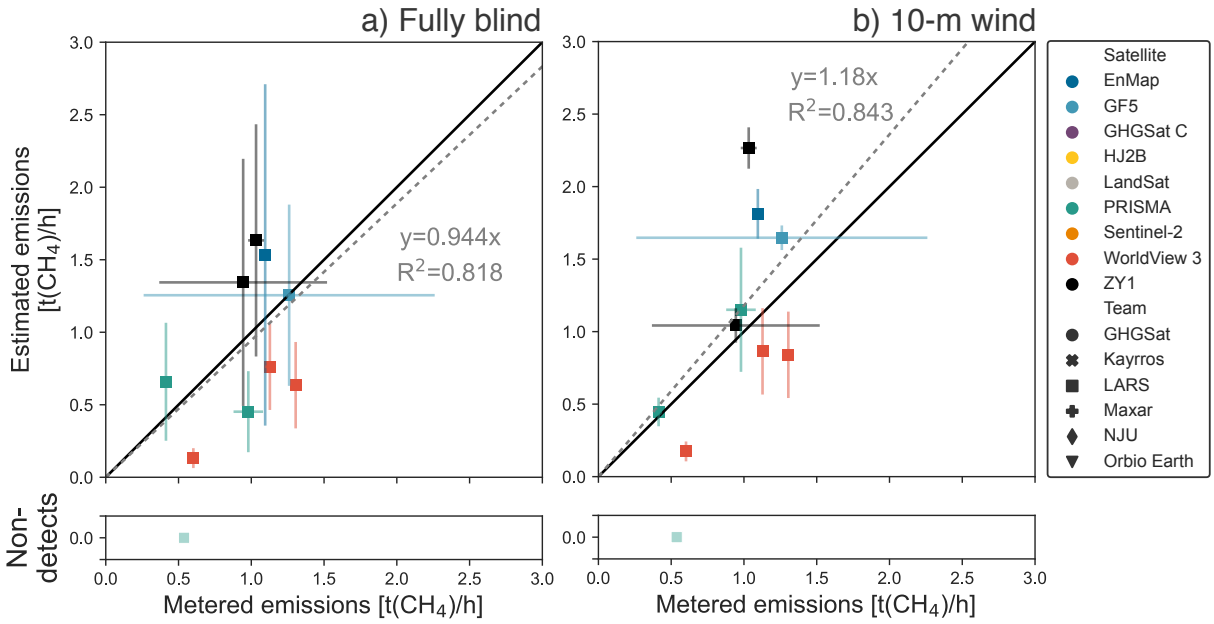


Figure S7. Quantification performance for LARS across all satellites, with 95% X and Y confidence intervals. a) presents fully blinded results, while in b) were produced using 10 m in situ wind measurements. The black solid line denotes exact 1:1 agreement. Fitted slope and uncentered $R^2$ shown for an ordinary least squares fit with the intercept fixed at zero (gray dashed line). Note that LARS researcher Javier Gorroño submitted Stage 1 WorldView 3 estimates after LARS researcher Javier Roger Juan had received unblinded in situ wind data. Javier Gorroño then submitted Stage 2 WorldView 3 estimates, not included in the main manuscript, after release volumes were unblinded. Although Stanford researchers believe LARS WorldView 3 estimates did not use the ground truth wind data for their Stage 1 estimates or the metered volumes for their Stage 2 estimates, we include them only in the SI to maintain strict adherence to our experimental design.

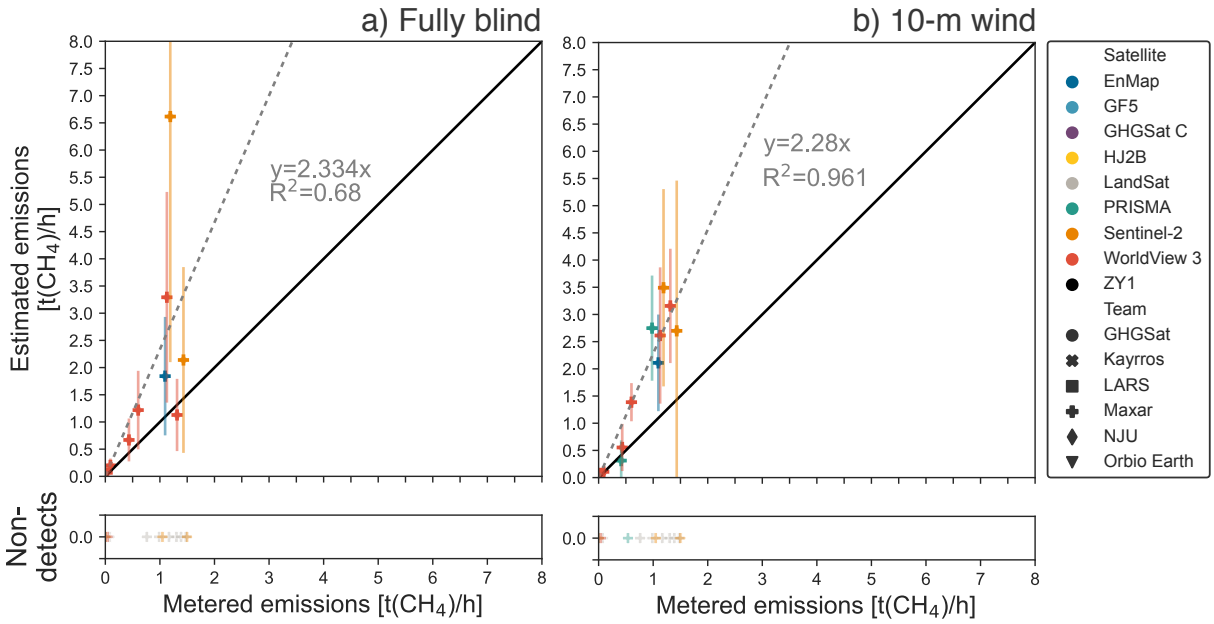


Figure S8. Quantification performance for Maxar across all satellites, with 95% X and Y confidence intervals. a) presents fully blinded results, while in b) were produced using 10 m in situ wind measurements. The black solid line denotes exact 1:1 agreement. Fitted slope and uncentered $R^2$ shown for an ordinary least squares fit with the intercept fixed at zero (gray dashed line). Note that Maxar concluded after results were unblinded that their results were high by a factor of 2.3 due to use of a deprecated spectral library (Hayden and Christy, 2023).

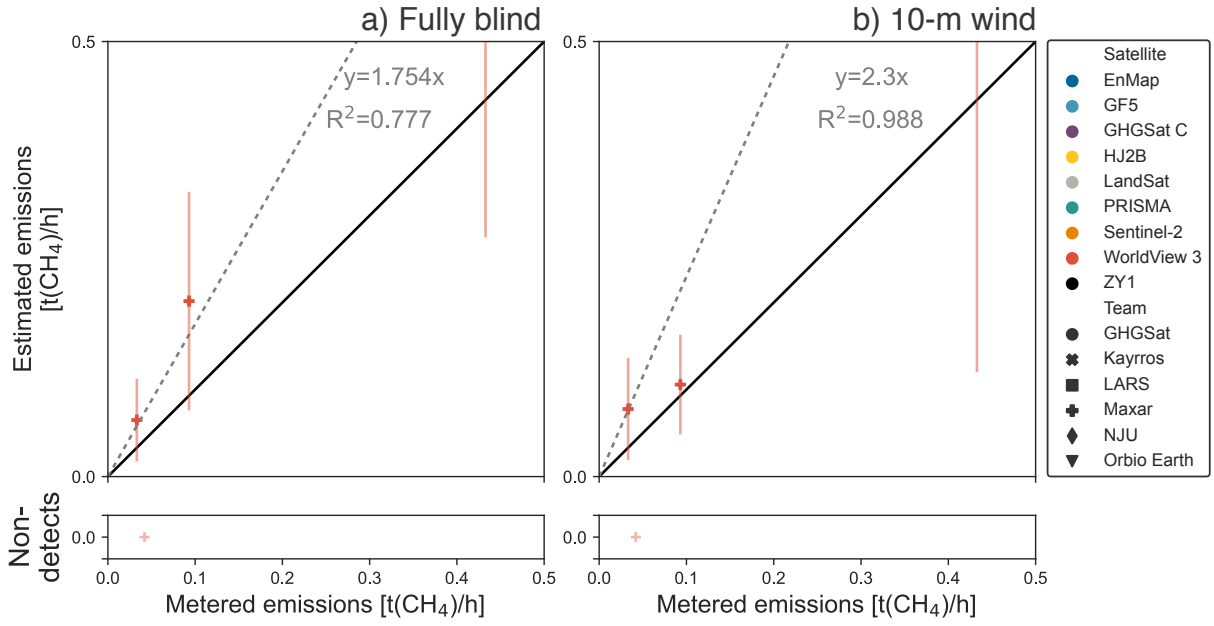


Figure S9 Quantification performance for Maxar for WorldView-3 showing only 0.5 t/h or less. Error bars represent 95% X and Y confidence intervals. a) presents fully blinded results, while in b) were produced using 10 m in situ wind measurements. The black solid line denotes exact 1:1 agreement. Fitted slope and uncentered $R^2$ shown for an ordinary least squares fit with the intercept fixed at zero (gray dashed line).

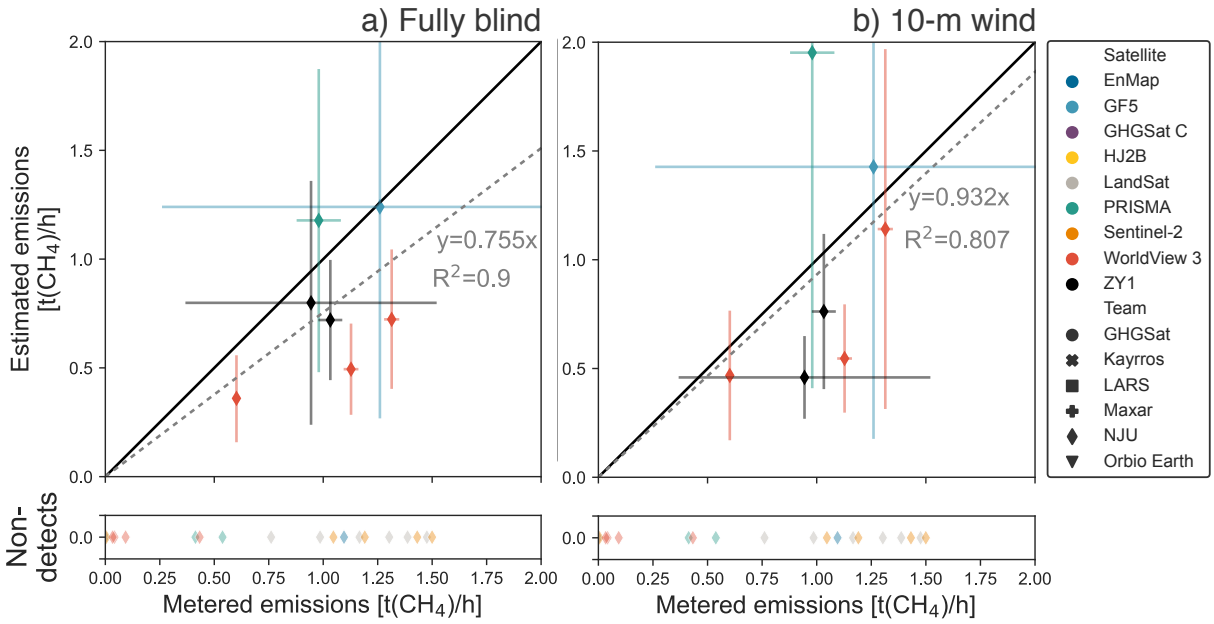


Figure S10. Quantification performance for NJU across all satellites, with 95% X and Y confidence intervals. a) presents fully blinded results, while in b) were produced using 10 m in situ wind measurements. The black solid line denotes exact 1:1 agreement. Fitted slope and uncentered $R^2$ shown for an ordinary least squares fit with the intercept fixed at zero (gray dashed line).

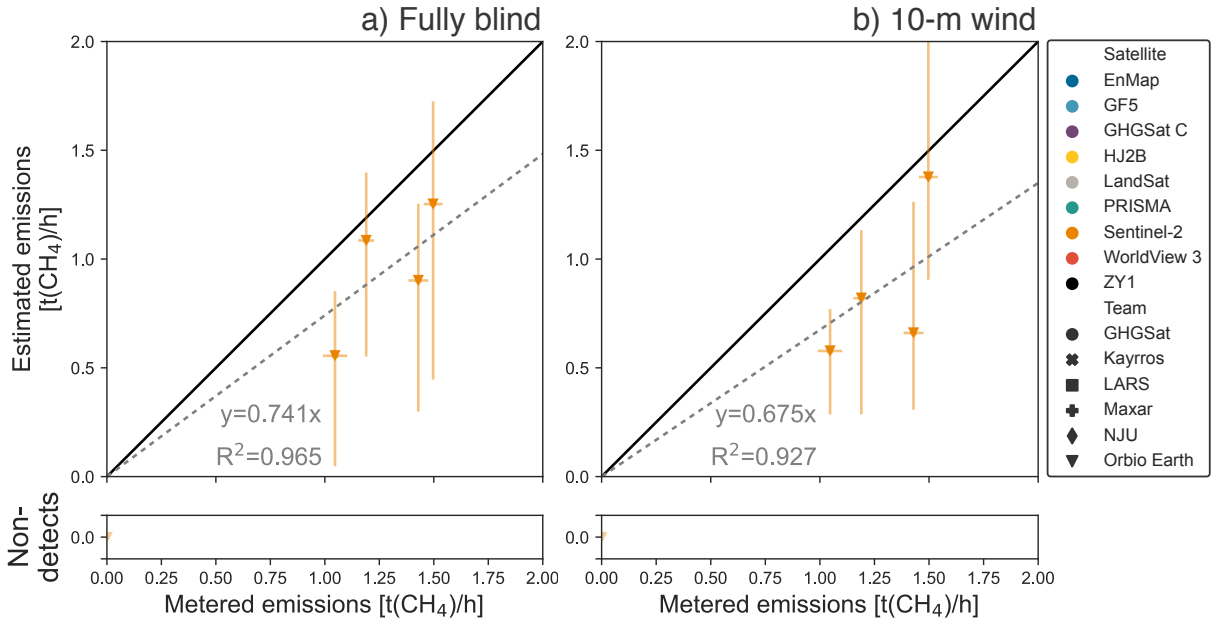


Figure S11. Quantification performance for Orbio Earth across all satellites, with 95% X and Y confidence intervals. a) presents fully blinded results, while in b) were produced using 10 m in situ wind measurements. The black solid line denotes exact 1:1 agreement. Fitted slope and uncentered $R^2$ shown for an ordinary least squares fit with the intercept fixed at zero (gray dashed line).

### S4.6.2. Satellite-specific parity charts

Recall that Maxar concluded after results were unblinded that their results were high by a factor of 2.3 due to use of a deprecated spectral library (Hayden and Christy, 2023). This would add upward average bias to all below linear fits that include Maxar estimates.

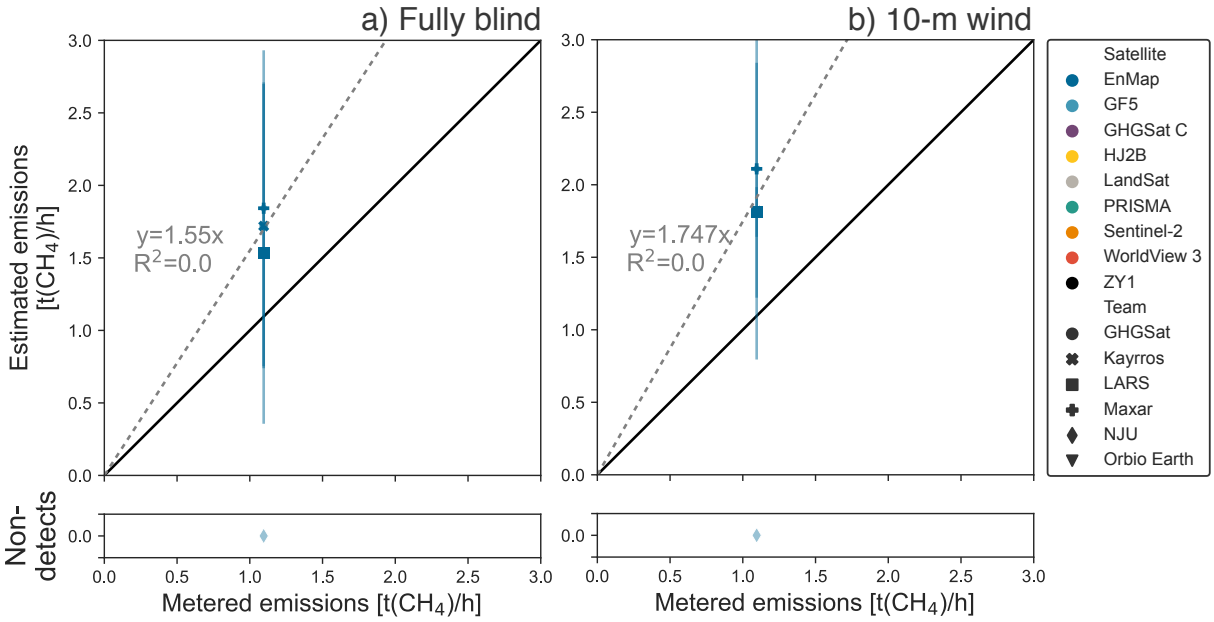


Figure S12. Quantification performance for EnMAP across all teams, with 95% X and Y confidence intervals. The black solid line denotes exact 1:1 agreement. Fitted slope and uncentered $R^2$ shown for an ordinary least squares fit with the intercept fixed at zero (gray dashed line).

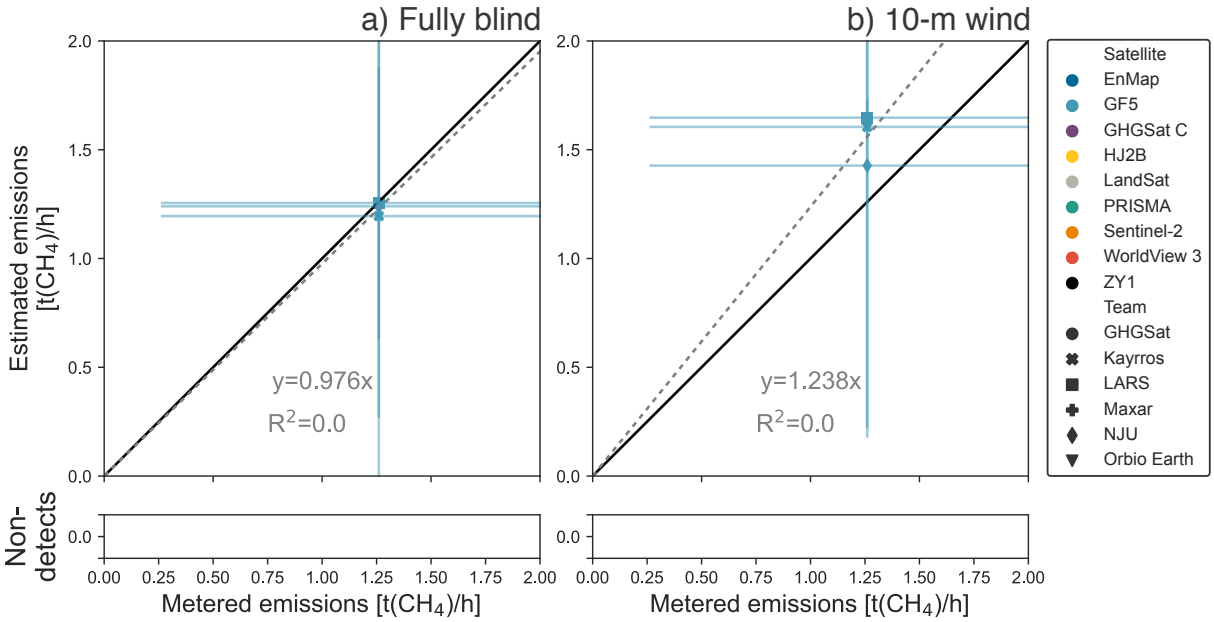


Figure S13. Quantification performance for GF5 across all teams, with 95% X and Y confidence intervals. The black solid line denotes exact 1:1 agreement. Fitted slope and uncentered $R^2$ shown for an ordinary least squares fit with the intercept fixed at zero (gray dashed line). $R^2$ is zero here because all points have an identical x-coordinate.

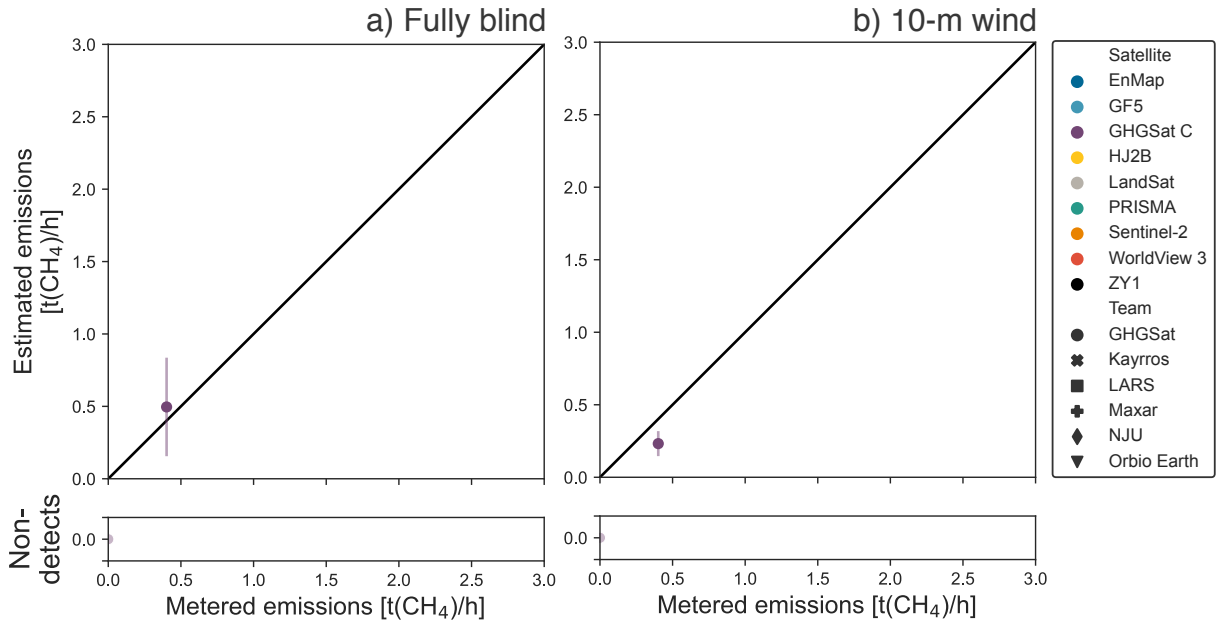


Figure S14. Quantification performance for GHGSat C across all teams, with 95% X and Y confidence intervals. The black solid line denotes exact 1:1 agreement.

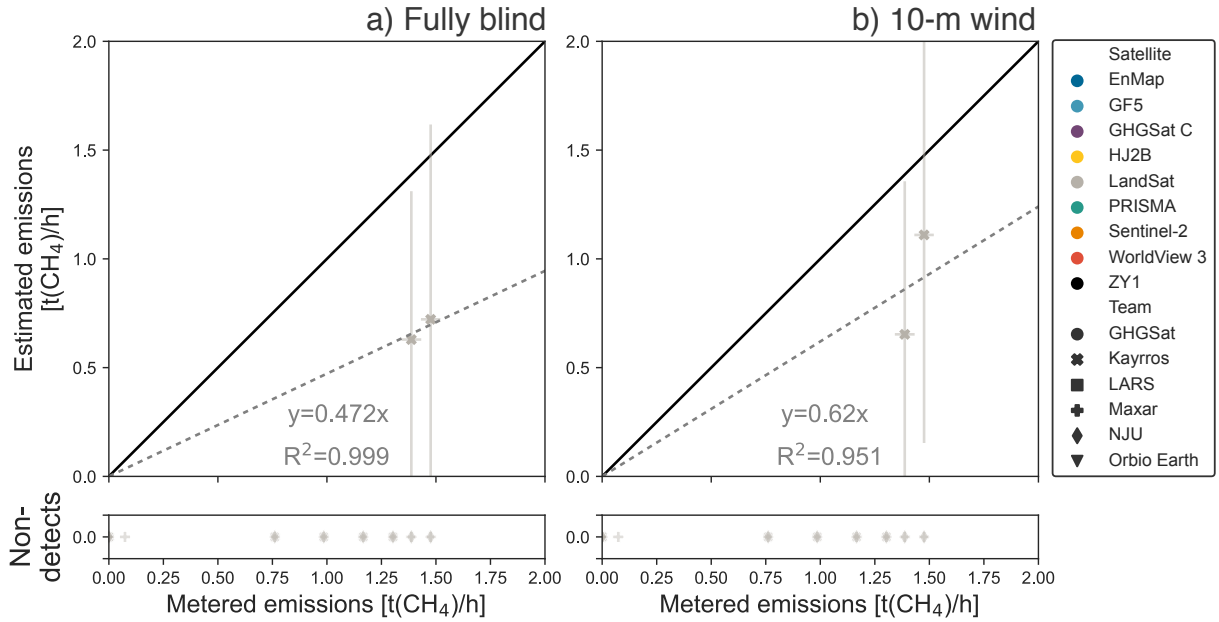


Figure S15. Quantification performance for LandSat 8/9 across all teams, with 95% X and Y confidence intervals. The black solid line denotes exact 1:1 agreement. Fitted slope and uncentered $R^2$ shown for an ordinary least squares fit with the intercept fixed at zero (gray dashed line).

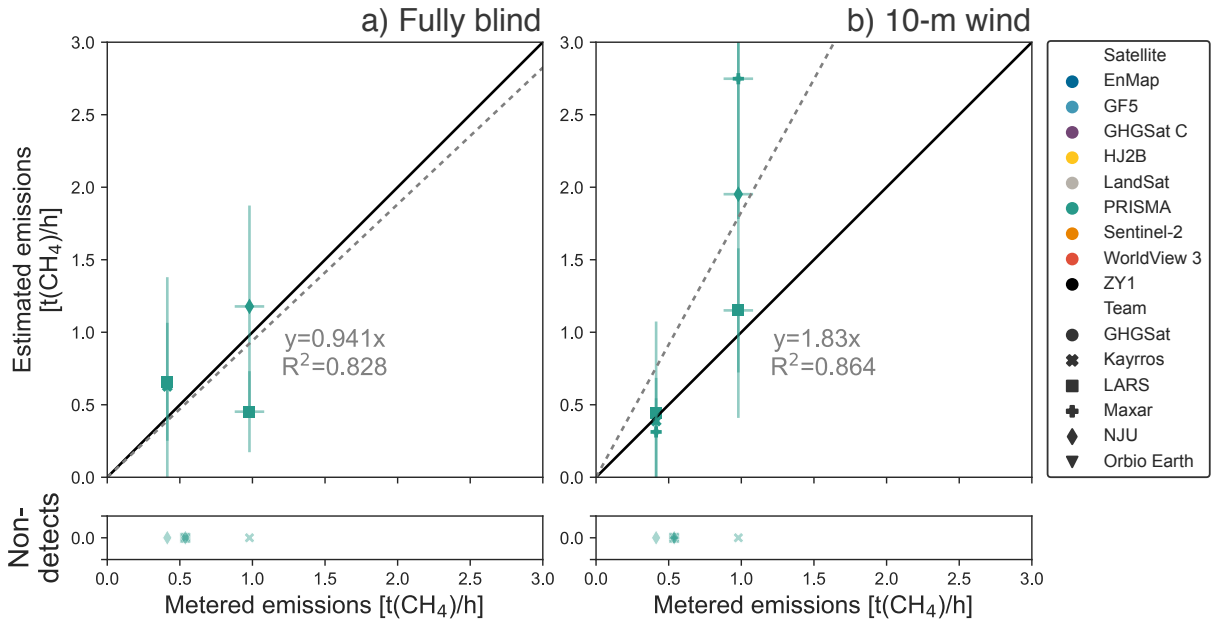


Figure S16. Quantification performance for PRISMA across all teams, with 95% X and Y confidence intervals. The black solid line denotes exact 1:1 agreement. Fitted slope and uncentered $R^2$ shown for an ordinary least squares fit with the intercept fixed at zero (gray dashed line).

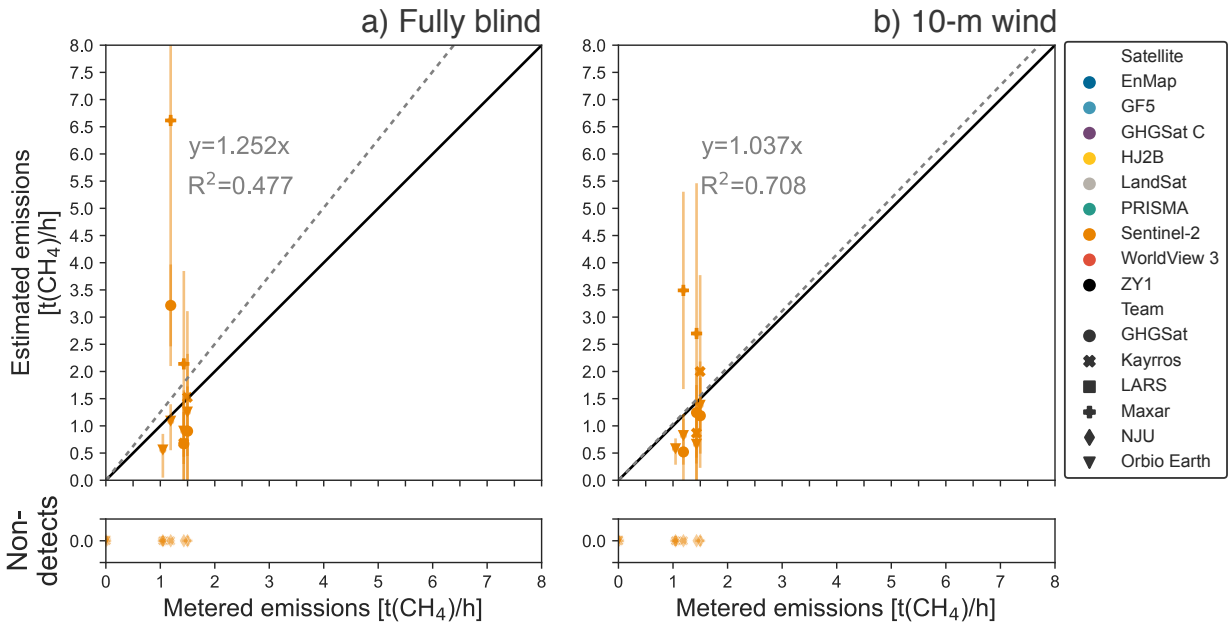


Figure S17. Quantification performance for Sentinel-2 across all teams, with 95% X and Y confidence intervals. The black dashed line denotes exact 1:1 agreement. Fitted slope and uncentered $R^2$ shown for an ordinary least squares fit with the intercept fixed at zero.

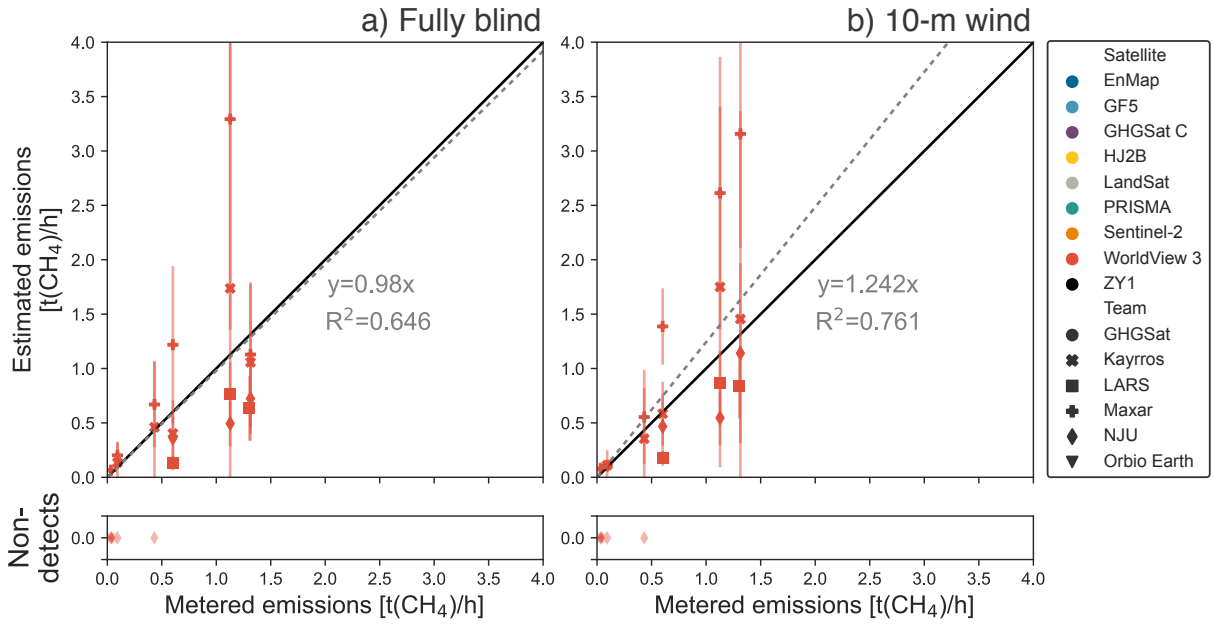


Figure S18. Quantification performance for WorldView-3 across all teams, with 95% X and Y confidence intervals. The black solid line denotes exact 1:1 agreement. Fitted slope and uncentered $R^2$ shown for an ordinary least squares fit with the intercept fixed at zero (gray dashed line). Note that LARS researcher Javier Gorroño submitted Stage 1 WorldView 3 estimates after LARS researcher Javier Roger Juan had received unblinded in situ wind data. Javier Gorroño then submitted Stage 2 WorldView 3 estimates, not included in the main manuscript, after release volumes were unblinded. Although Stanford researchers believe LARS WorldView 3 estimates did not use the ground truth wind data for their Stage 1 estimates or the metered volumes for their Stage 2 estimates, we include them only in the SI to maintain strict adherence to our experimental design.

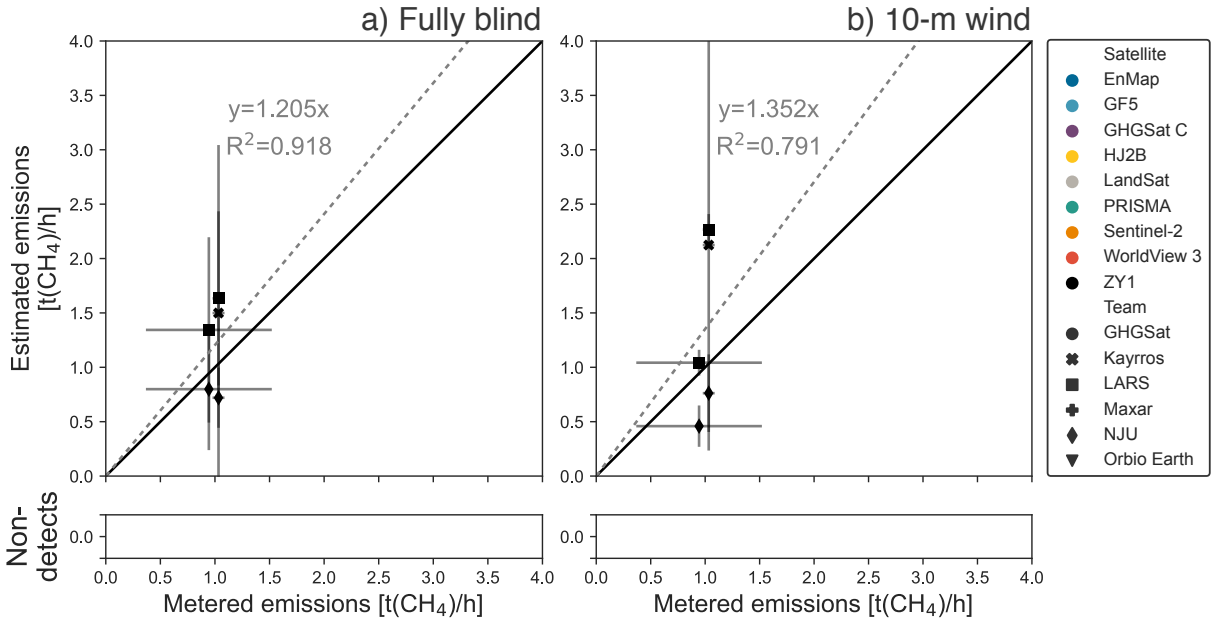


Figure S19. Quantification performance for ZY1 across all teams, with 95% X and Y confidence intervals. The black solid line denotes exact 1:1 agreement. Fitted slope and uncentered $R^2$ shown for an ordinary least squares fit with the intercept fixed at zero (gray dashed line). Includes estimates submitted for the October 20th release, which was filtered in the main analysis due to a system malfunction. See the SI, Section S3.3 for further discussion of this data point.

## S4.7. Retrieval images

The following are masked and unmasked methane retrieval images from each of the participating teams. Masking refers to the process of identifying a methane plume and differentiating its outline from its surroundings. Submitting these images was optional, and not all teams submitted all images for retrievals they conducted. Note the level of variability in unmasked scenes across teams operating with precisely the same spectral data.

### S4.7.1. EnMAP

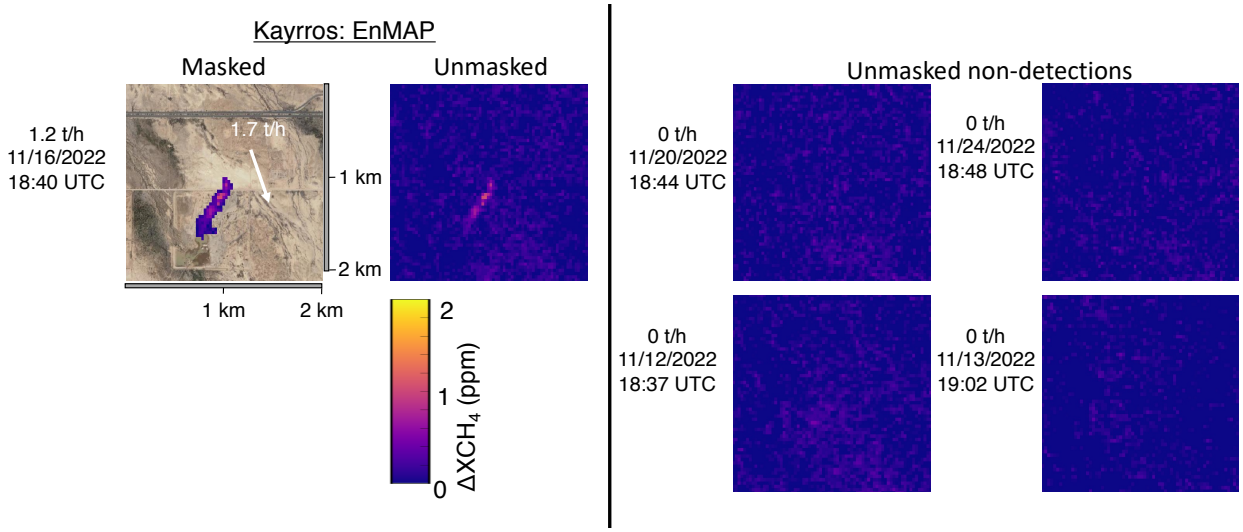


Figure S20. Provided masked and unmasked methane enhancement estimates from Kayrros for EnMAP retrievals. True emission rates and timestamps in black text. For nonzero estimated emissions, mean stage 1 estimated emission rate in white inset text. The white arrow represents 5-minute average measured in situ wind speed. Surface imagery © 2023 Google Earth, CNES/Airbus, Maxar Technologies, USDA/FPAC/GEO.

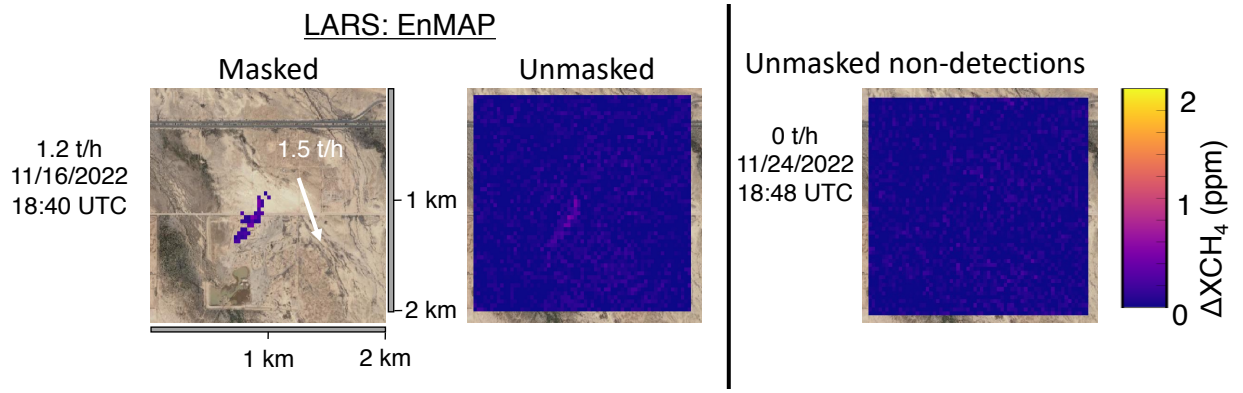


Figure S21. Provided masked and unmasked methane enhancement estimates from LARS for EnMAP retrievals. True emission rates and timestamps in black text. For nonzero estimated emissions, mean estimated emission rate in white inset text. The white arrow represents 5-minute average measured in situ wind speed. Surface imagery © 2023 Google Earth, CNES/Airbus, Maxar Technologies, USDA/FPAC/GEO.

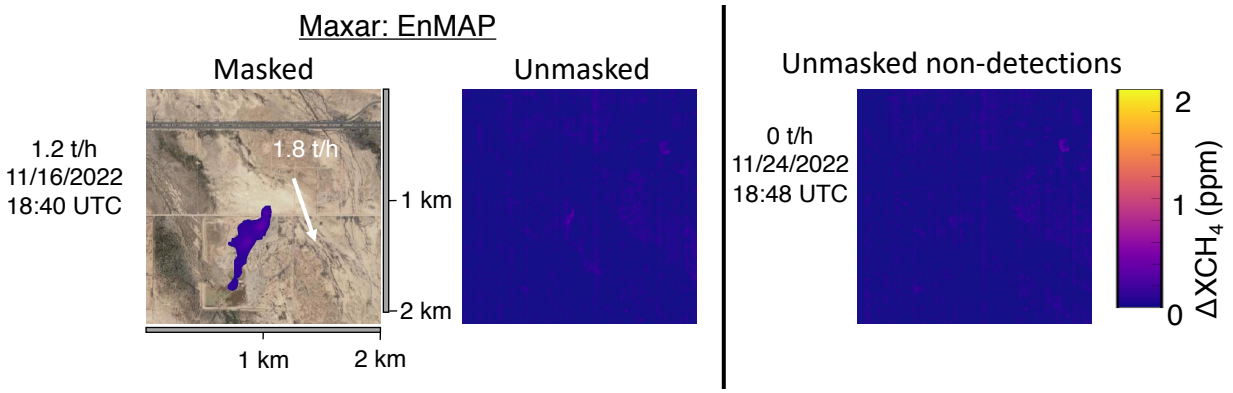


Figure S22. Provided masked and unmasked methane enhancement estimates from Maxar for EnMAP retrievals. True emission rates and timestamps in black text. For nonzero estimated emissions, mean estimated emission rate in white inset text. The white arrow represents 5-minute average measured in situ wind speed. Surface imagery © 2023 Google Earth, CNES/Airbus, Maxar Technologies, USDA/FPAC/GEO.

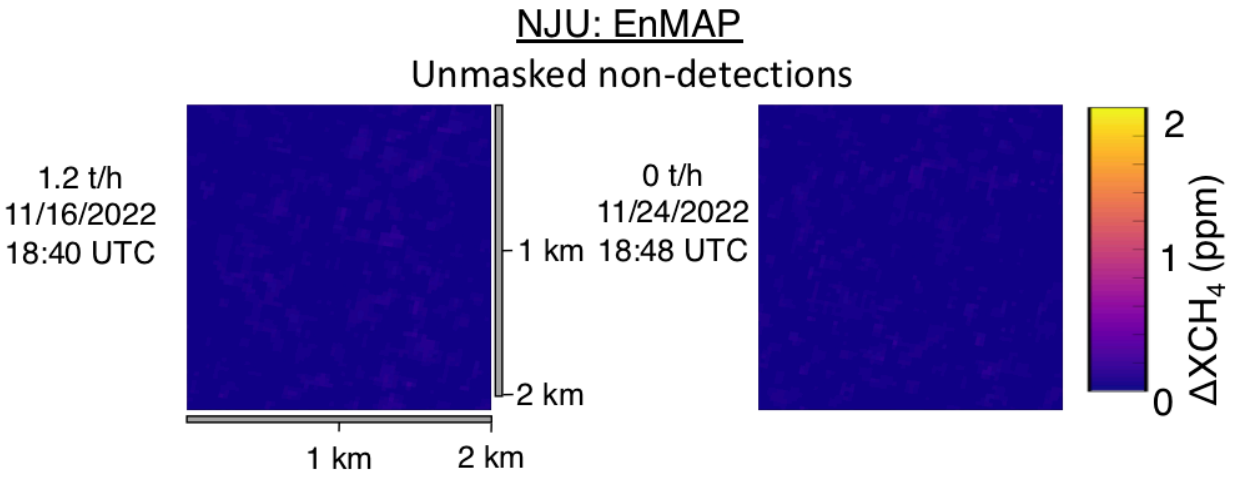


Figure S23. Provided masked and unmasked methane enhancement estimates from NJU for EnMAP retrievals. Surface imagery © 2023 Google Earth, CNES/Airbus, Maxar Technologies, USDA/FPAC/GEO.

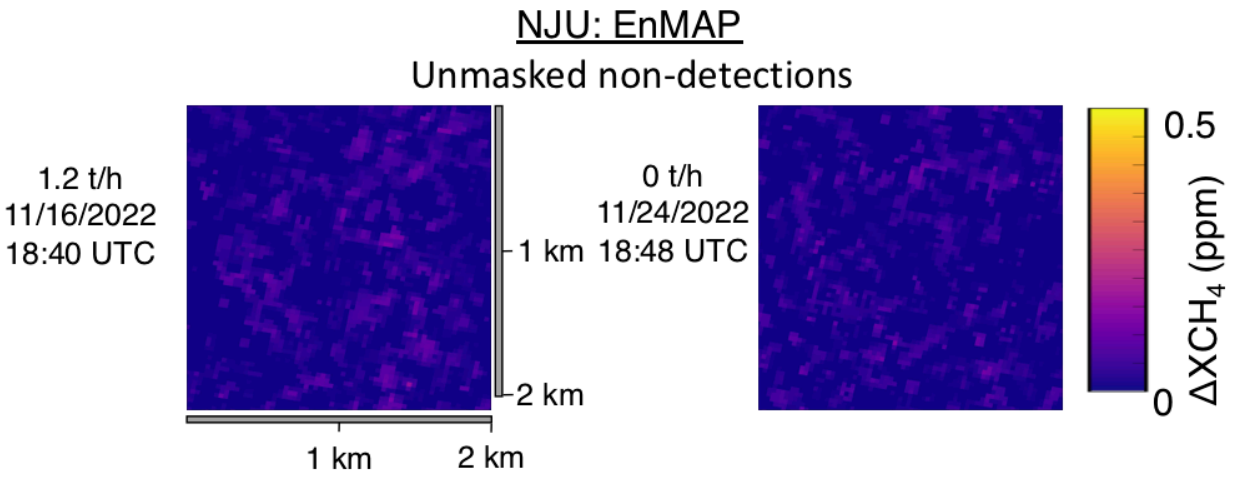


Figure S24. Custom-PPM scale, provided masked and unmasked methane enhancement estimates from NJU for EnMAP retrievals. Surface imagery © 2023 Google Earth, CNES/Airbus, Maxar Technologies, USDA/FPAC/GEO.

### S4.7.2. Gaofen 5 (GF5)

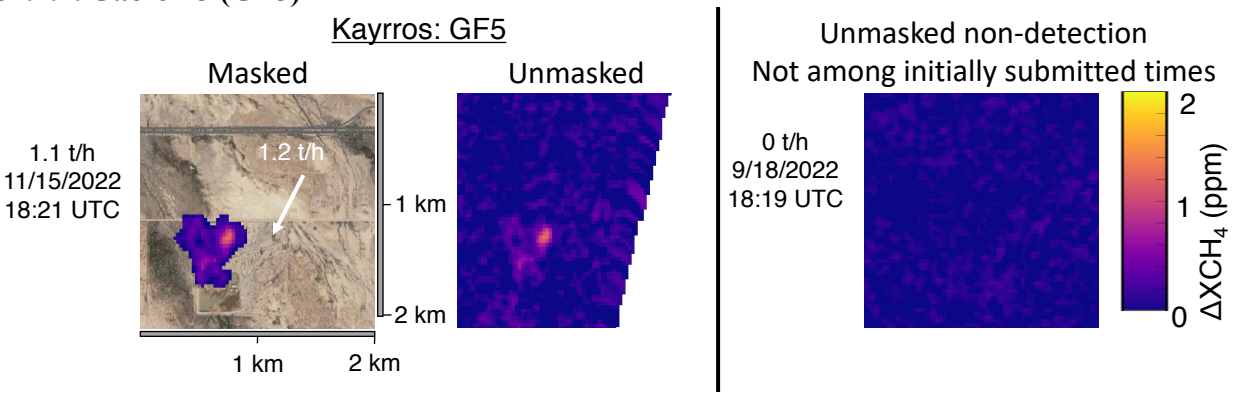


Figure S25. Provided masked and unmasked methane enhancement estimates from Kayrros for GF5 retrievals. True emission rates and timestamps in black text. For nonzero estimated emissions, mean estimated emission rate in white inset text. The white arrow represents 5-minute average measured in situ wind speed. Surface imagery © 2023 Google Earth, CNES/Airbus, Maxar Technologies, USDA/FPAC/GEO.

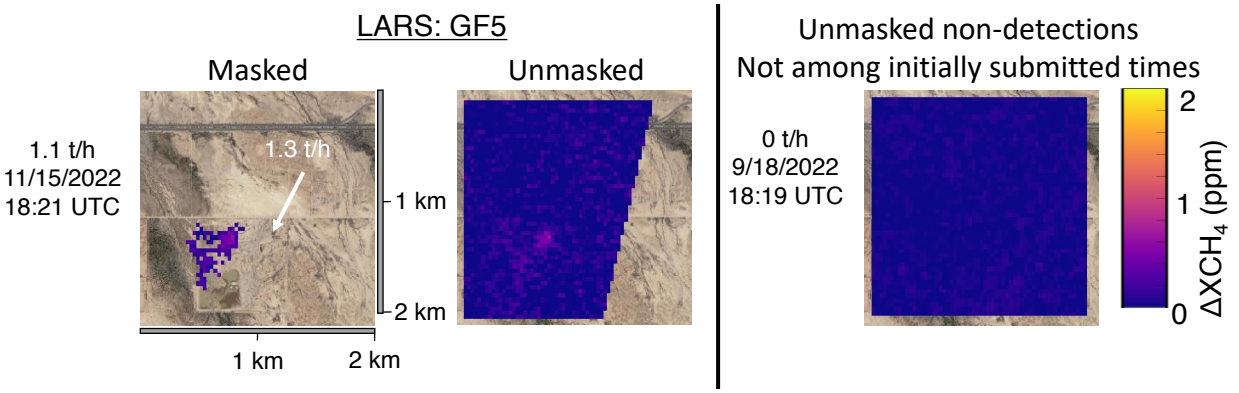


Figure S26. Provided masked and unmasked methane enhancement estimates from LARS for GF5 retrievals. True emission rates and timestamps in black text. For nonzero estimated emissions, mean estimated emission rate in white inset text. The white arrow represents 5-minute average measured in situ wind speed. Surface imagery © 2023 Google Earth, CNES/Airbus, Maxar Technologies, USDA/FPAC/GEO.

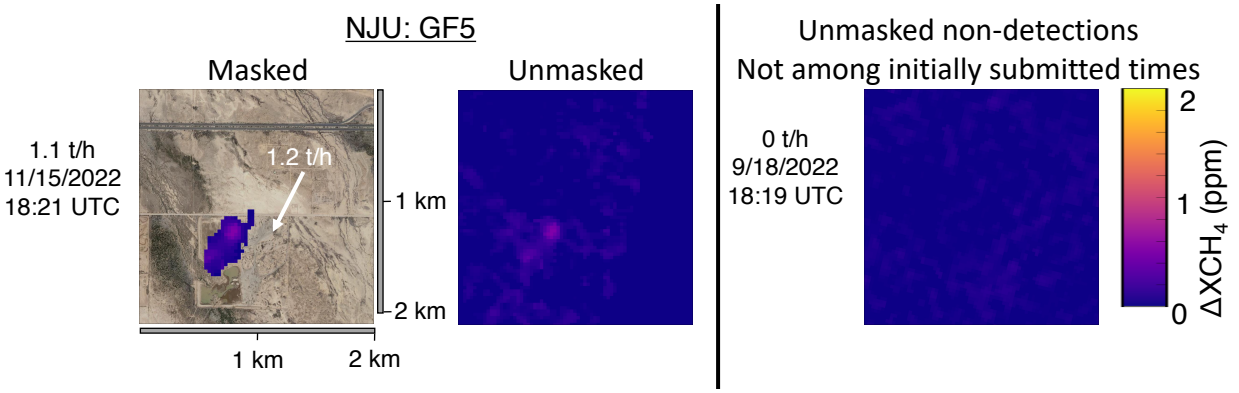


Figure S27. Provided masked and unmasked methane enhancement estimates from NJU for GF5 retrievals. True emission rates and timestamps in black text. For nonzero estimated emissions, mean estimated emission rate in white inset text. The white arrow represents 5-minute average measured in situ wind speed. Surface imagery © 2023 Google Earth, CNES/Airbus, Maxar Technologies, USDA/FPAC/GEO.

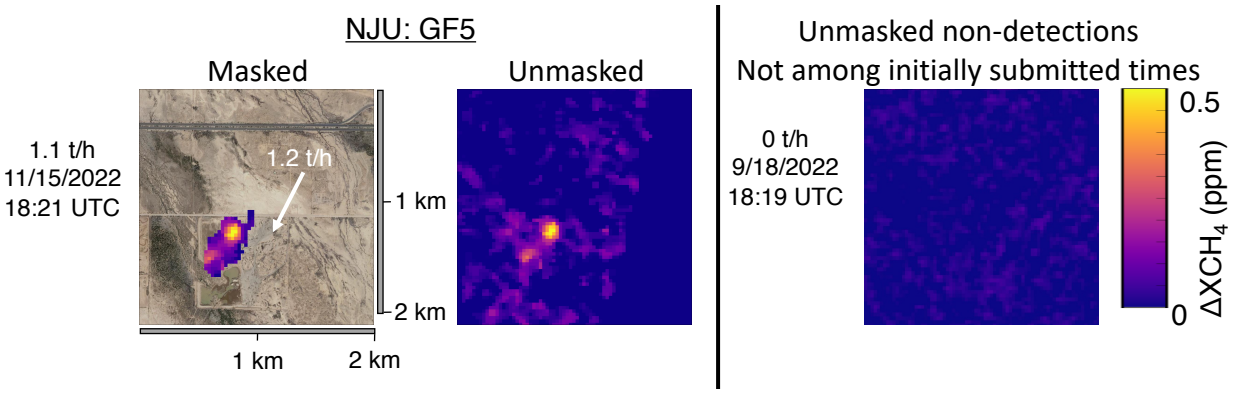


Figure S28. Custom-PPM scale, provided masked and unmasked methane enhancement estimates from NJU for GF5 retrievals. True emission rates and timestamps in black text. For nonzero estimated emissions, mean estimated emission rate in white inset text. The white arrow represents 5-minute average measured in situ wind speed. Surface imagery © 2023 Google Earth, CNES/Airbus, Maxar Technologies, USDA/FPAC/GEO.

### S4.7.3. GHGSat C

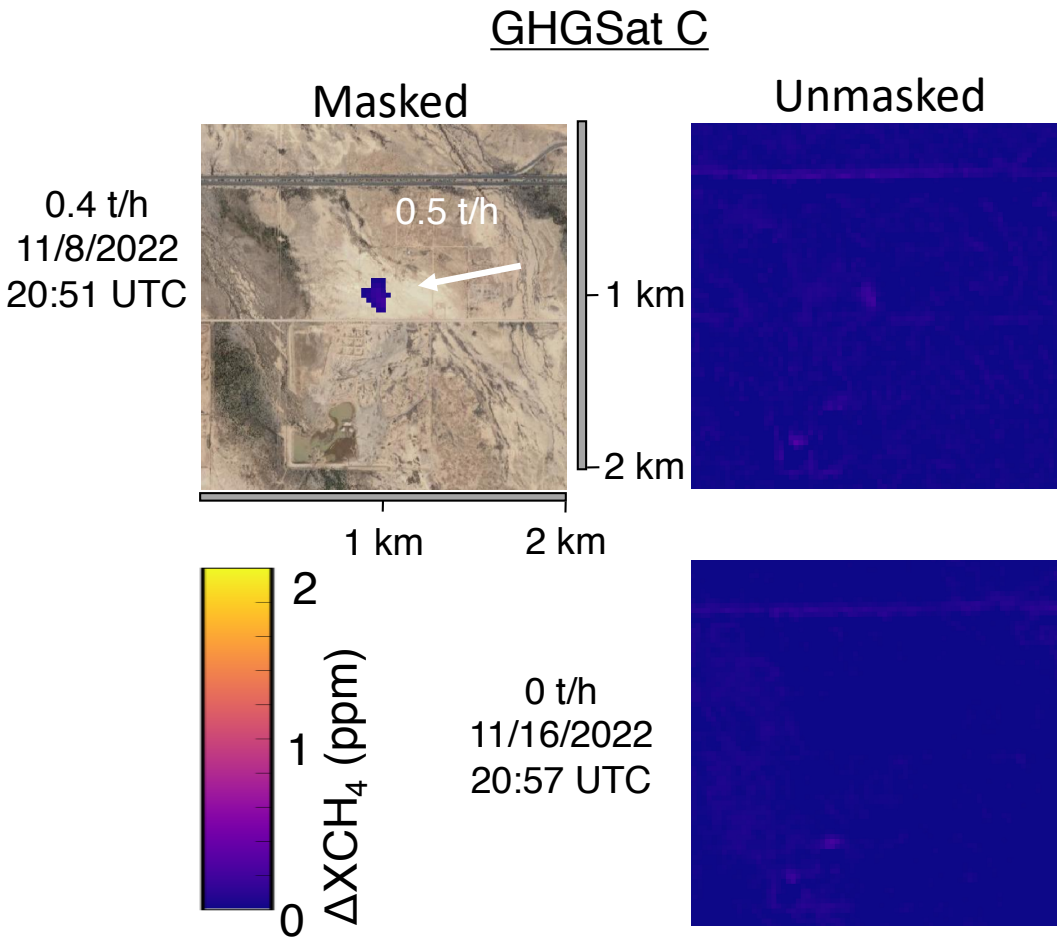


Figure S29. Provided masked and unmasked methane enhancement estimates from GHGSat for GHGSat C retrievals. True emission rates and timestamps in black text. For nonzero estimated emissions, mean estimated emission rate in white inset text. The white arrow represents 5-minute average measured in situ wind speed. Surface imagery © 2023 Google Earth, CNES/Airbus, Maxar Technologies, USDA/FPAC/GEO.

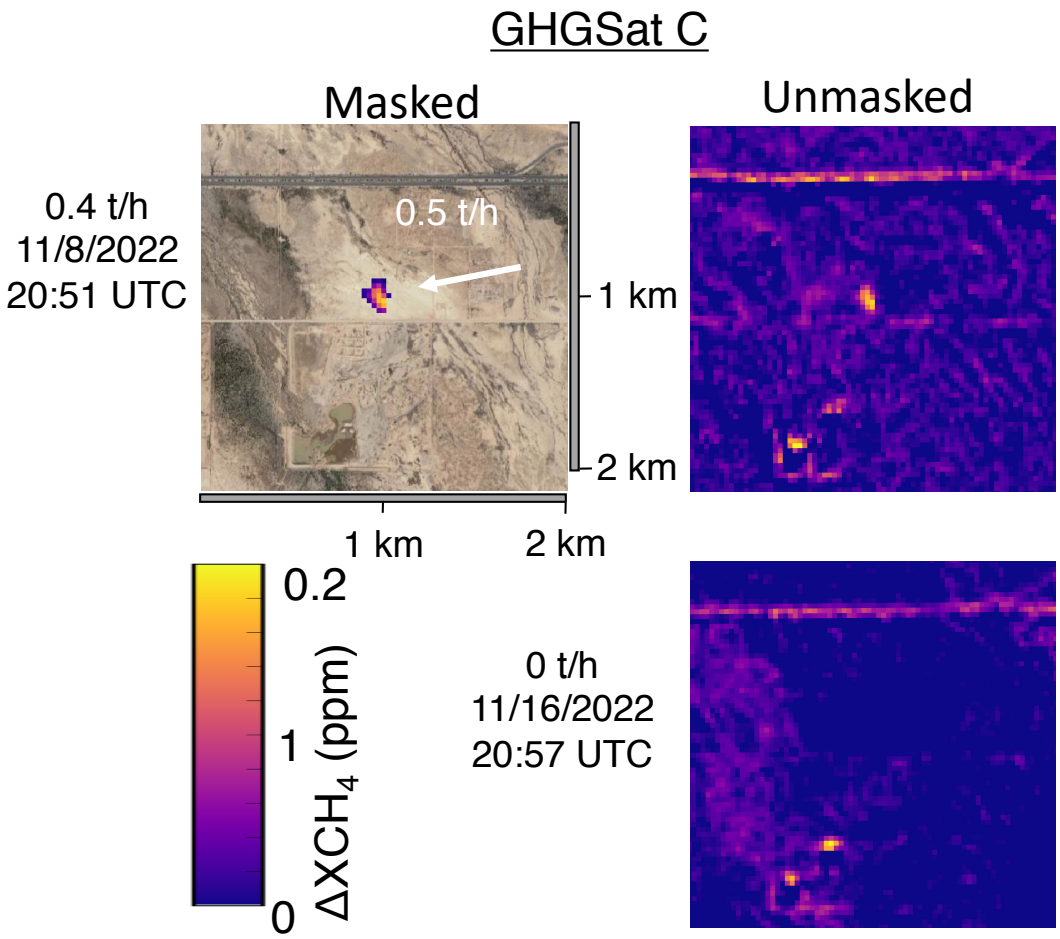


Figure S30. Provided masked and unmasked methane enhancement estimates from GHGSat for GHGSat C retrievals. True emission rates and timestamps in black text. For nonzero estimated emissions, mean estimated emission rate in white inset text. The white arrow represents 5-minute average measured in situ wind speed. Uses a maximum ppm scale value of 0.2 ppm instead of the 2 ppm used for intercomparison across technologies. Surface imagery © 2023 Google Earth, CNES/Airbus, Maxar Technologies, USDA/FPAC/GEO.

### S4.7.4. Huanjing 2B (HJ2B)

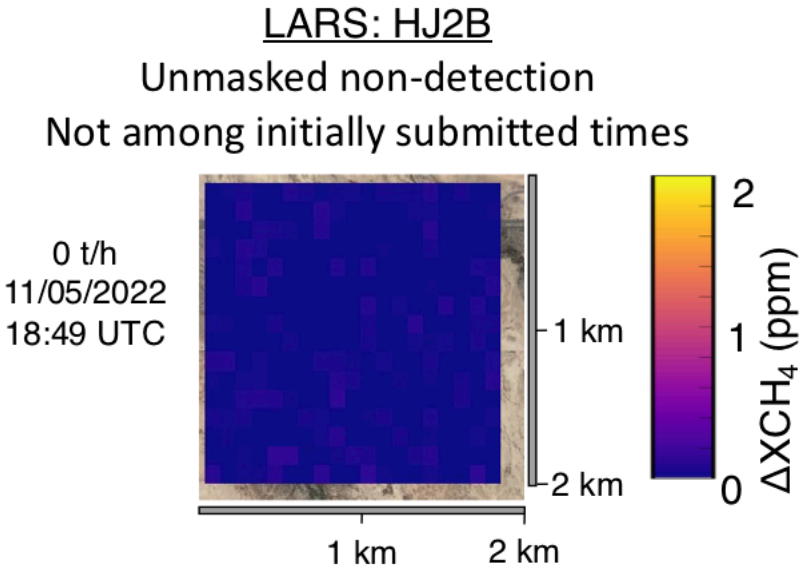


Figure S31. Provided masked and unmasked methane enhancement estimates from LARS for the HJ2B retrieval. True emission rates and timestamps in black text. Surface imagery © 2023 Google Earth, CNES/Airbus, Maxar Technologies, USDA/FPAC/GEO.

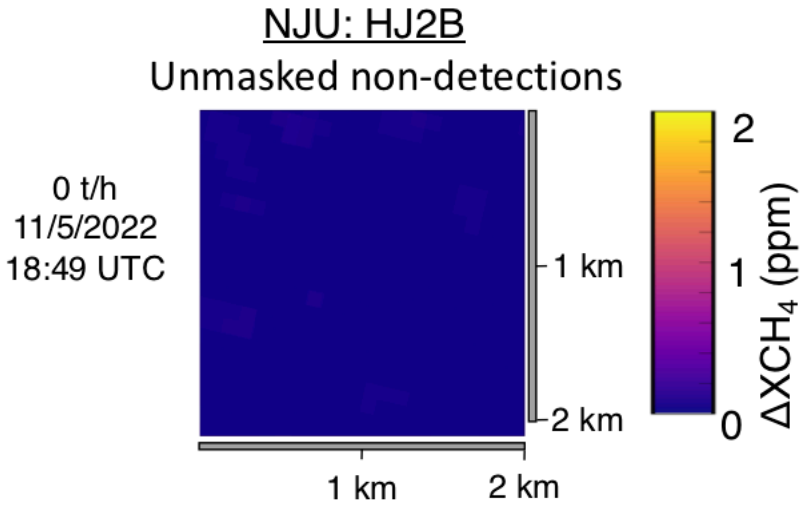


Figure S32. Provided masked and unmasked methane enhancement estimates from NJU for the HJ2B retrieval. True emission rates and timestamps in black text. Surface imagery © 2023 Google Earth, CNES/Airbus, Maxar Technologies, USDA/FPAC/GEO.

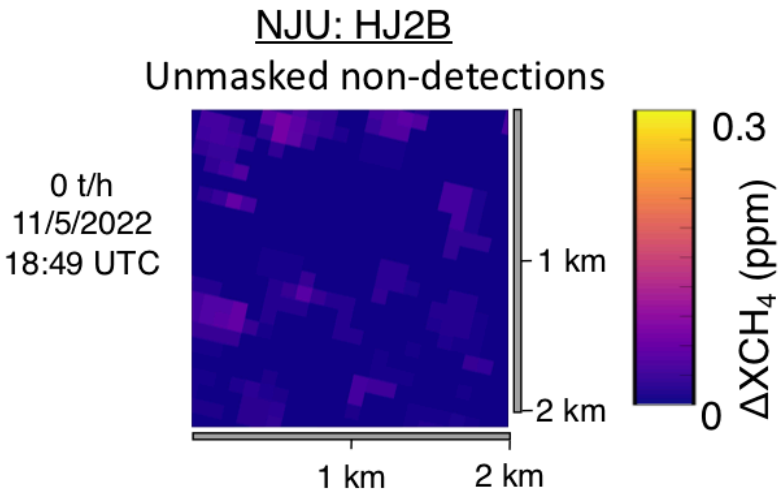


Figure S33. Custom-ppm scale, provided masked and unmasked methane enhancement estimates from NJU for the HJ2B retrieval. True emission rates and timestamps in black text. Surface imagery © 2023 Google Earth, CNES/Airbus, Maxar Technologies, USDA/FPAC/GEO.

### S4.7.5. LandSat

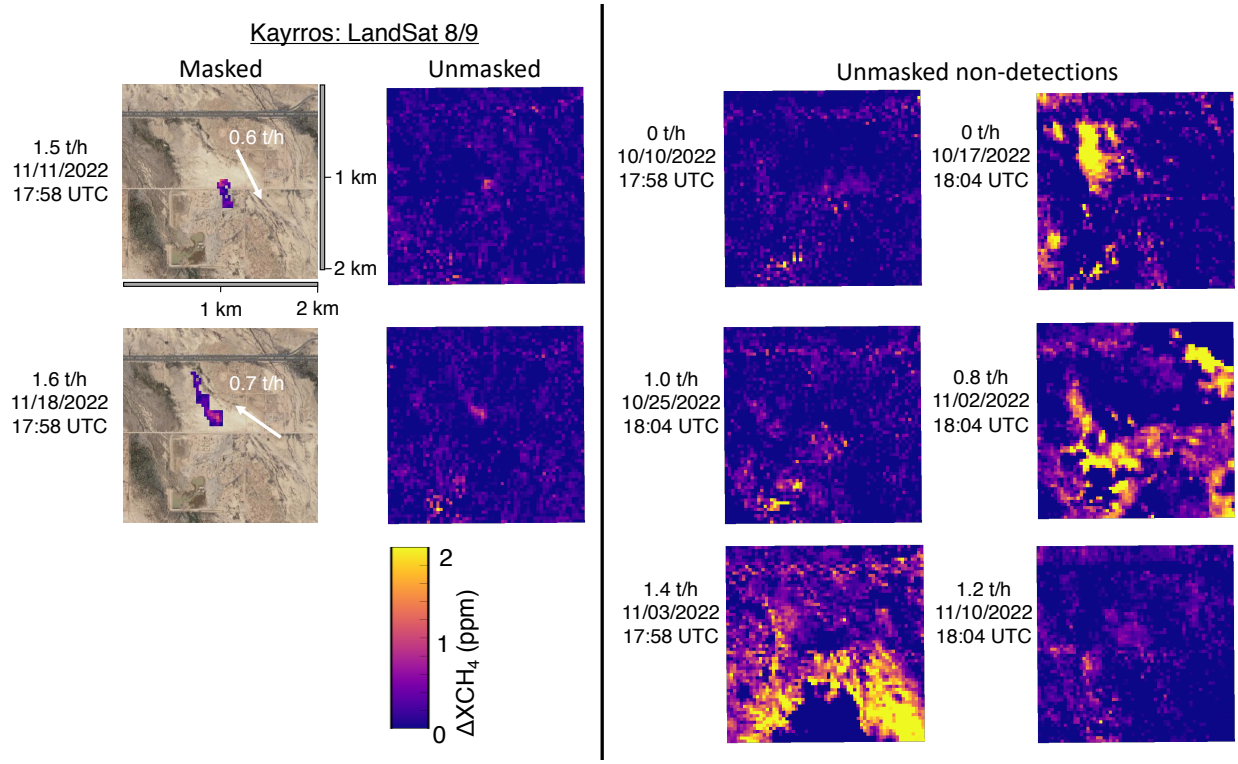


Figure S34. Provided masked and unmasked methane enhancement estimates from Kayrros for LandSat 8/9 retrievals. True emission rates and timestamps in black text. For nonzero estimated emissions, mean estimated emission rate in white inset text. The white arrows represent 5-minute average measured in situ wind speed. Surface imagery © 2023 Google Earth, CNES/Airbus, Maxar Technologies, USDA/FPAC/GEO.

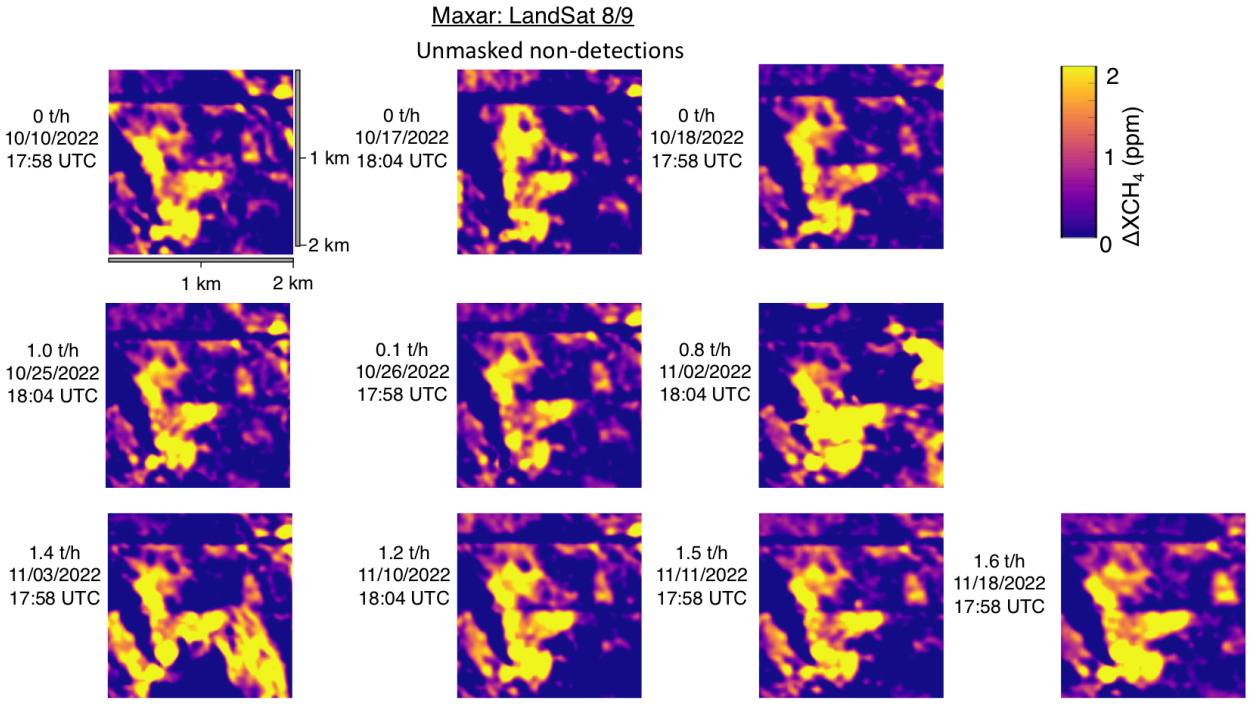


Figure S35. Provided masked and unmasked methane enhancement estimates from Maxar for LandSat 8/9 retrievals. All retrievals were reported as non-detections. Surface imagery © 2023 Google Earth, CNES/Airbus, Maxar Technologies, USDA/FPAC/GEO.

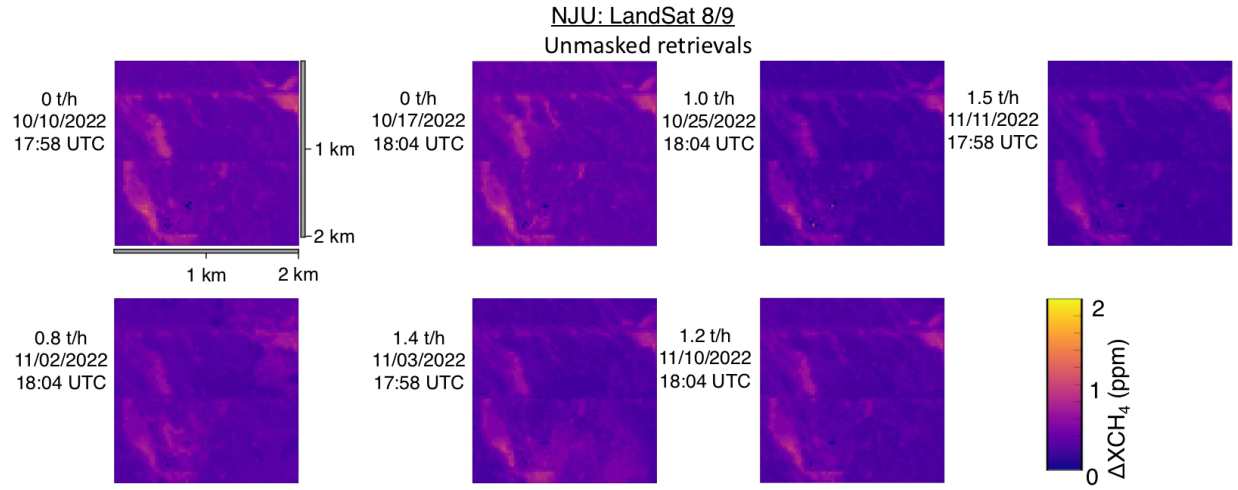


Figure S36. Provided masked and unmasked methane enhancement estimates from NJU for LandSat 8/9 retrievals. True emission rates and timestamps in black text. All retrievals were reported as non-detections. Surface imagery © 2023 Google Earth, CNES/Airbus, Maxar Technologies, USDA/FPAC/GEO.

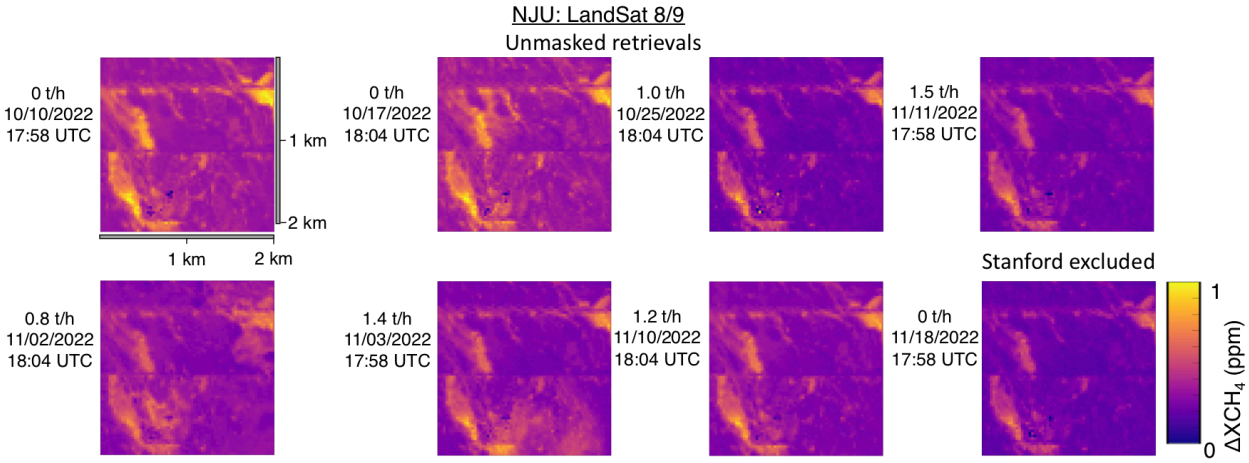


Figure S37. Custom-PPM scale, provided masked and unmasked methane enhancement estimates from NJU for LandSat 8/9 retrievals. True emission rates and timestamps in black text. For nonzero estimated emissions. All retrievals were reported as non-detections. Surface imagery © 2023 Google Earth, CNES/Airbus, Maxar Technologies, USDA/FPAC/GEO.

## S4.7.6. PRISMA

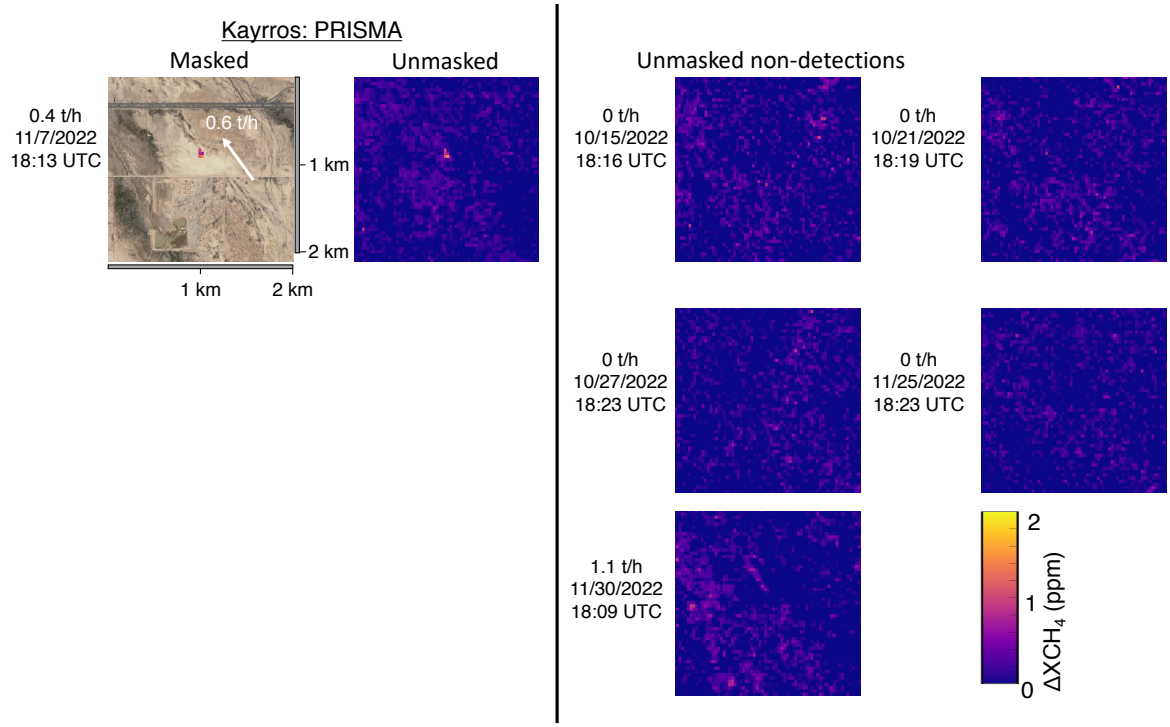


Figure S38. Provided masked and unmasked methane enhancement estimates from Kayrros for PRISMA retrievals. True emission rates and timestamps in black text. For nonzero estimated emissions, mean estimated emission rate in white inset text. The white arrow represents 5-minute average measured in situ wind speed. Surface imagery © 2023 Google Earth, CNES/Airbus, Maxar Technologies, USDA/FPAC/GEO.

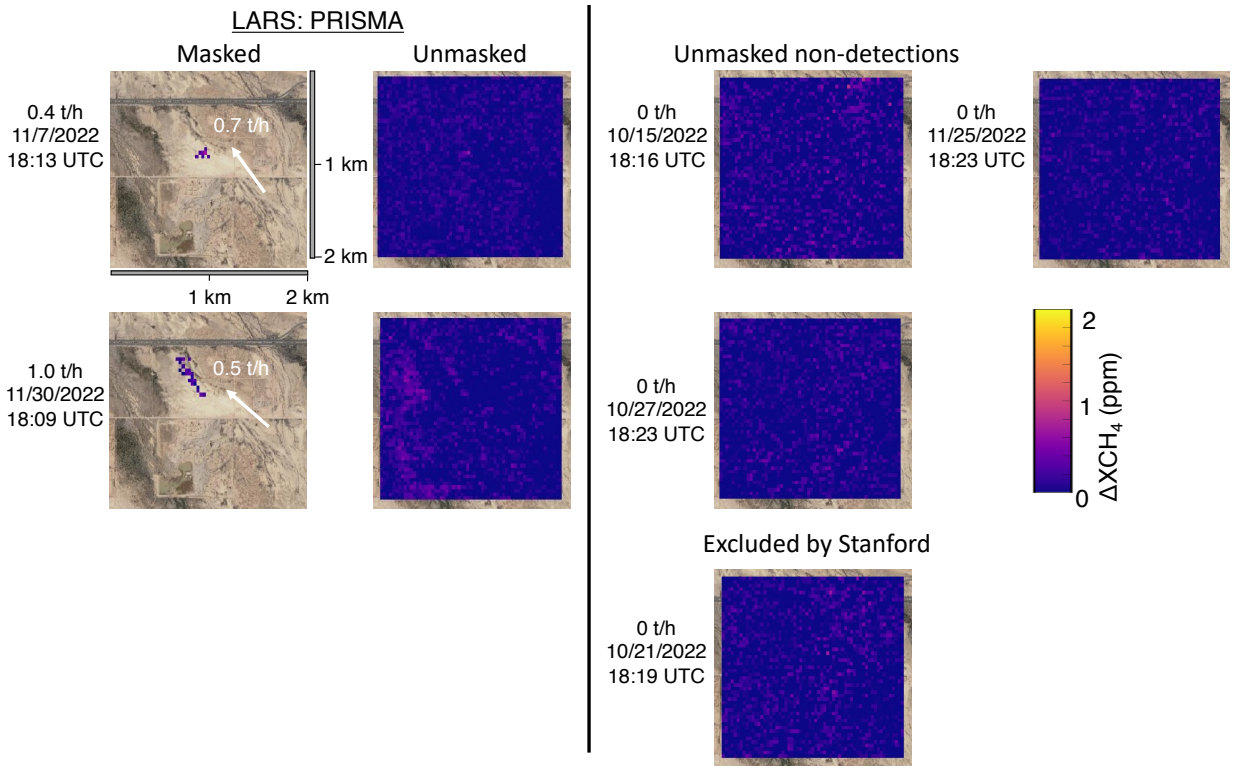


Figure S39. Provided masked and unmasked methane enhancement estimates from LARS for PRISMA retrievals. True emission rates and timestamps in black text. For nonzero estimated emissions, mean estimated emission rate in white inset text. The white arrows represent 5-minute average measured in situ wind speed. Surface imagery © 2023 Google Earth, CNES/Airbus, Maxar Technologies, USDA/FPAC/GEO.

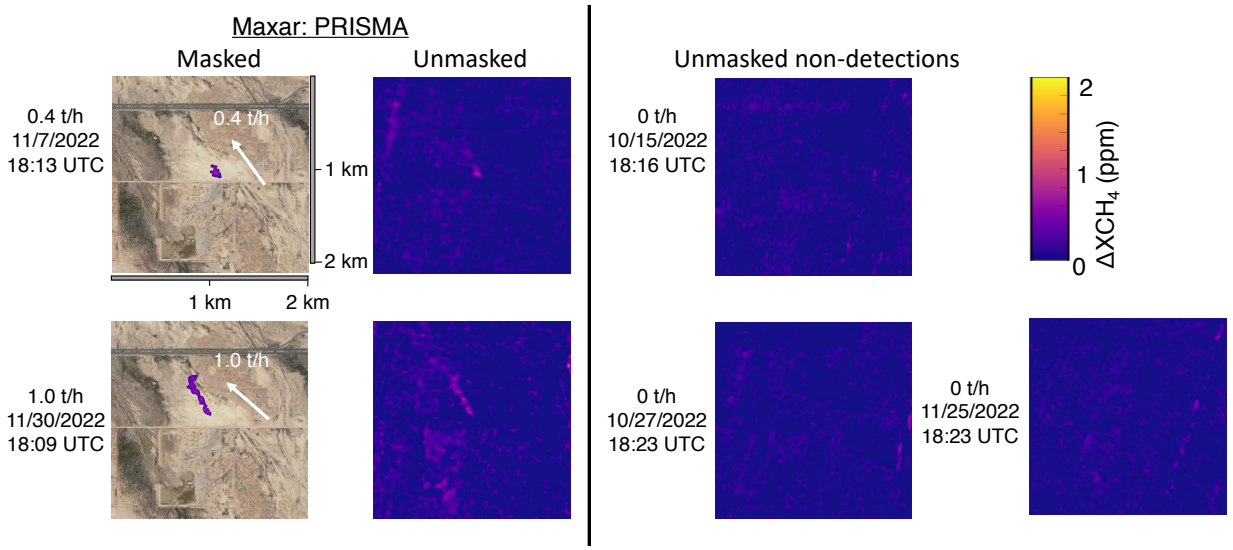


Figure S40. Provided masked and unmasked methane enhancement estimates from Maxar for PRISMA retrievals. True emission rates and timestamps in black text. For nonzero estimated emissions, mean estimated emission rate in white inset text. The white arrows represent 5-minute average measured in situ wind speed. Surface imagery © 2023 Google Earth, CNES/Airbus, Maxar Technologies, USDA/FPAC/GEO.

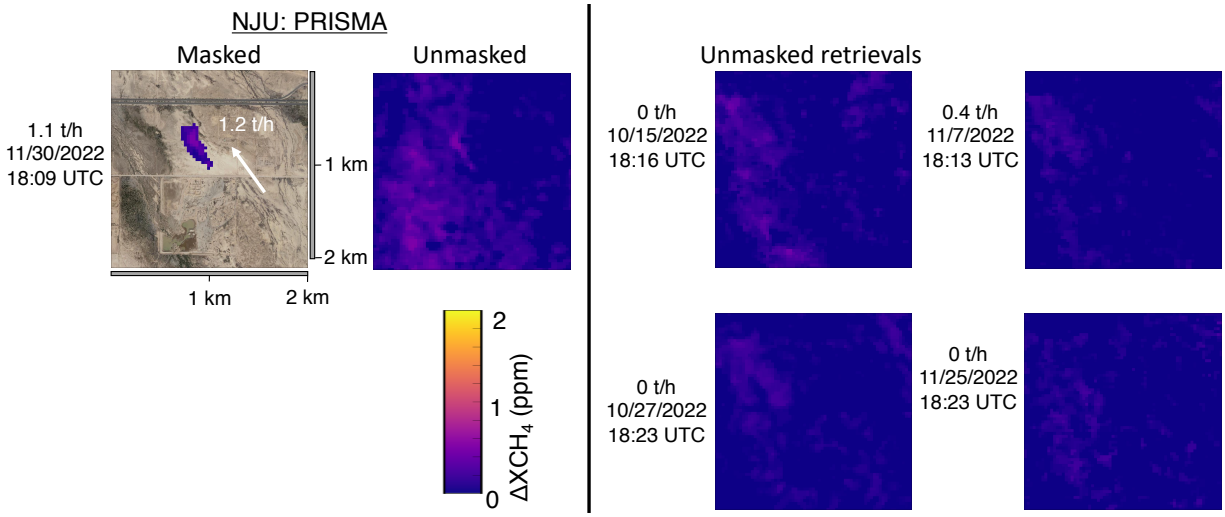


Figure S41. Provided masked and unmasked methane enhancement estimates from NJU for PRISMA retrievals. True emission rates and timestamps in black text. For nonzero estimated emissions, mean estimated emission rate in white inset text (in this case, the Stage 1 estimate submitted past the deadline by Maxar). The white arrow represents 5-minute average measured in situ wind speed. Surface imagery © 2023 Google Earth, CNES/Airbus, Maxar Technologies, USDA/FPAC/GEO.

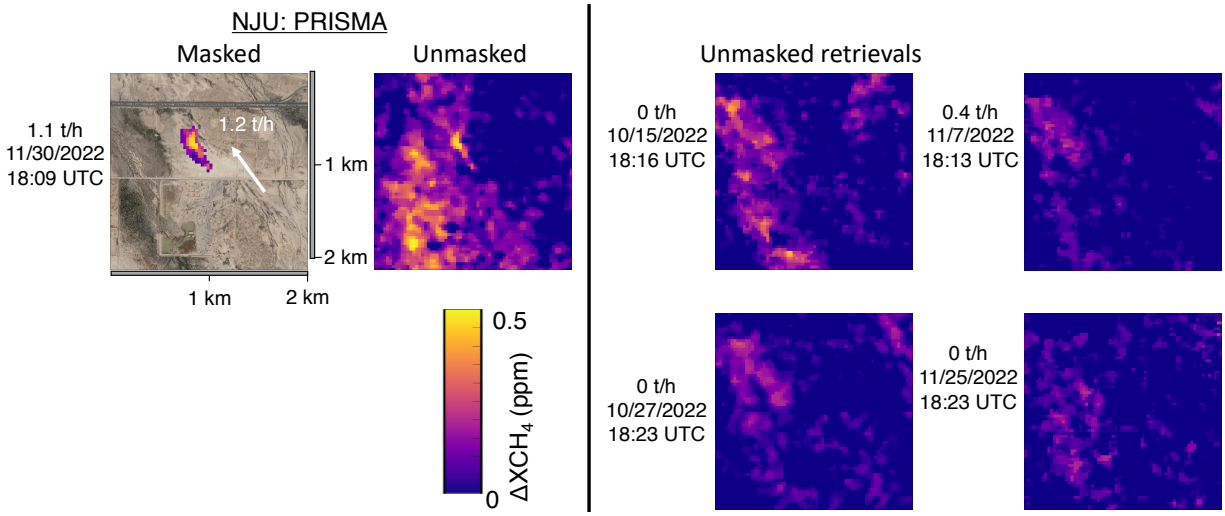


Figure S42. Custom-PPM scale provided masked and unmasked methane enhancement estimates from NJU for PRISMA retrievals. True emission rates and timestamps in black text. For nonzero estimated emissions, mean estimated emission rate in white inset text. The white arrow represents 5-minute average measured in situ wind speed. Surface imagery © 2023 Google Earth, CNES/Airbus, Maxar Technologies, USDA/FPAC/GEO.

### S4.7.7. Sentinel-2

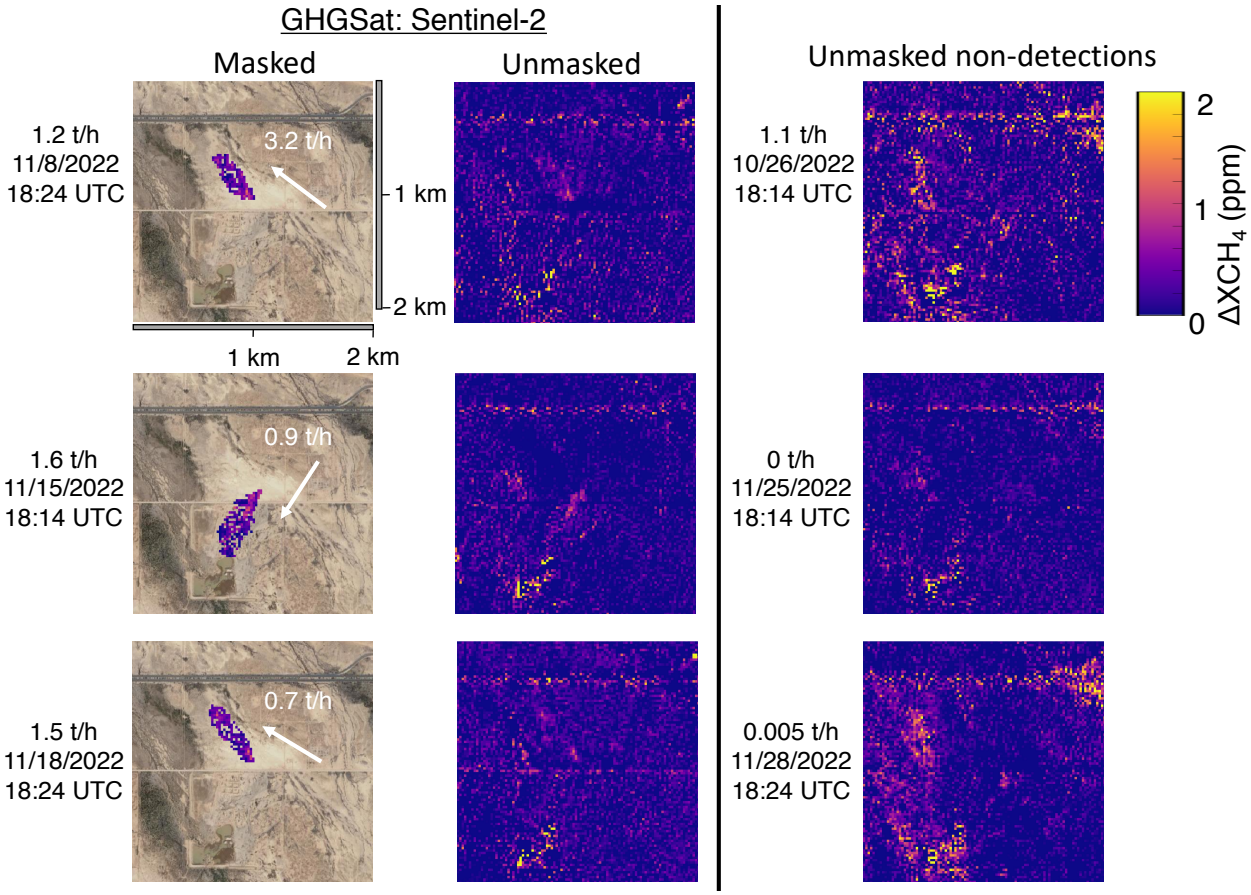


Figure S43. Provided masked and unmasked methane enhancement estimates from GHGSat for Sentinel-2 retrievals. True emission rates and timestamps in black text. For nonzero estimated emissions, mean estimated emission rate in white inset text. The white arrows represent 5-minute average measured in situ wind speed. Surface imagery © 2023 Google Earth, CNES/Airbus, Maxar Technologies, USDA/FPAC/GEO.

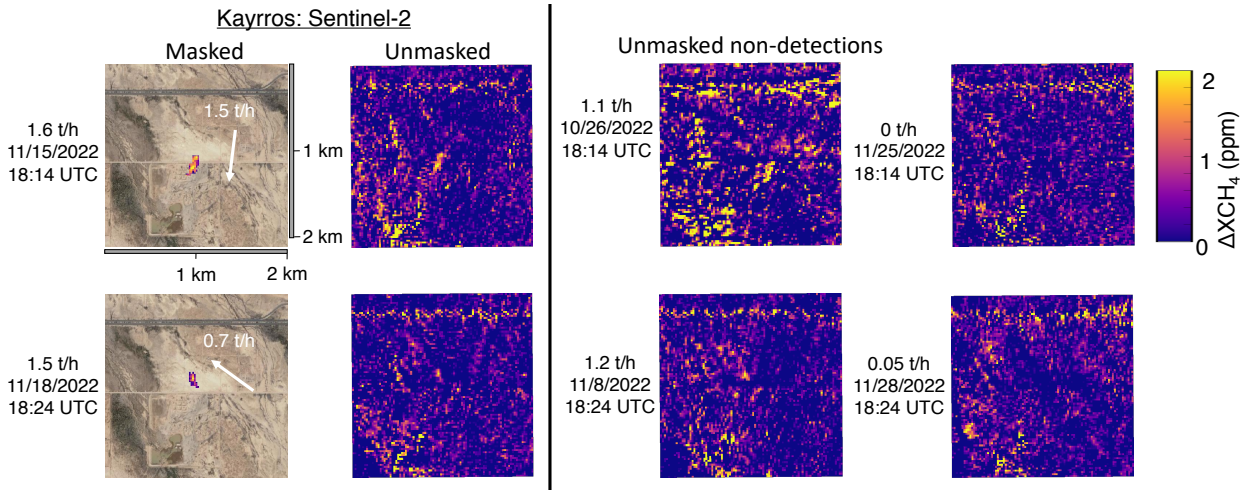


Figure S44. Provided masked and unmasked methane enhancement estimates from Kayrros for Sentinel-2 retrievals. True emission rates and timestamps in black text. For nonzero estimated emissions, mean estimated emission rate in white inset text. The white arrows represent 5-minute average measured in situ wind speed. Surface imagery © 2023 Google Earth, CNES/Airbus, Maxar Technologies, USDA/FPAC/GEO.

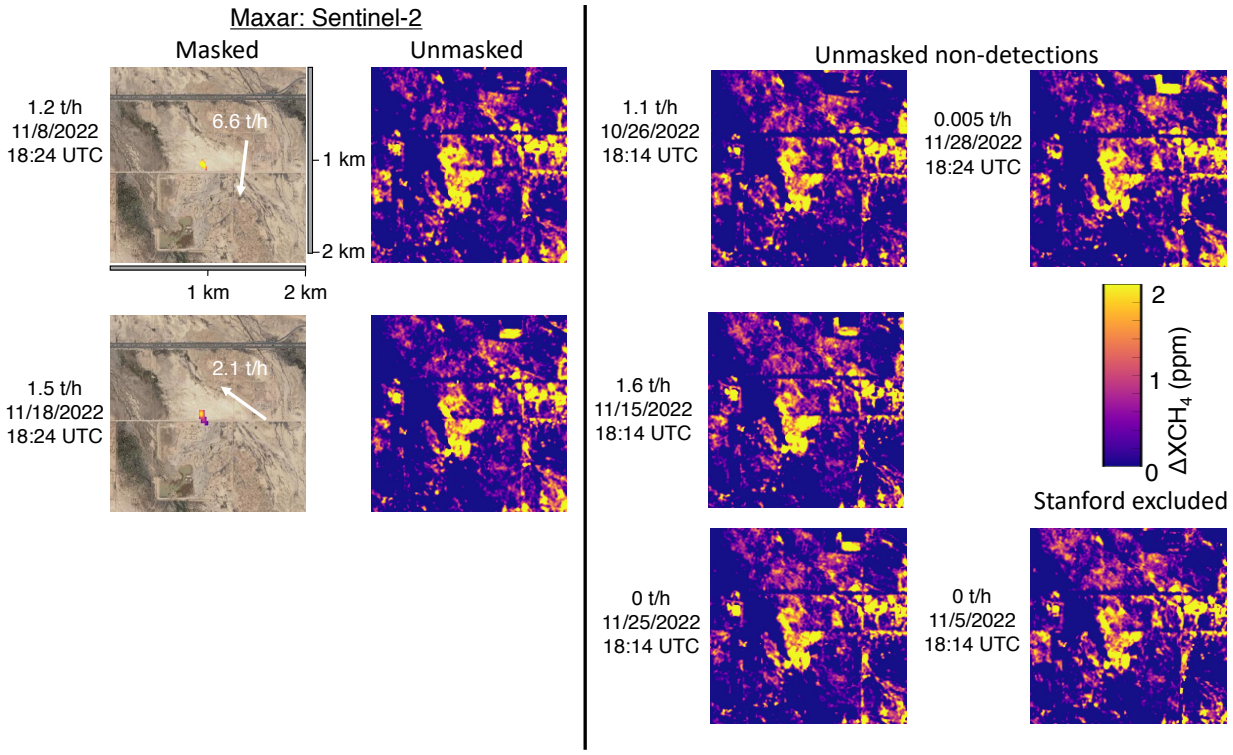


Figure S45. Provided masked and unmasked methane enhancement estimates from Maxar for Sentinel-2 retrievals. True emission rates and timestamps in black text. For nonzero estimated emissions, mean estimated emission rate in white inset text. The white arrows represent 5-minute average measured in situ wind speed. Surface imagery © 2023 Google Earth, CNES/Airbus, Maxar Technologies, USDA/FPAC/GEO.

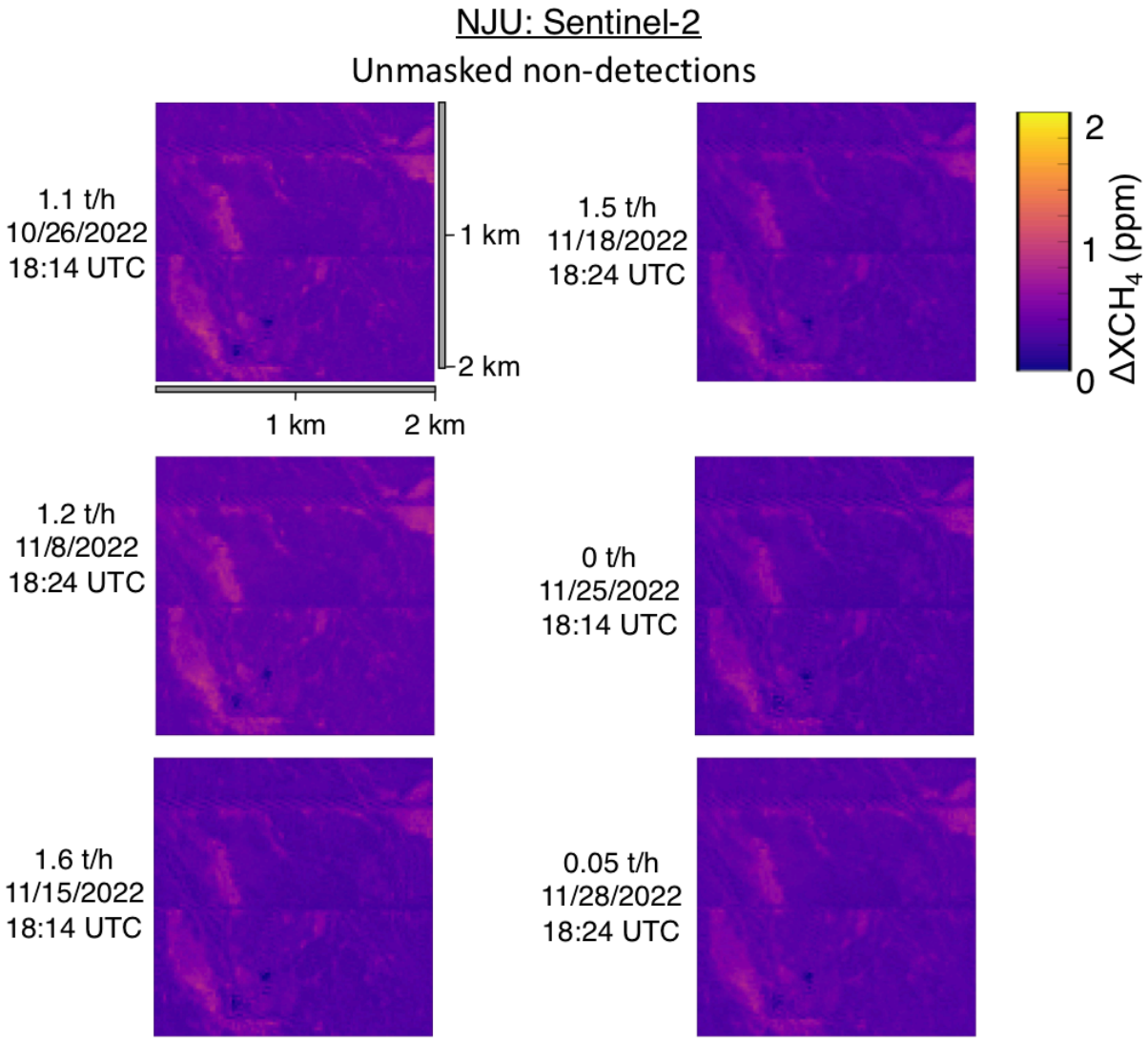


Figure S46. Provided masked and unmasked methane enhancement estimates from NJU for Sentinel-2 retrievals. True emission rates and timestamps in black text. For nonzero estimated emissions, mean estimated emission rate in white inset text. The white arrow represents 5-minute average measured in situ wind speed. Surface imagery © 2023 Google Earth, CNES/Airbus, Maxar Technologies, USDA/FPAC/GEO.

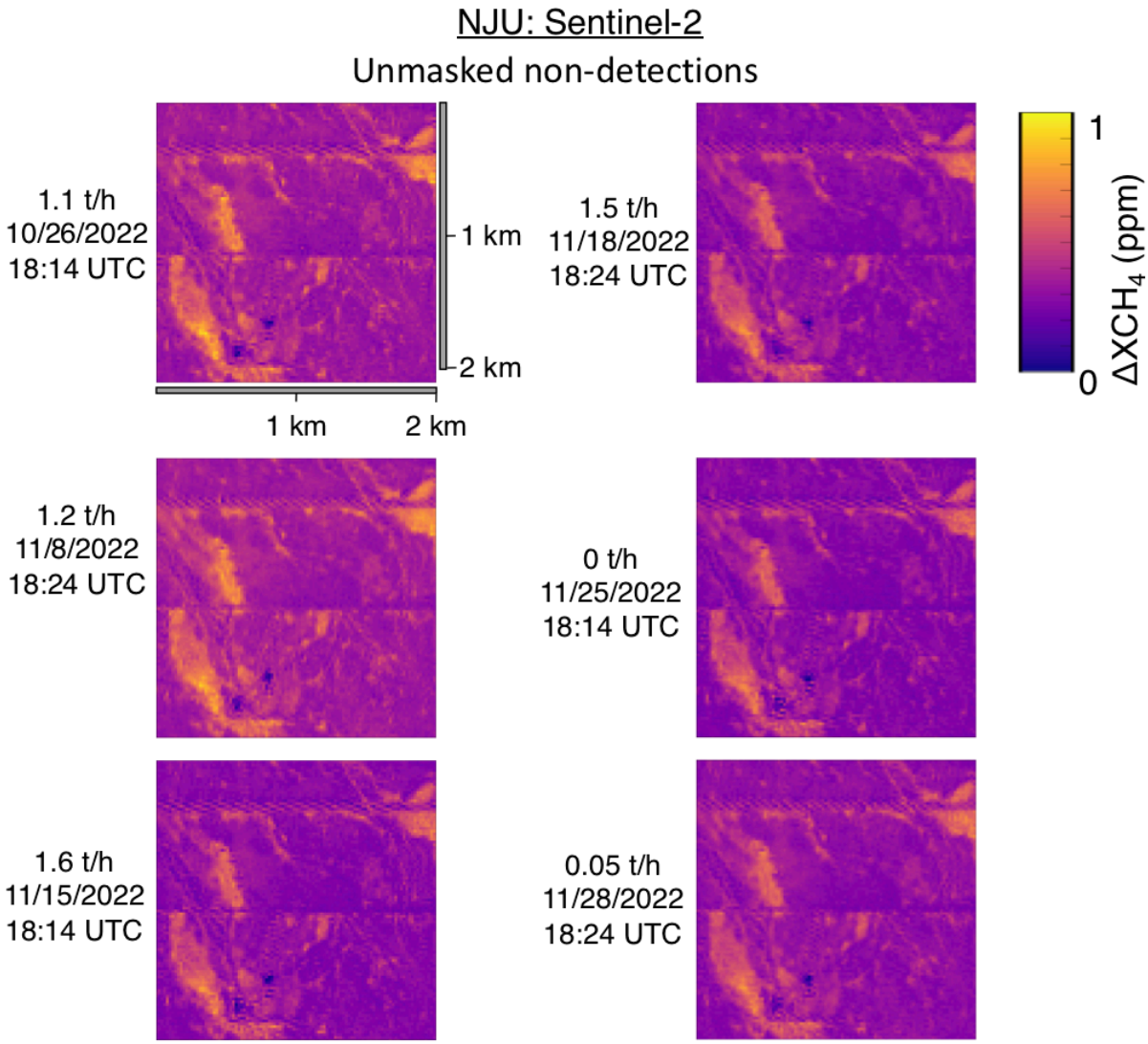


Figure S47. Custom-PPM scale, provided masked and unmasked methane enhancement estimates from NJU for Sentinel-2 retrievals. True emission rates and timestamps in black text. For nonzero estimated emissions, mean estimated emission rate in white inset text. The white arrow represents 5-minute average measured in situ wind speed. Surface imagery © 2023 Google Earth, CNES/Airbus, Maxar Technologies, USDA/FPAC/GEO.

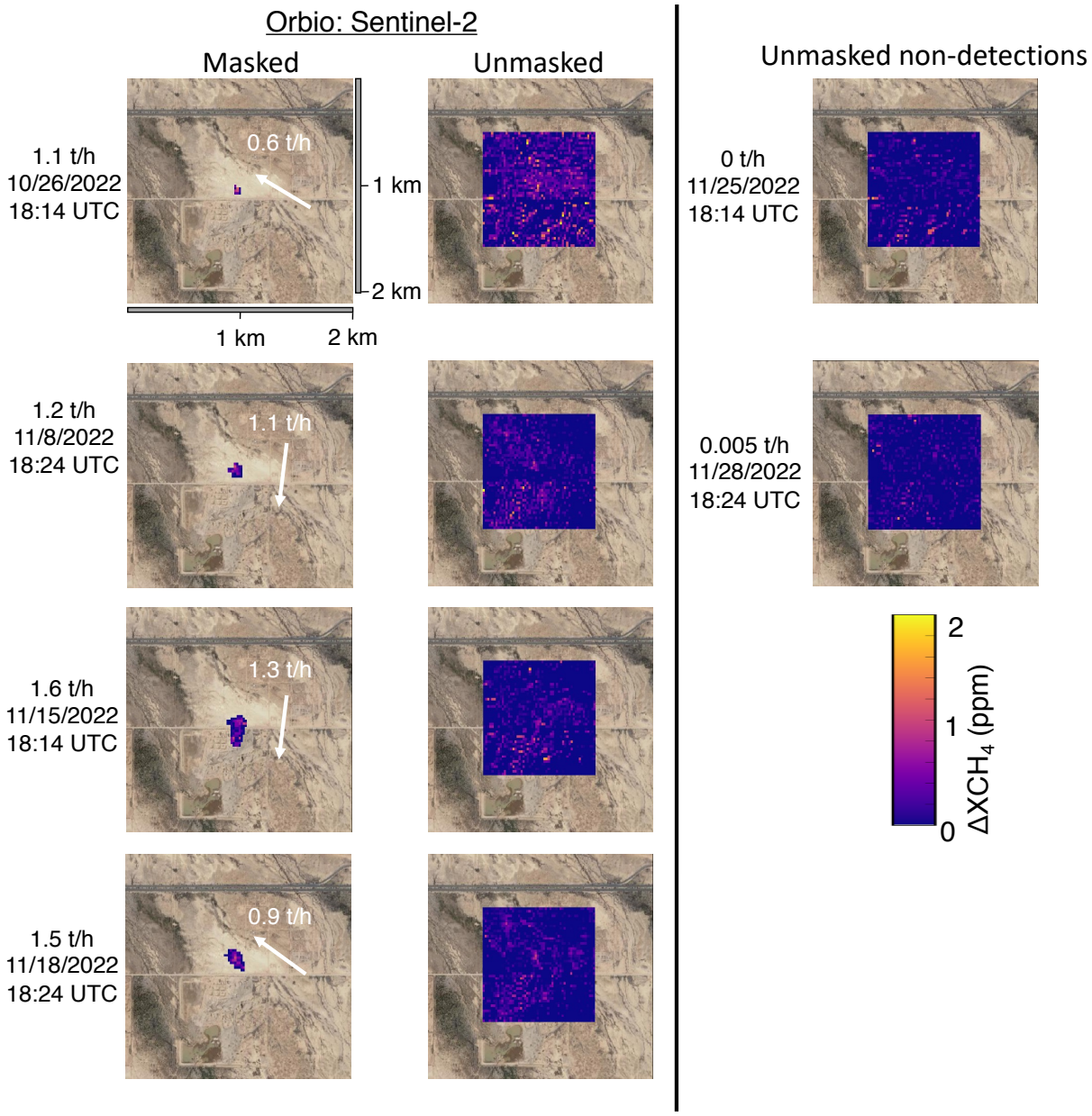


Figure S48. Provided masked and unmasked methane enhancement estimates from Orbio Earth for Sentinel-2 retrievals. True emission rates and timestamps in black text. For nonzero estimated emissions, mean estimated emission rate in white inset text. The white arrows represent 5-minute average measured in situ wind speed. Surface imagery © 2023 Google Earth, CNES/Airbus, Maxar Technologies, USDA/FPAC/GEO.

## S4.7.8. WorldView-3

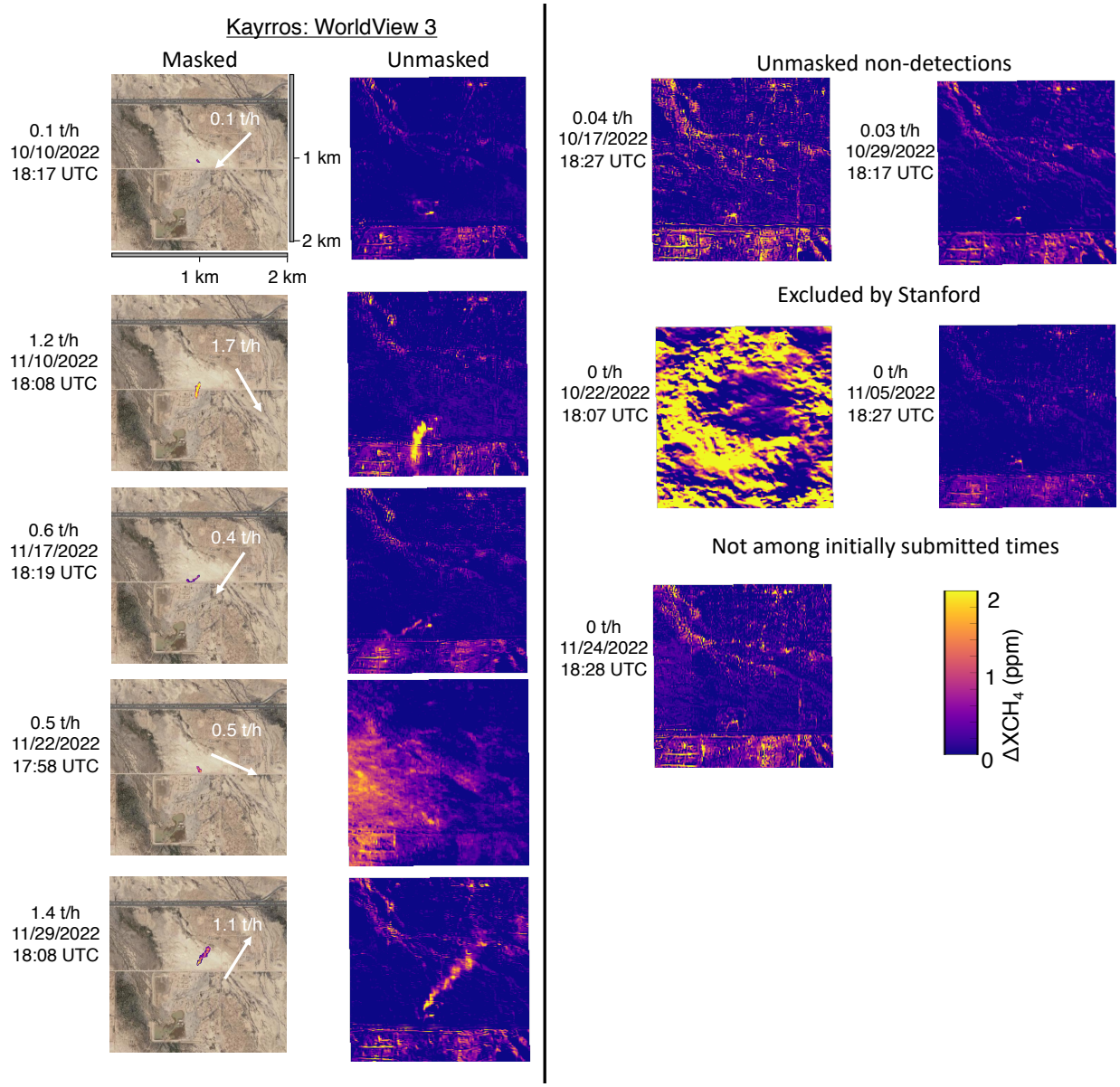


Figure S49. Provided masked and unmasked methane enhancement estimates from Kayrros for WorldView-3 retrievals. True emission rates and timestamps in black text. For nonzero estimated emissions, mean estimated emission rate in white inset text. The white arrows represent 5-minute average measured in situ wind speed. Note that unmasked images shift the frame roughly 1 km north compared with the masked images and zoom in on a smaller area. Surface imagery © 2023 Google Earth, CNES/Airbus, Maxar Technologies, USDA/FPAC/GEO.

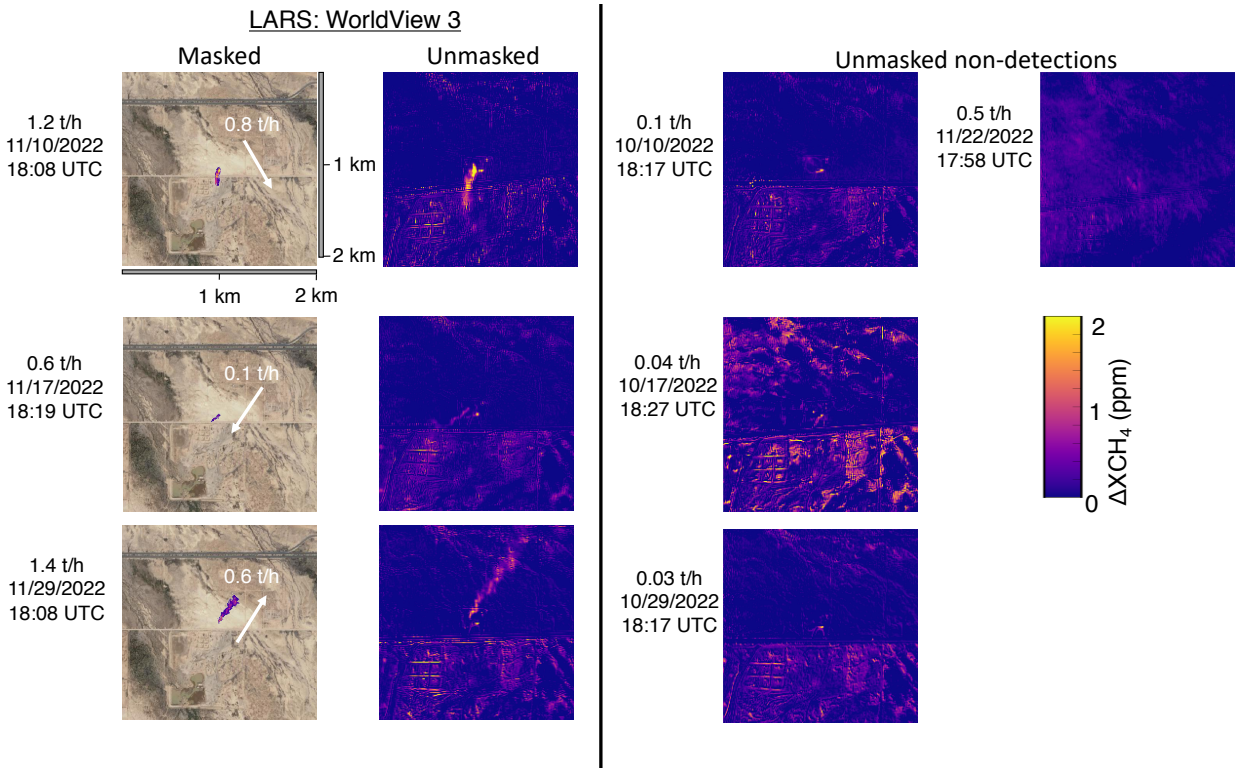


Figure S50. Provided masked and unmasked methane enhancement estimates from LARS for WorldView-3 retrievals. Note that unmasked images focus on a smaller area. True emission rates and timestamps in black text. For nonzero estimated emissions, mean estimated emission rate in white inset text. The white arrows represent 5-minute average measured in situ wind speed. Surface imagery © 2023 Google Earth, CNES/Airbus, Maxar Technologies, USDA/FPAC/GEO. Note that LARS researcher Javier Gorroño submitted Stage 1 WorldView 3 estimates after LARS researcher Javier Roger Juan had received unblinded in situ wind data. Javier Gorroño then submitted Stage 2 WorldView 3 estimates, not included in the main manuscript, after release volumes were unblinded. Although Stanford researchers believe LARS WorldView 3 estimates did not use the ground truth wind data for their Stage 1 estimates or the metered volumes for their Stage 2 estimates, we include them only in the SI to maintain strict adherence to our experimental design.

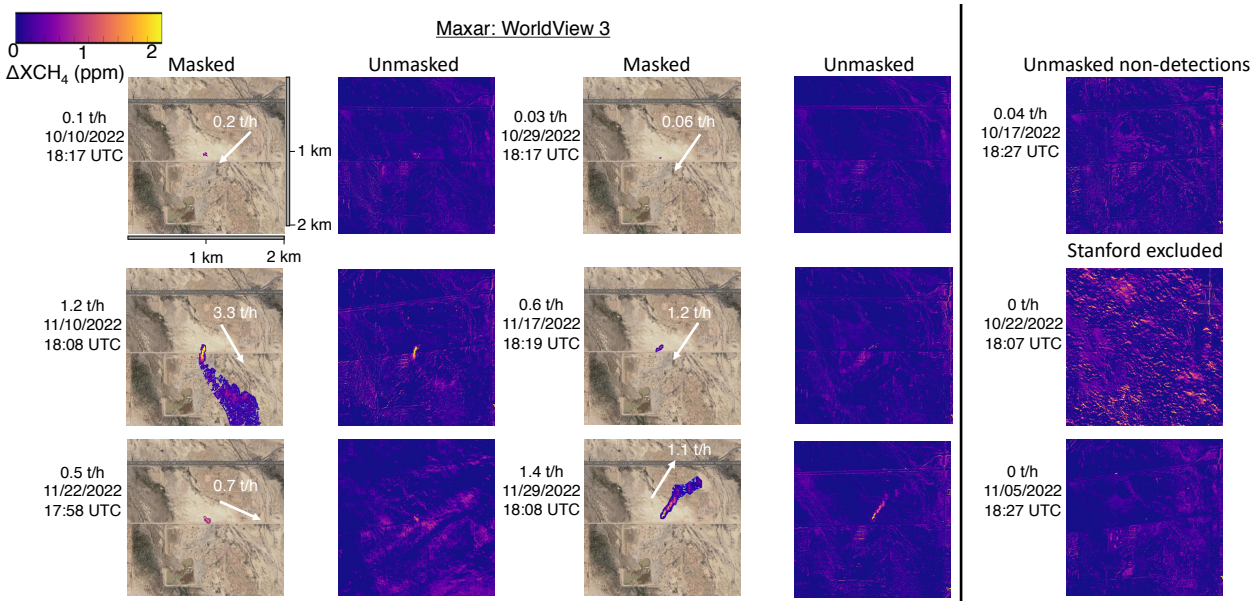


Figure S51. Provided masked and unmasked methane enhancement estimates from Maxar for WorldView-3 retrievals. True emission rates and timestamps in black text. For nonzero estimated emissions, mean estimated emission rate in white inset text. The white arrows represent 5-minute average measured in situ wind speed. Surface imagery © 2023 Google Earth, CNES/Airbus, Maxar Technologies, USDA/FPAC/GEO.

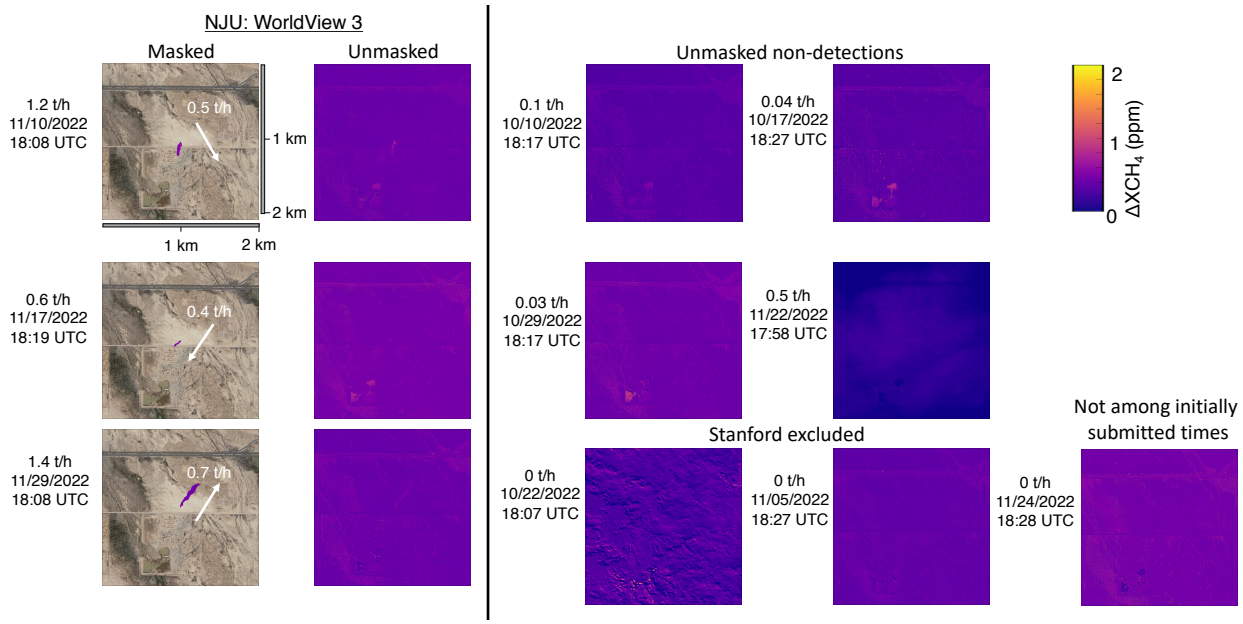


Figure S52. Provided masked and unmasked methane enhancement estimates from NJU for WorldView-3 retrievals. True emission rates and timestamps in black text. For nonzero estimated emissions, mean estimated emission rate in white inset text. The white arrows represent 5-minute average measured in situ wind speed. Surface imagery © 2023 Google Earth, CNES/Airbus, Maxar Technologies, USDA/FPAC/GEO.

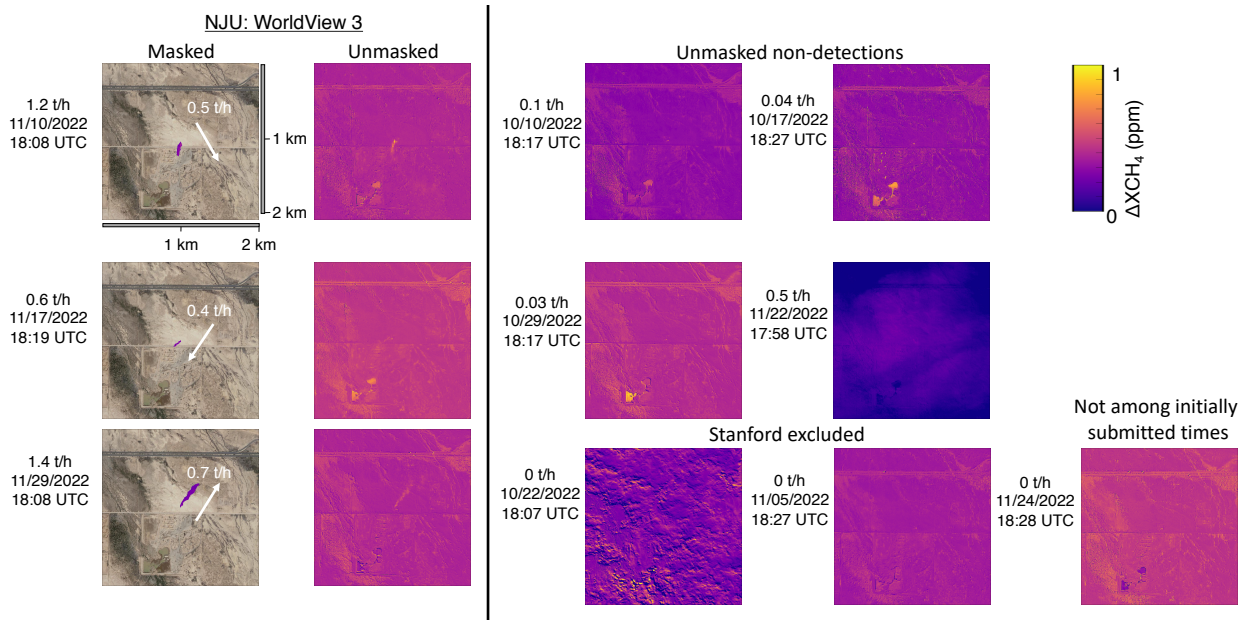


Figure S53. Custom-PPM scale, provided masked and unmasked methane enhancement estimates from NJU for WorldView-3 retrievals. True emission rates and timestamps in black text. For nonzero estimated emissions, mean estimated emission rate in white inset text. The white arrows represent 5-minute average measured in situ wind speed. Surface imagery © 2023 Google Earth, CNES/Airbus, Maxar Technologies, USDA/FPAC/GEO.

### S4.7.9. Ziyuan (ZY1)

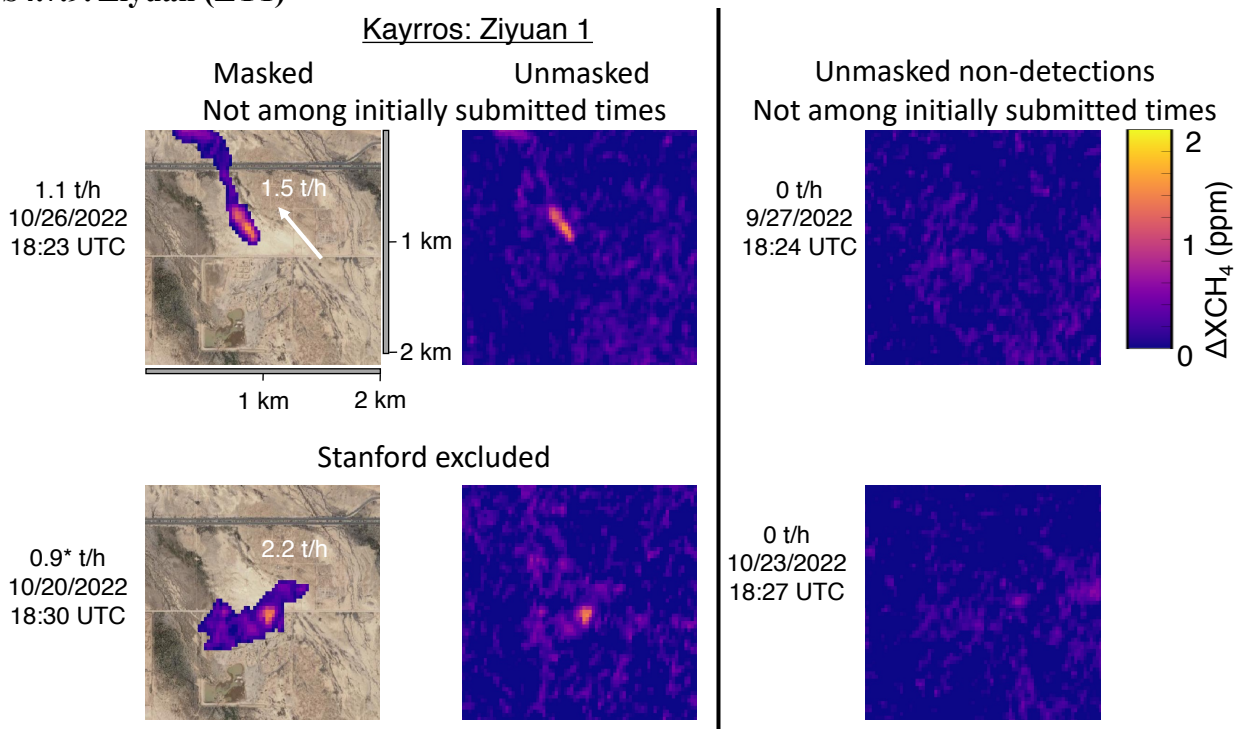


Figure S54. Provided masked and unmasked methane enhancement estimates from Kayrros for ZY1 retrievals. True emission rates and timestamps in black text. For nonzero estimated emissions, mean estimated emission rate in white inset text. The white arrow represents 5-minute average measured in situ wind speed. *The October 20th release volume is estimated, as described in S1.4, due to a system malfunction that prevented data logging. Surface imagery © 2023 Google Earth, CNES/Airbus, Maxar Technologies, USDA/FPAC/GEO.

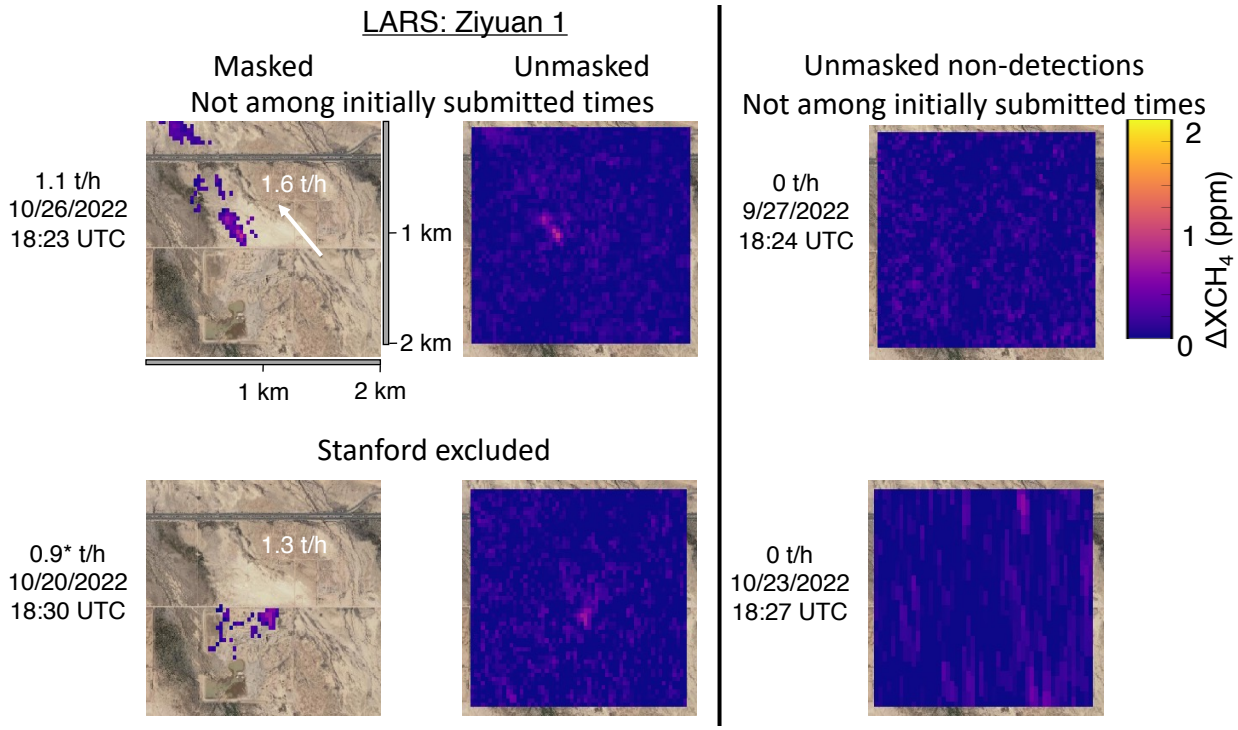


Figure S55. Provided masked and unmasked methane enhancement estimates from LARS for ZY1 retrievals. True emission rates and timestamps in black text. For nonzero estimated emissions, mean estimated emission rate in white inset text. The white arrow represents 5-minute average measured in situ wind speed. *The October 20th release volume is estimated, as described in S1.4, due to a system malfunction that prevented data logging. Surface imagery © 2023 Google Earth, CNES/Airbus, Maxar Technologies, USDA/FPAC/GEO.

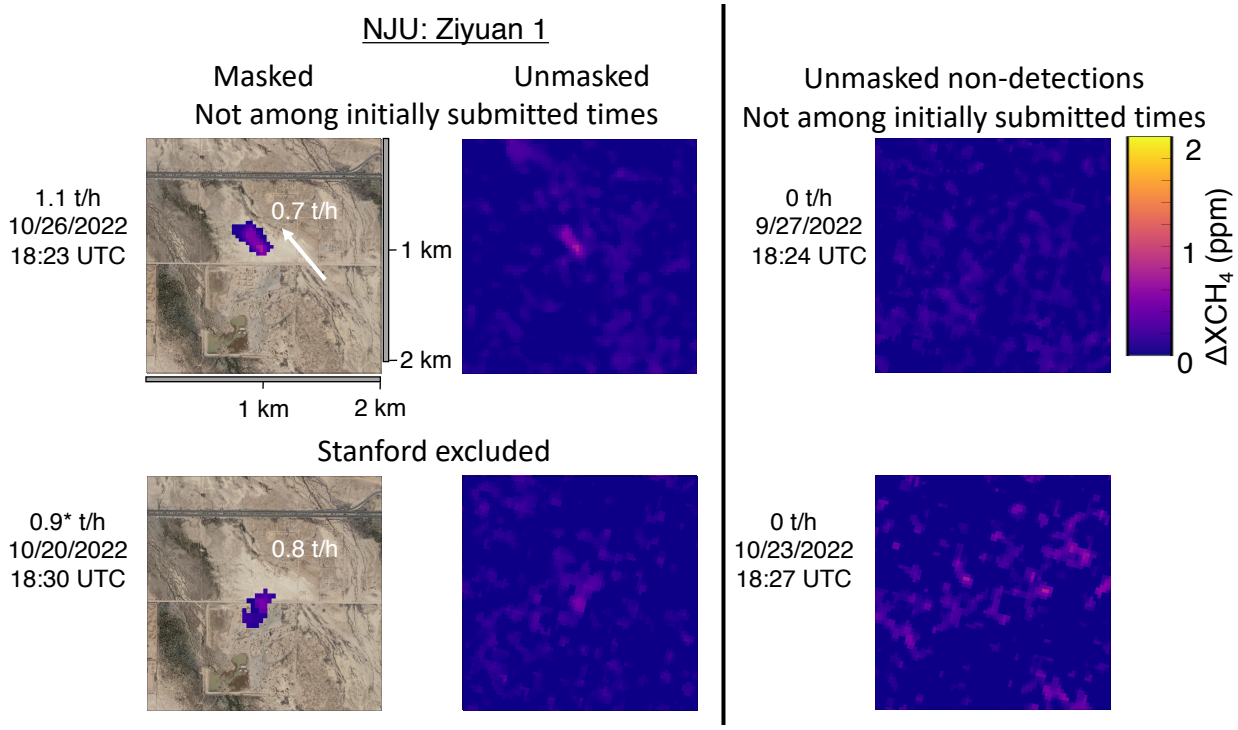

Figure S56. Provided masked and unmasked methane enhancement estimates from NJU for ZY1 retrievals. True emission rates and timestamps in black text. For nonzero estimated emissions, mean estimated emission rate in white inset text. The white arrow represents 5-minute average measured in situ wind speed. *The October 20th release volume is estimated, as described in S1.4, due to a system malfunction that prevented data logging. Surface imagery © 2023 Google Earth, CNES/Airbus, Maxar Technologies, USDA/FPAC/GEO.

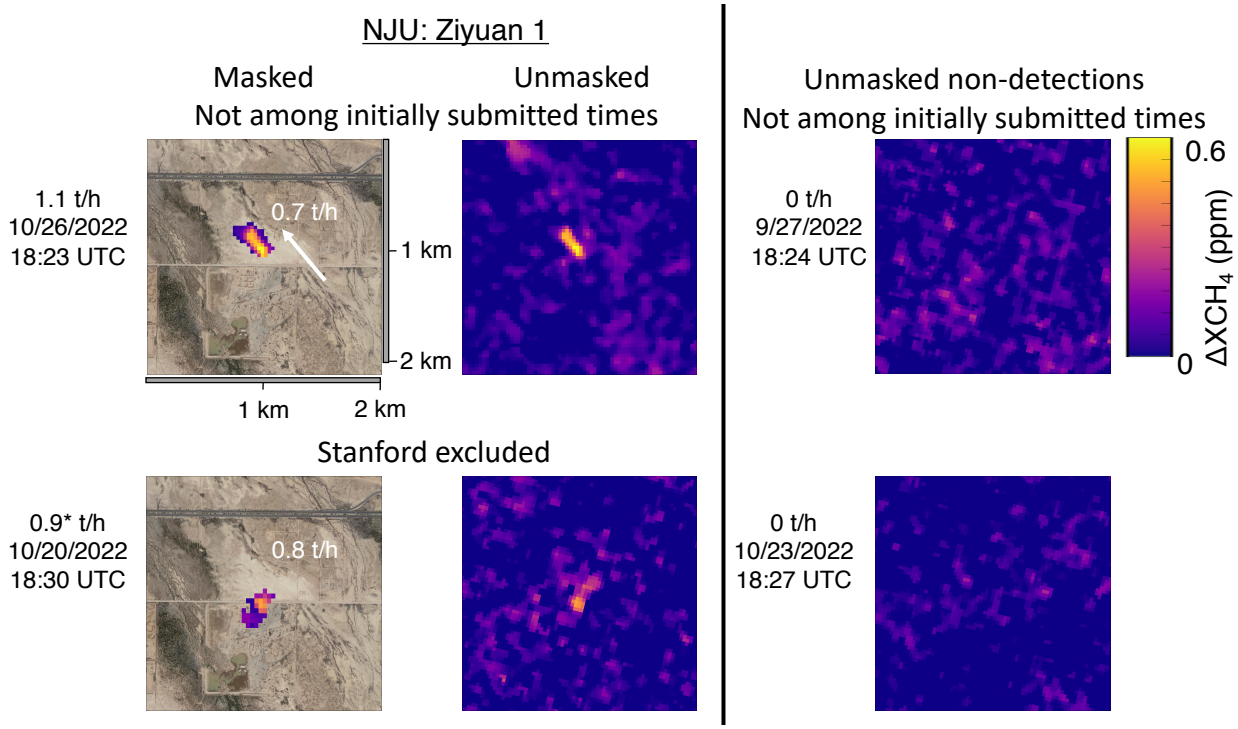


Figure S57. Custom-PPM scale, provided masked and unmasked methane enhancement estimates from NJU for ZY1 retrievals. True emission rates and timestamps in black text. For nonzero estimated emissions, mean estimated emission rate in white inset text. The white arrow represents 5-minute average measured in situ wind speed. *The October 20th release volume is estimated, as described in S1.4, due to a system malfunction that prevented data logging. Surface imagery © 2023 Google Earth, CNES/Airbus, Maxar Technologies, USDA/FPAC/GEO.

## S4.8. Optical satellite images

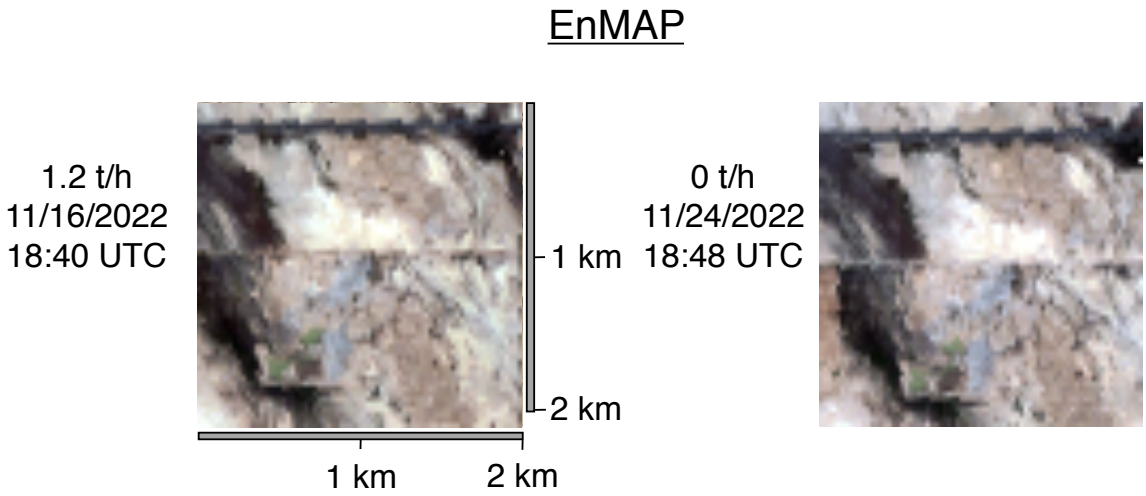


Figure S58. Optical images of the release site derived from EnMAP spectral data.

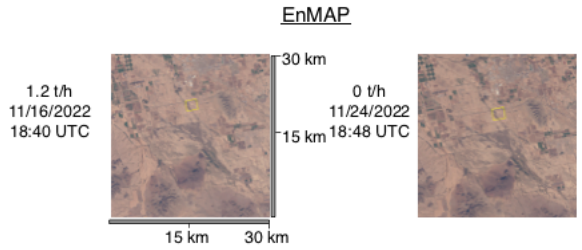


Figure S59. Wider field-of-view optical images of the release site derived from EnMAP spectral data. The 2x2 km area around the release point is highlighted in a yellow square.

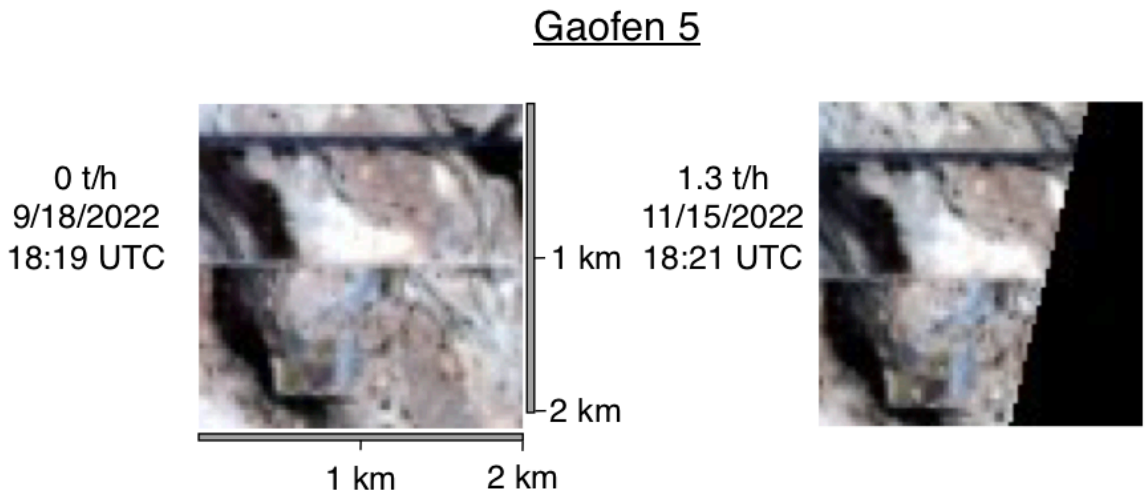


Figure S60. Optical images of the release site derived from Gaofen 5 spectral data.

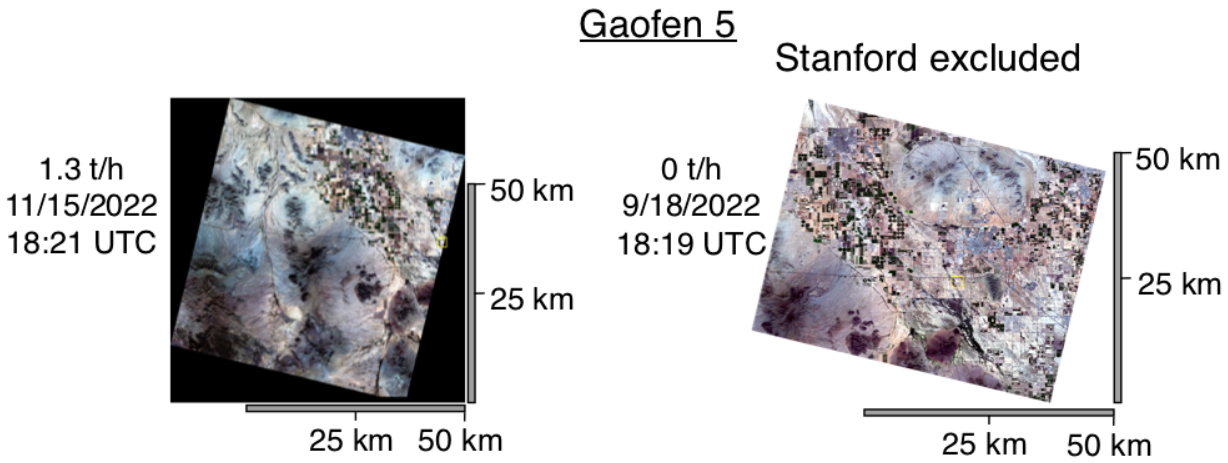


Figure S61. Wider field-of-view optical images of the release site derived from Gaofen 5 spectral data. The 2x2 km area around the release point is highlighted in a yellow square.

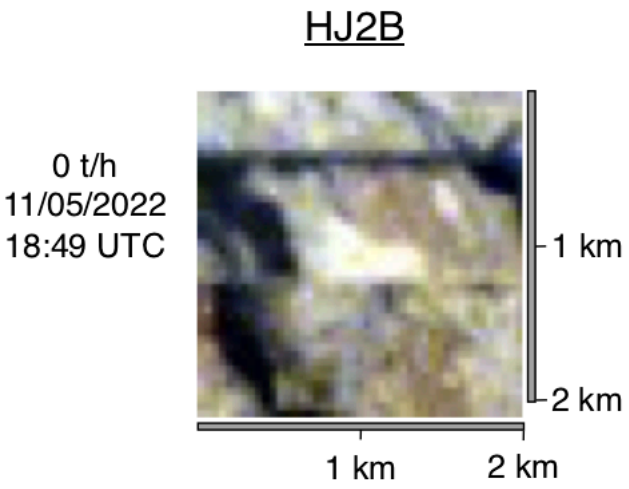


Figure S62. Optical images of the release site derived from Huanjin 2B spectral data.

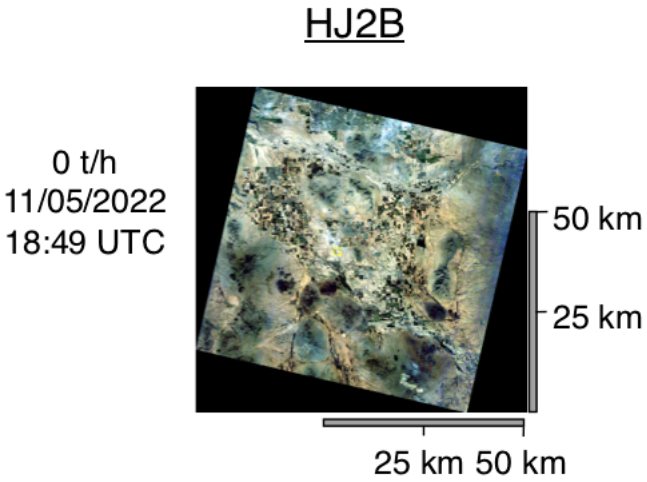


Figure S63. Wider field-of-view optical images of the release site derived from Huanjin 2B spectral data. The 2x2 km area around the release point is highlighted in a yellow square.

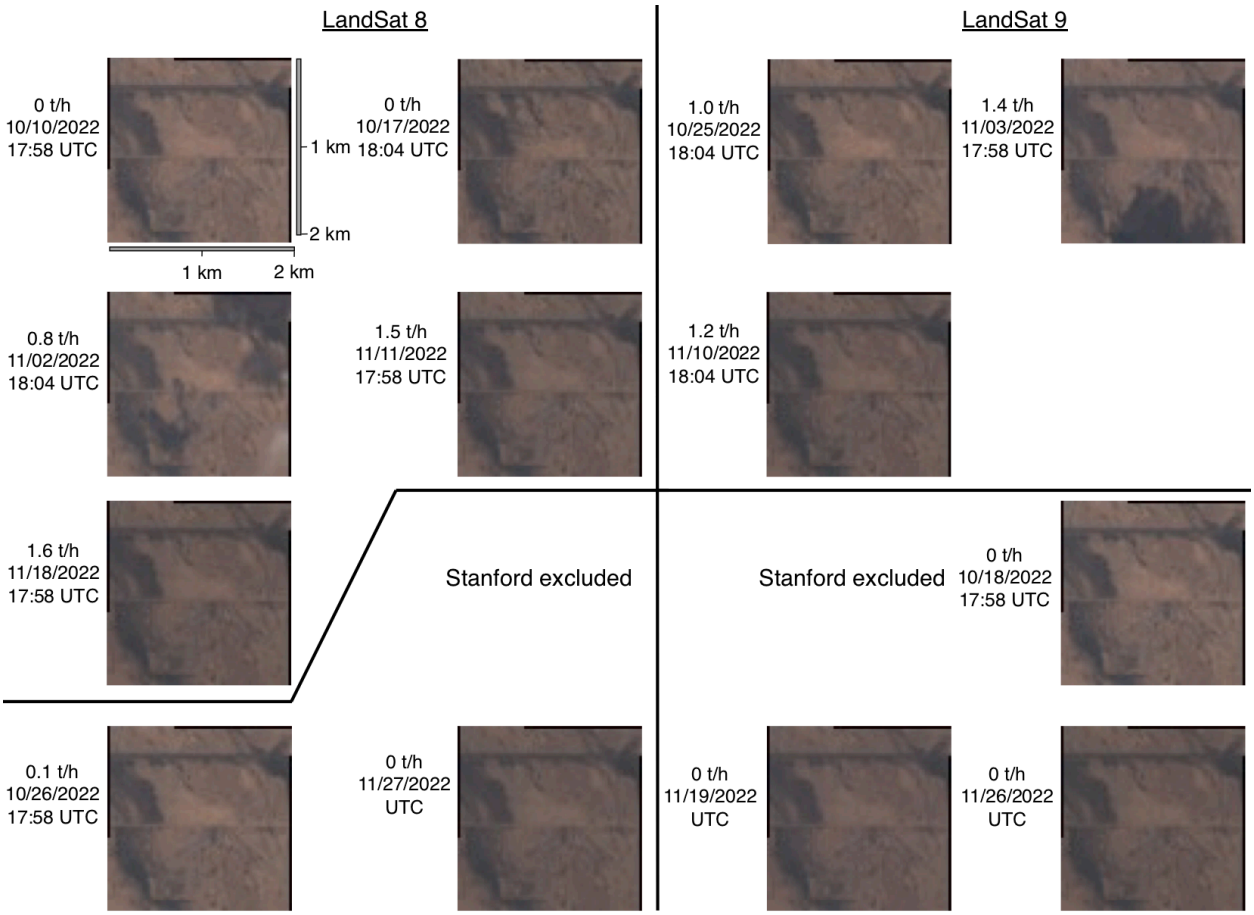

Figure S64. Optical images of the release site derived from LandSat 8/9 spectral data.

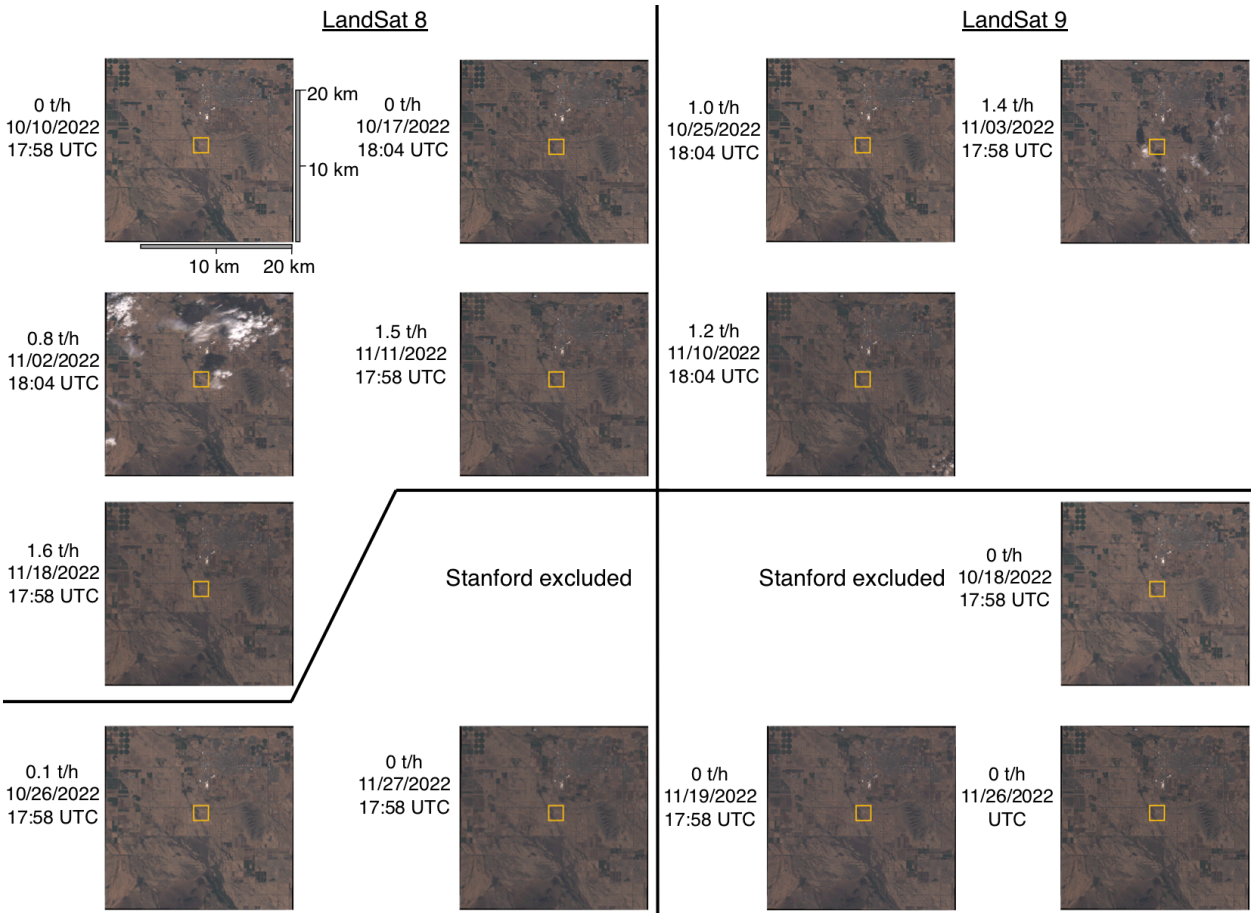

Figure S65. Wider field-of-view optical images of the release site derived from LandSat 8/9 spectral data. The 2x2 km area around the release point is highlighted in a yellow square.

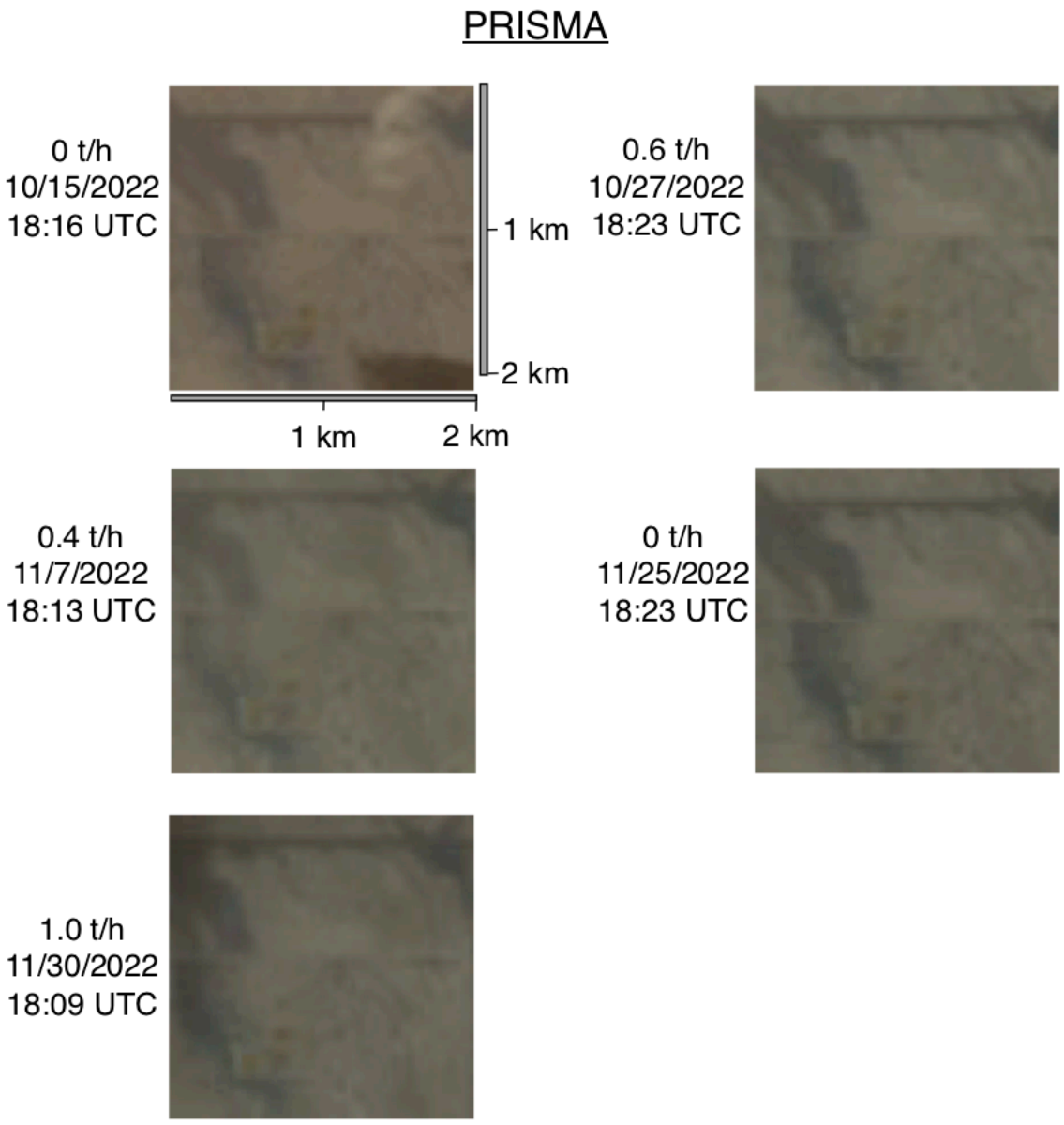


Figure S66. Optical images of the release site derived from PRISMA spectral data.

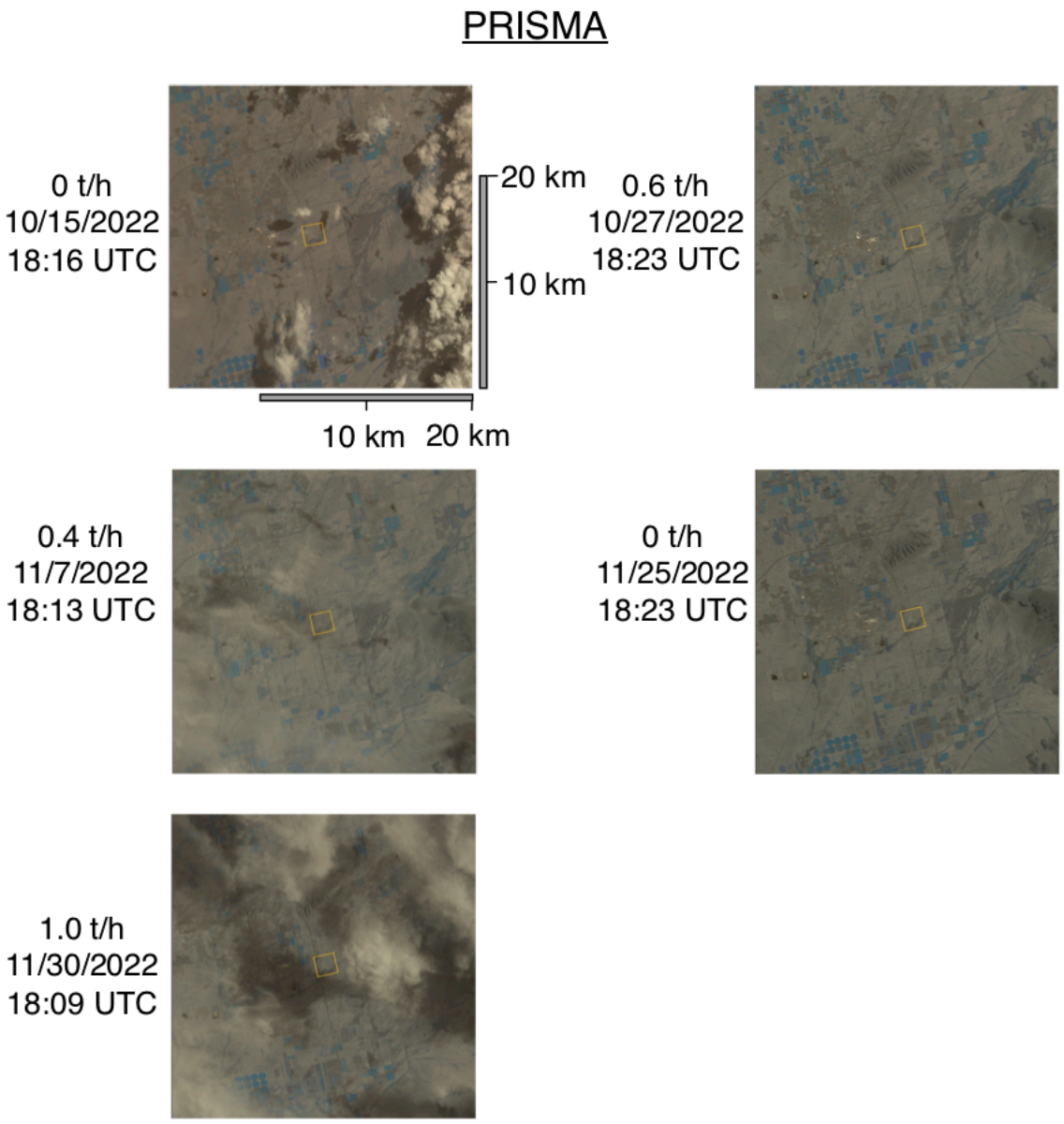


Figure S67. Wider field-of-view optical images of the release site derived from PRISMA spectral data. The 2x2 km area around the release point is highlighted in a yellow square.

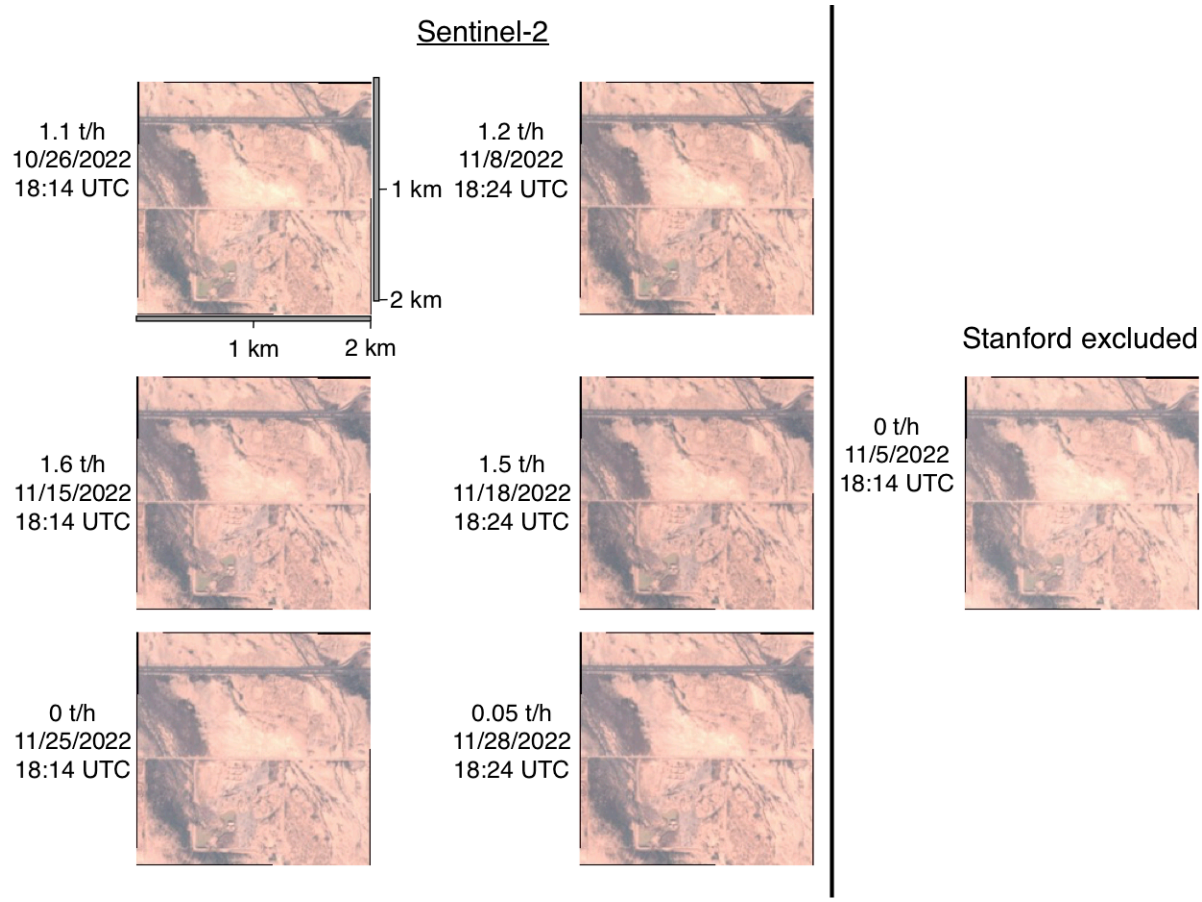


Figure S68. Optical images of the release site derived from Sentinel-2 spectral data.

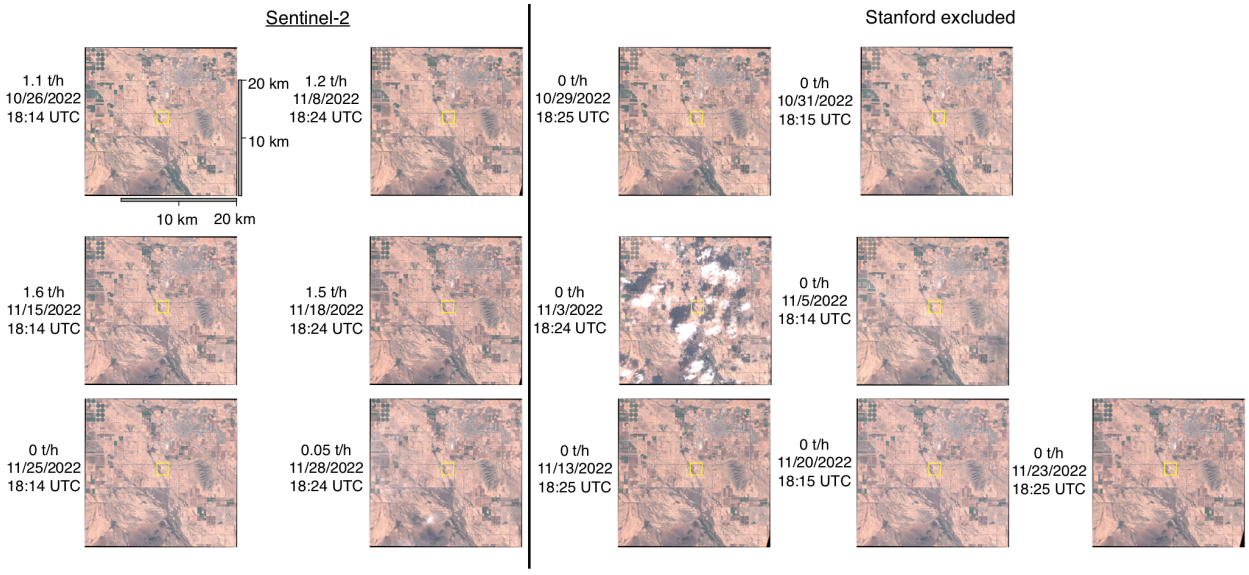


Figure S69. Wider field-of-view optical images of the release site derived from Sentinel-2 spectral data. The 2x2 km area around the release point is highlighted in a yellow square.

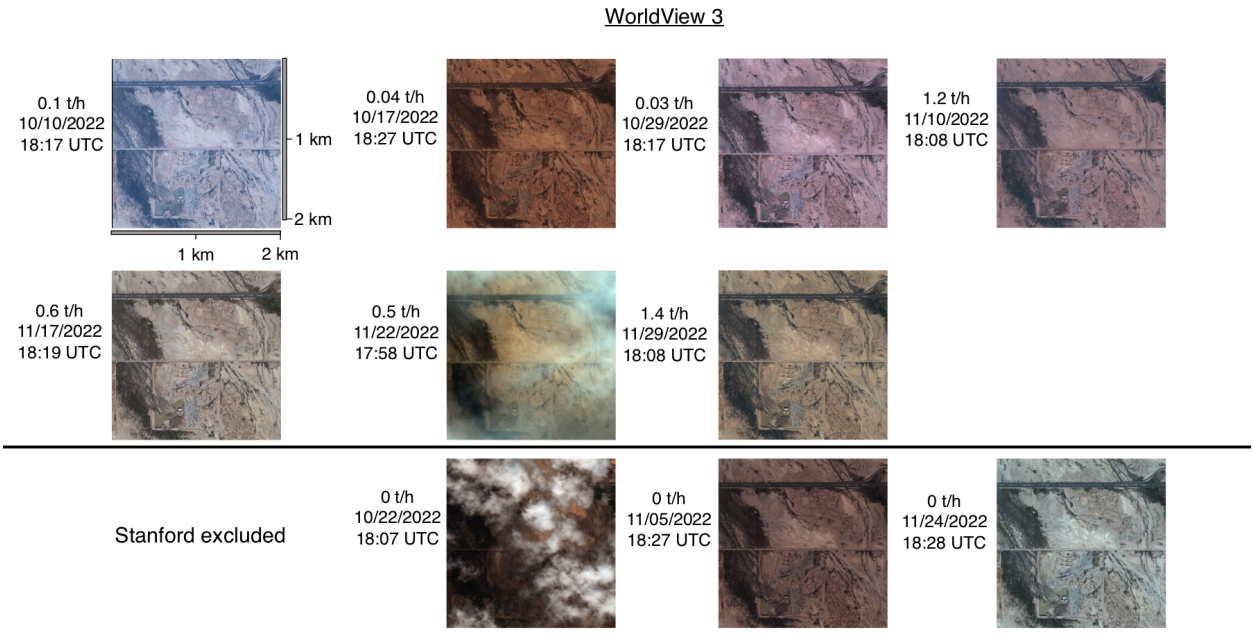


Figure S70. Optical images of the release site derived from WorldView-3 spectral data.

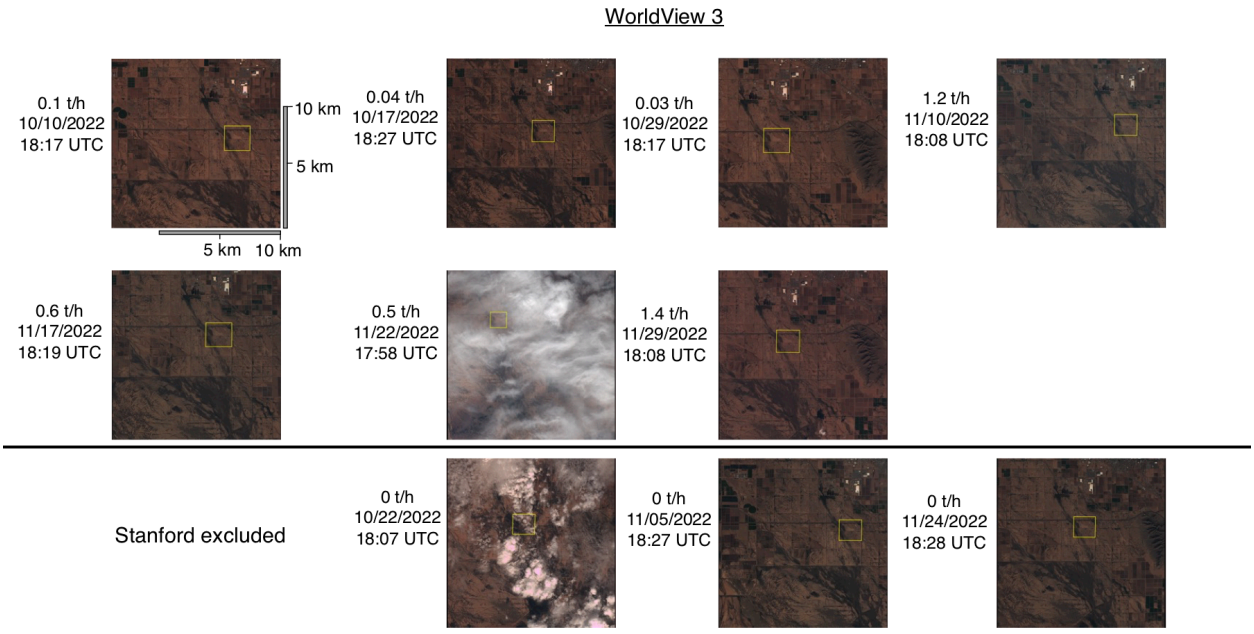


Figure S71. Wider field-of-view optical images of the release site derived from WorldView-3 spectral data. The 2x2 km area around the release point is highlighted in a yellow square.

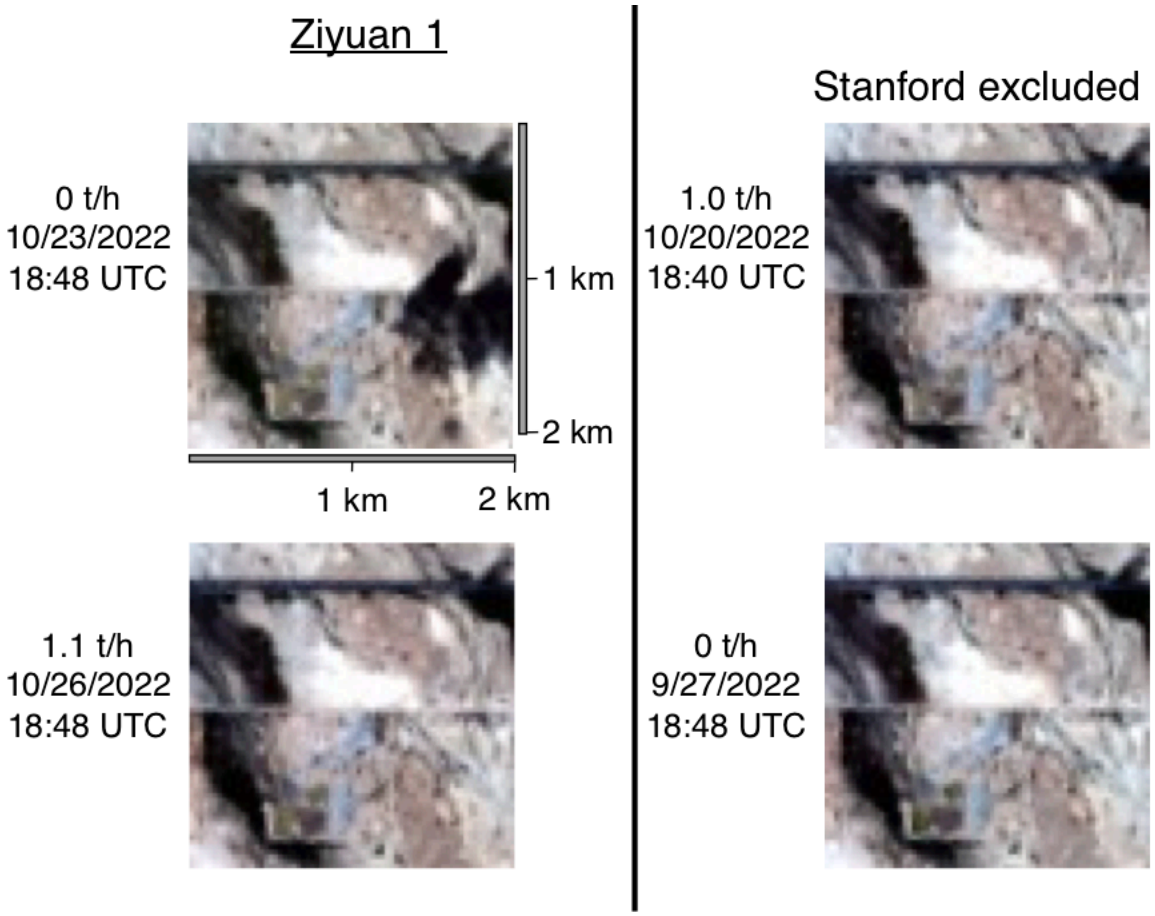


Figure S72. Optical images of the release site derived from Ziyuan 1 spectral data.

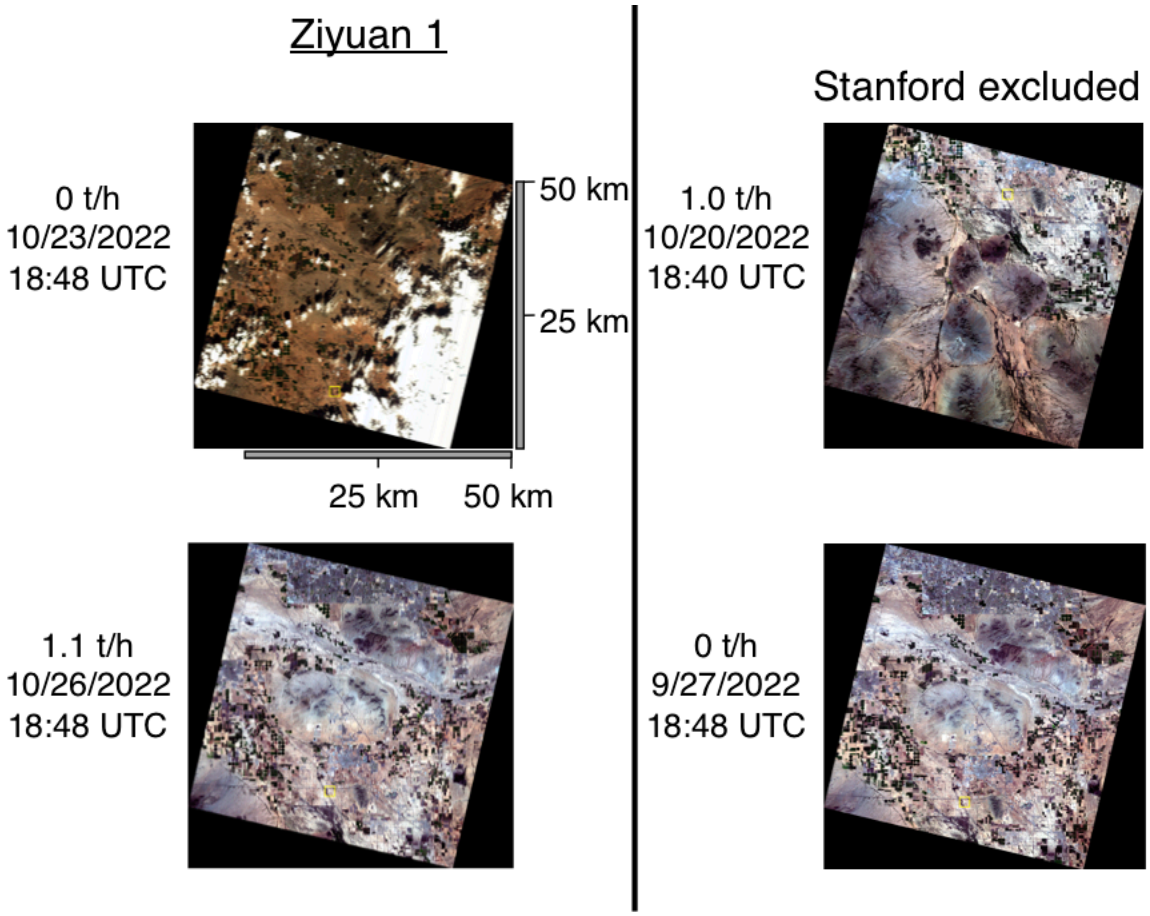


Figure S73. Wider field-of-view optical images of the release site derived from Ziyuan 1 spectral data. The 2x2 km area around the release point is highlighted in a yellow square.

## S4.9. Sky photographs

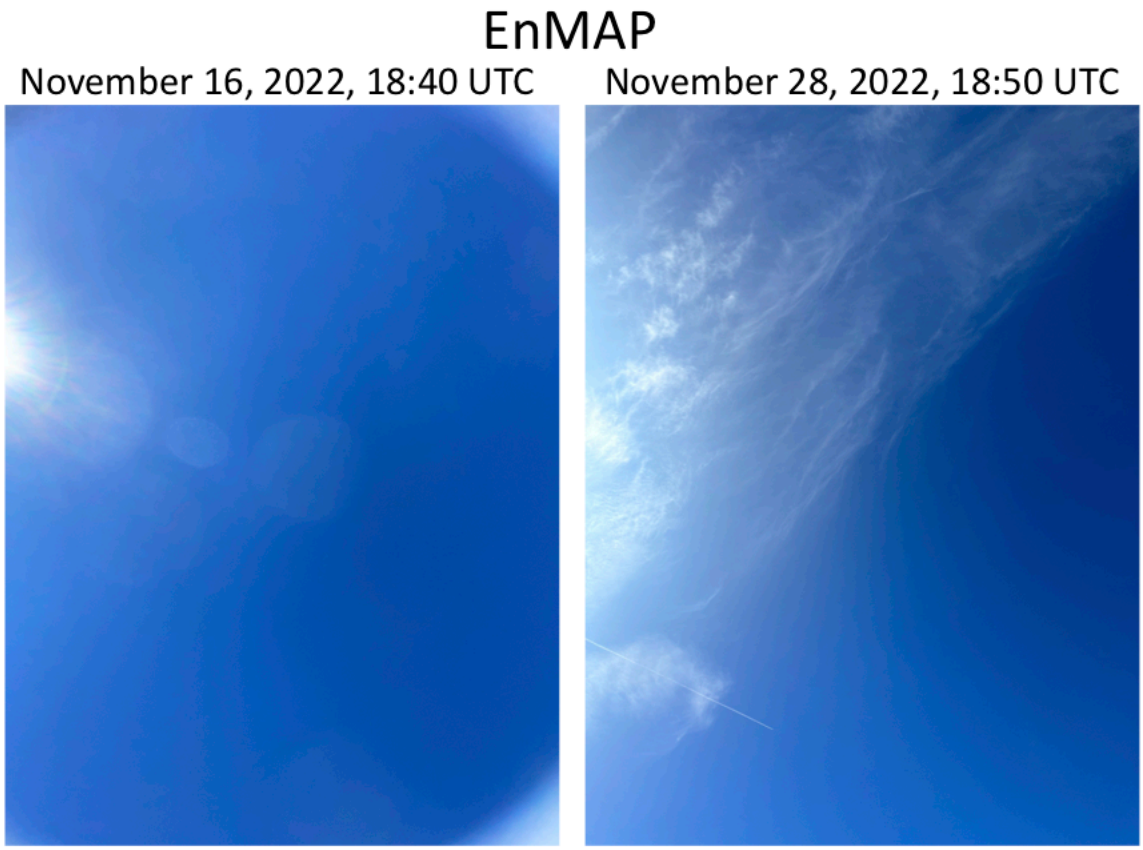


Figure S74. Photographs of the sky above the release site, taken by Stanford researchers near EnMAP satellite overpass times. The Stanford team did not take sky photographs for the November 11th, 13th, 20th, or 24th overpasses, all of which had zero methane emissions.


Figure S75. Photographs of the sky above the release site, taken by Stanford researchers near Gaofen 5 (GF5) satellite overpass times. The Stanford team did not take sky photographs for the September 18th overpass, which had zero methane emissions and occurred prior to the start of the experiment.

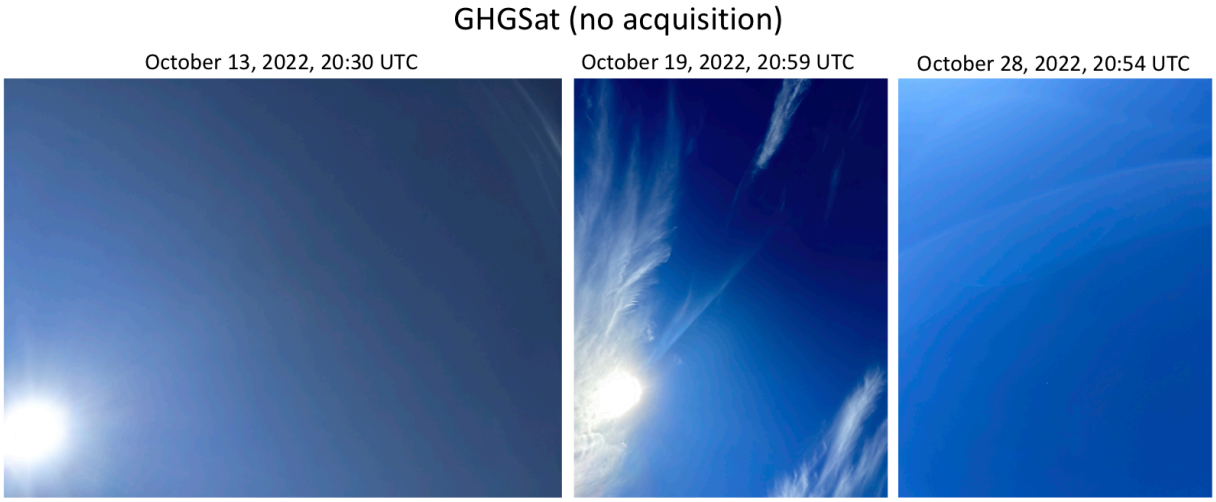


Figure S76. Photographs of the sky above the release site, taken by Stanford researchers near GHGSat satellite overpass times during October, when the satellite was not tasked due to a miscommunication. The Stanford team did not take sky photographs for the October 21st and 22nd overpasses, during which the Stanford team was troubleshooting on-site hardware systems.

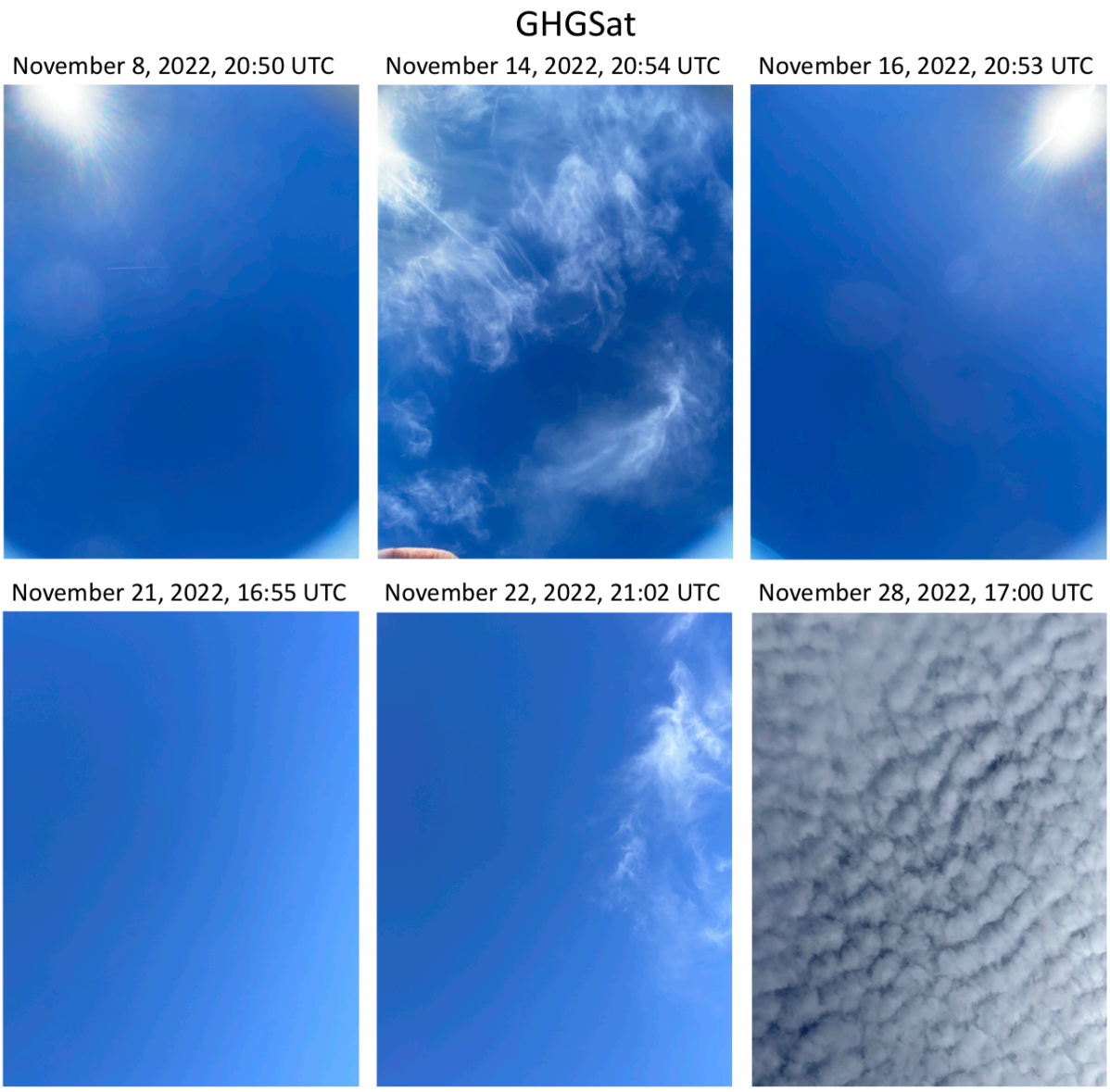


Figure S77. Photographs of the sky above the release site, taken by Stanford researchers near all GHGSat overpass times in November.

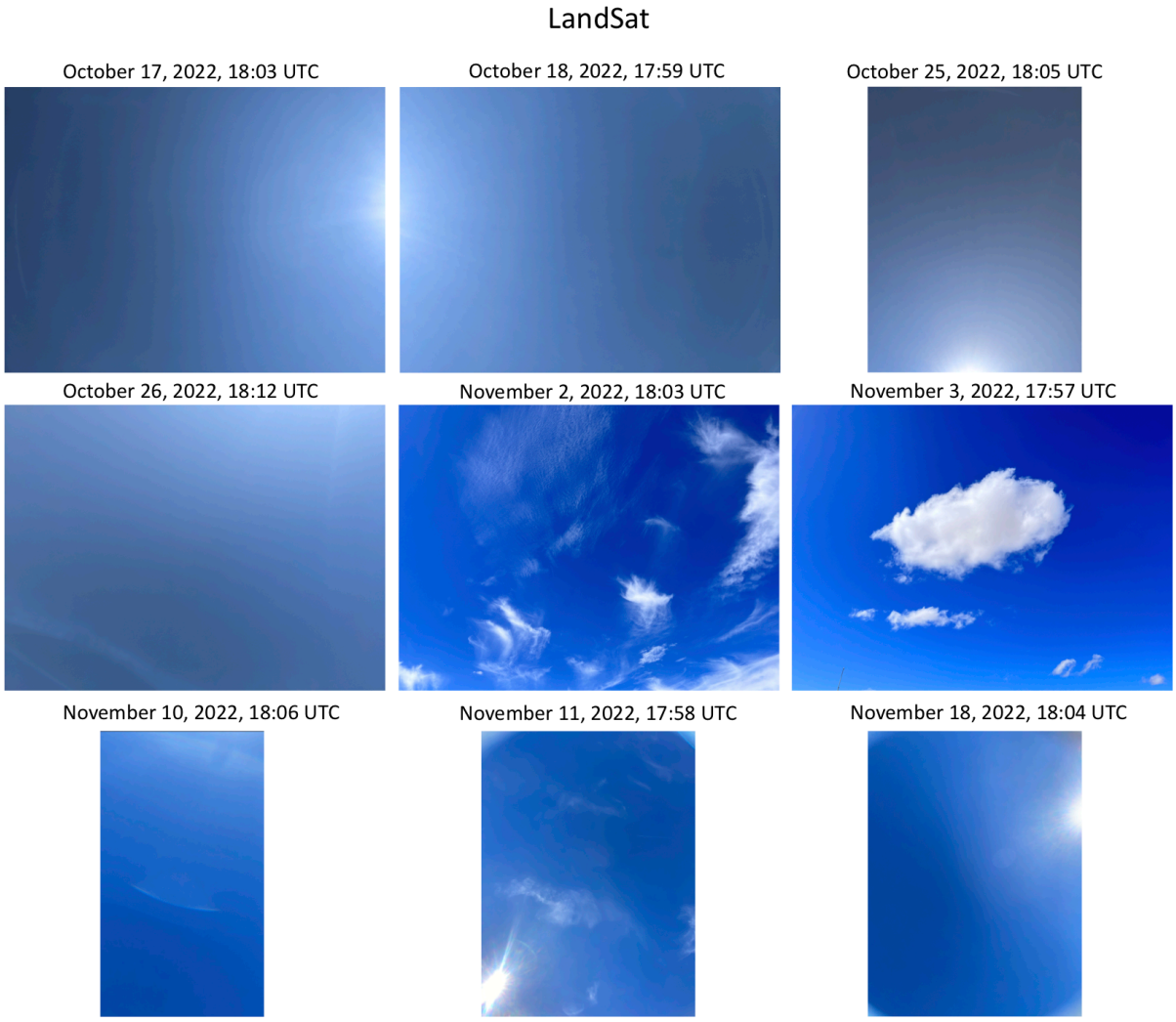


Figure S78. Photographs of the sky above the release site, taken by Stanford researchers near LandSat overpass times. The Stanford team did not take a sky photographs for the October 10th overpass, which had zero methane emissions.

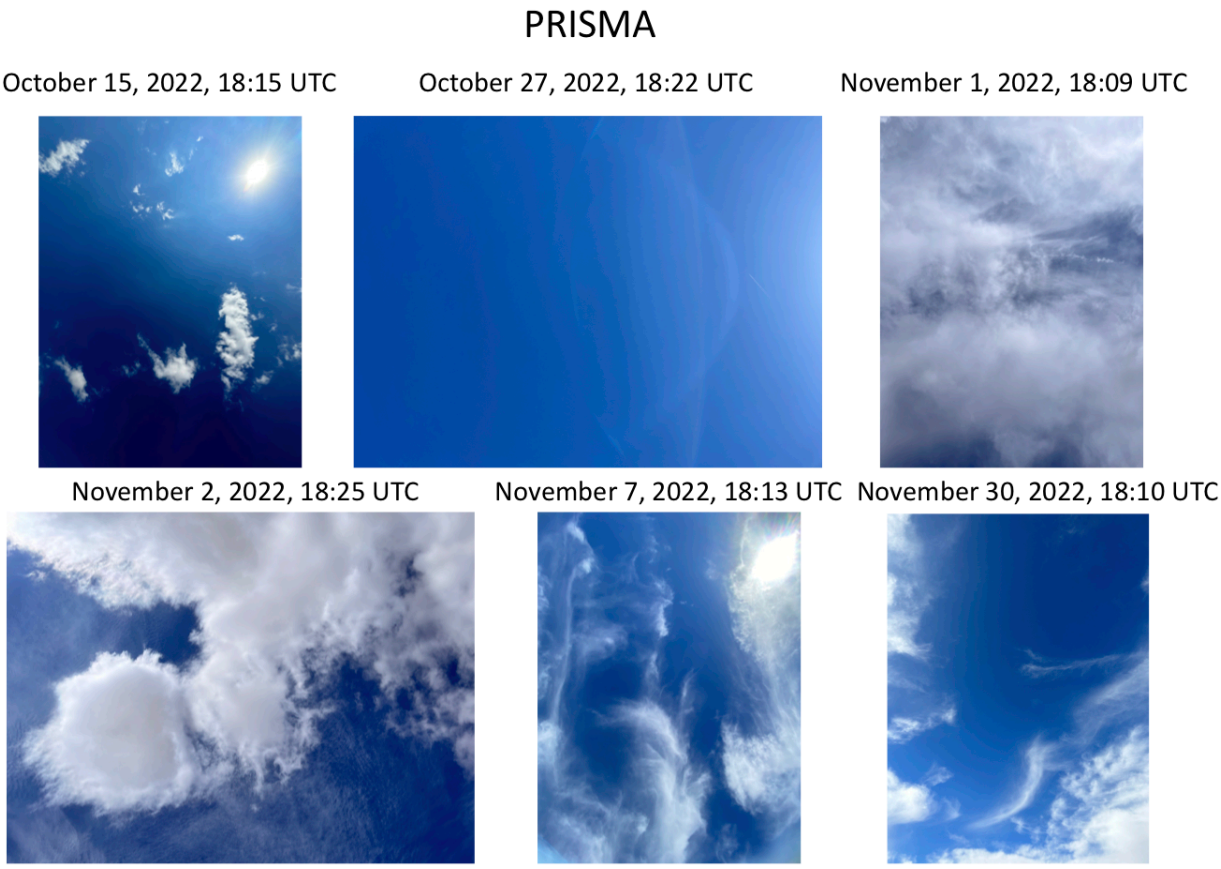


Figure S79. Photographs of the sky above the release site, taken by Stanford researchers near PRISMA overpass times. The Stanford team did not take a sky photographs for the October 21st and November 13th, 19th, and 25th overpasses, all of which had zero methane emissions. On October 21st, the Stanford team was conducting system troubleshooting and cancelled gas releases; all the November dates were weekends, and the Stanford team could not be present at the field site due to personnel shortage.

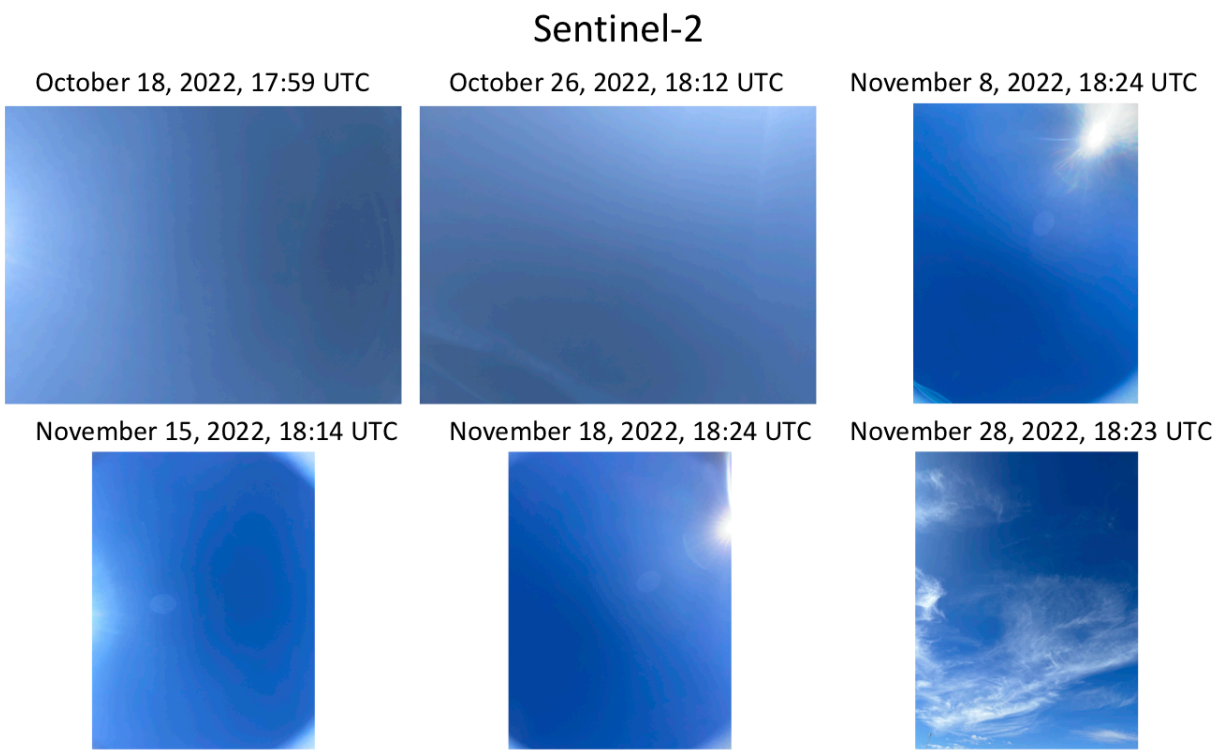


Figure S80. Photographs of the sky above the release site, taken by Stanford researchers near Sentinel-2 overpass times. The Stanford team did not take a sky photographs for the November 5th and 25th overpasses, which had zero methane emissions. The Stanford team could not be present at the field site on these dates due to personnel shortage.

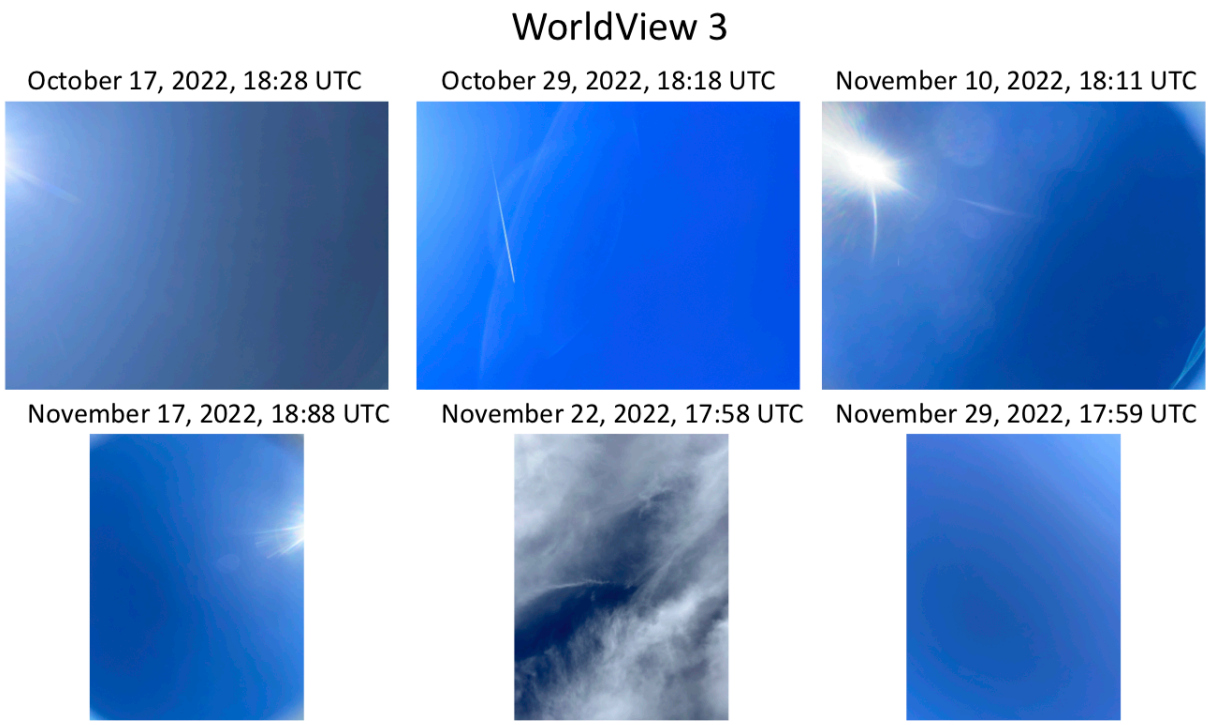


Figure S81. Photographs of the sky above the release site, taken by Stanford researchers near Sentinel-2 overpass times. The Stanford team did not take a sky photographs for the October 10th and 22nd and November 5th and 24th overpasses, all of which had zero methane emissions.

# S5. Supplementary references

CEOS: A Constellation Architecture for Monitoring Carbon Dioxide and Methane from Space, Committee on Earth Observation Satellites Atmospheric Composition Virtual Constellation Greenhouse Gas Team, 2018.

ECMWF: ERA5, European Centre for Medium-Range Weather Forecasts, Bonn, Germany, 2022.

El Abbadi, S., Chen, Z., Burdeau, P., Rutherford, J., Chen, Y., Zhang, Z., Sherwin, E., and Brandt, A.: Comprehensive evaluation of aircraft-based methane sensing for greenhouse gas mitigation, Engineering, https://doi.org/10.31223/X51D4C, 2023.

EnMAP: EnMAP Instrument Planning, EnMap, Bonn, Germany, 2022.

EnMAP: EnMAP: Mission, EnMAP, EnMAP, 2023.

ESA: eoPortal: PRISMA (Hyperspectral), European Space Agency, Paris, France, 2012.

ESA: Sentinel-2 User Handbook, European Space Agency, Paris, France, 2015.

ESA: Sentinel-2: About the launch, European Space Agency, Paris, France, 2017.

ESA: Access to Sentinel data via download, European Space Agency, Paris, France, 2021a.

ESA: GHGSat data now available through ESA's Earthnet programme, European Space Agency, Paris, France, 2021b.

ESA: Sentinel-2, European Space Agency, Paris, France, 2021c.

ESA: About GHGSat, European Space Agency, Paris, France, 2022a.

ESA: Earth Online: Worldview-3, European Space Agency, Paris, France, 2022b.

ESA: Sentinel-5P: Global Air Monitoring for Copernicus, European Space Agency, Paris, France, 2022c.

ESA: WorldView-3 full archive and tasking, European Space Agency, Paris, France, 2022d.

Frankenberg, C., Thorpe, A. K., Thompson, D. R., Hulley, G., Kort, E. A., Vance, N., Borchardt, J., Krings, T., Gerilowski, K., Sweeney, C., Conley, S., Bue, B. D., Aubrey, A. D., Hook, S., and Green, R. O.: Airborne methane remote measurements reveal heavy-tail flux distribution in Four Corners region, Proc Natl Acad Sci USA, 113, 9734–9739, https://doi.org/10.1073/pnas.1605617113, 2016.

GHGSat: Greenhouse Gas Monitoring from Space: GHGSat Launches Three New Satellites with SpaceX, GHGSat, Montréal, Canada, 2022.

GHGSat: 3 New Methane Monitoring Satellites Make Contact in Record-Time, GHGSat, Montréal, Canada, 2023.

Hayden, A. and Christy, J.: Maxar's WorldView-3 Enables Low-Concentration Methane Detection from Space, https://doi.org/10.31223/X51T1C, 15 June 2023.

Irakulis-Loitxate, I., Guanter, L., Liu, Y.-N., Varon, D. J., Maasakkers, J. D., Zhang, Y., Chulakadabba, A., Wofsy, S. C., Thorpe, A. K., Duren, R. M., Frankenberg, C., Lyon, D. R., Hmiel, B., Cusworth, D. H., Zhang, Y., Segl, K., Gorroño, J., Sánchez-García, E., Sulprizio, M. P., Cao, K., Zhu, H., Liang, J., Li, X., Aben, I., and Jacob, D. J.: Satellite-based survey of extreme methane emissions in the Permian basin, Sci. Adv., 7, eabf4507, https://doi.org/10.1126/sciadv.abf4507, 2021.

Irakulis-Loitxate, I., Guanter, L., Maasakkers, J. D., Zavala-Araiza, D., and Aben, I.: Satellites Detect Abatable Super-Emissions in One of the World's Largest Methane Hotspot Regions, Environ. Sci. Technol., 56, 2143–2152, https://doi.org/10.1021/acs.est.1c04873, 2022.

Jacob, D. J., Varon, D. J., Cusworth, D. H., Dennison, P. E., Frankenberg, C., Gautam, R., Guanter, L., Kelley, J., McKeever, J., Ott, L. E., Poulter, B., Qu, Z., Thorpe, A. K., Worden, J. R., and Duren, R. M.: Quantifying methane emissions from the global scale down to point sources using satellite observations of atmospheric methane, Atmos. Chem. Phys., 22, 9617–9646, https://doi.org/10.5194/acp-22-9617-2022, 2022.

Lauvaux, T., Giron, C., Mazzolini, M., d'Aspremont, A., Duren, R., Cusworth, D., Shindell, D., and Ciais, P.: Global Assessment of Oil and Gas Methane Ultra-Emitters, Science, 375, 557–561, https://doi.org/10.31223/X5NS54, 2022.

Luo, H., Li, Z., Wu, Y., Qiu, Z., Shi, H., Wang, Q., and Xiong, W.: Greenhouse Gases Monitoring Instrument on GaoFen-5 Satellite-II: Optical Design and Evaluation, Remote Sensing, 15, 1105, https://doi.org/10.3390/rs15041105, 2023.

NASA: GEOS Near-Real Time Data Products, National Aeronotics and Space Administration, Global Modeling and Assimilation Office, Greenbelt, Maryland, USA, 2021.

NASA: Landsat 9, NASA, Washington, D.C., USA, 2023.

NOAA: The High-Resolution Rapid Refresh (HRRR), National Oceanographic & Atmospheric Administration, Global Systems Laboratory, Boulder, Colorado, USA, 2022.

OHBI: Satellites & Missions: PRISMA, Orbitale Hochtechnologie Bremen Italia S.p.A., Milan, Italy, 2022.

Orbio: Actionable Methane Intelligence: Filling the global methane gap with asset-level emissions data, Orbio, Köln, Germany, 2023.

Sánchez-García, E., Gorroño, J., Irakulis-Loitxate, I., Varon, D. J., and Guanter, L.: Mapping methane plumes at very high spatial resolution with the WorldView-3 satellite, Environmental Science & Technology, 56, 10517–10529, https://doi.org/10.1021/acs.est.1c08575, 2022.

Satelytics: Satelytics solves the most pressing industrial challenges, Satelytics, Perrysburg, Ohio, USA, 2023.

Sherwin, E. D., Rutherford, J. S., Chen, Y., Aminfard, S., Kort, E. A., Jackson, R. B., and Brandt, A. R.: Single-blind validation of space-based point-source detection and quantification of onshore methane emissions, Sci Rep, 13, 3836, https://doi.org/10.1038/s41598-023-30761-2, 2023.

Song, Q., Ma, C., Liu, J., and Wei, H.: Quantifying ocean surface green tides using high-spatial resolution thermal images, Opt. Express, 30, 36592, https://doi.org/10.1364/OE.472479, 2022.

USGS: Landsat 8, United States Geological Survey, Washington, D.C., 2022a.

USGS: Landsat Data Access, United States Geological Survey, Washington, D.C., 2022b.

Varon, D. J., Jacob, D. J., McKeever, J., Jervis, D., Durak, B. O. A., Xia, Y., and Huang, Y.: Quantifying methane point sources from fine-scale satellite observations of atmospheric methane plumes, Atmos. Meas. Tech., 11, 5673–5686, https://doi.org/10.5194/amt-11-5673-2018, 2018.

Varon, D. J., Jervis, D., McKeever, J., Spence, I., Gains, D., and Jacob, D. J.: High-frequency monitoring of anomalous methane point sources with multispectral Sentinel-2 satellite

observations, Atmos. Meas. Tech., 14, 2771–2785, https://doi.org/10.5194/amt-14-2771-2021, 2021.

Zhang, B., Guo, B., Zou, B., Wei, W., Lei, Y., and Li, T.: Retrieving soil heavy metals concentrations based on GaoFen-5 hyperspectral satellite image at an opencast coal mine, Inner Mongolia, China, Environmental Pollution, 300, 118981, https://doi.org/10.1016/j.envpol.2022.118981, 2022.

Zhong, B., Yang, A., Liu, Q., Wu, S., Shan, X., Mu, X., Hu, L., and Wu, J.: Analysis Ready Data of the Chinese GaoFen Satellite Data, Remote Sensing, 13, 1709, https://doi.org/10.3390/rs13091709, 2021.

Zimmerle, D.: METEC Controlled Test Protocol: Survey Emission Detection And Quantification, Colorado State University, Fort Collins, CO, USA, 2022.